

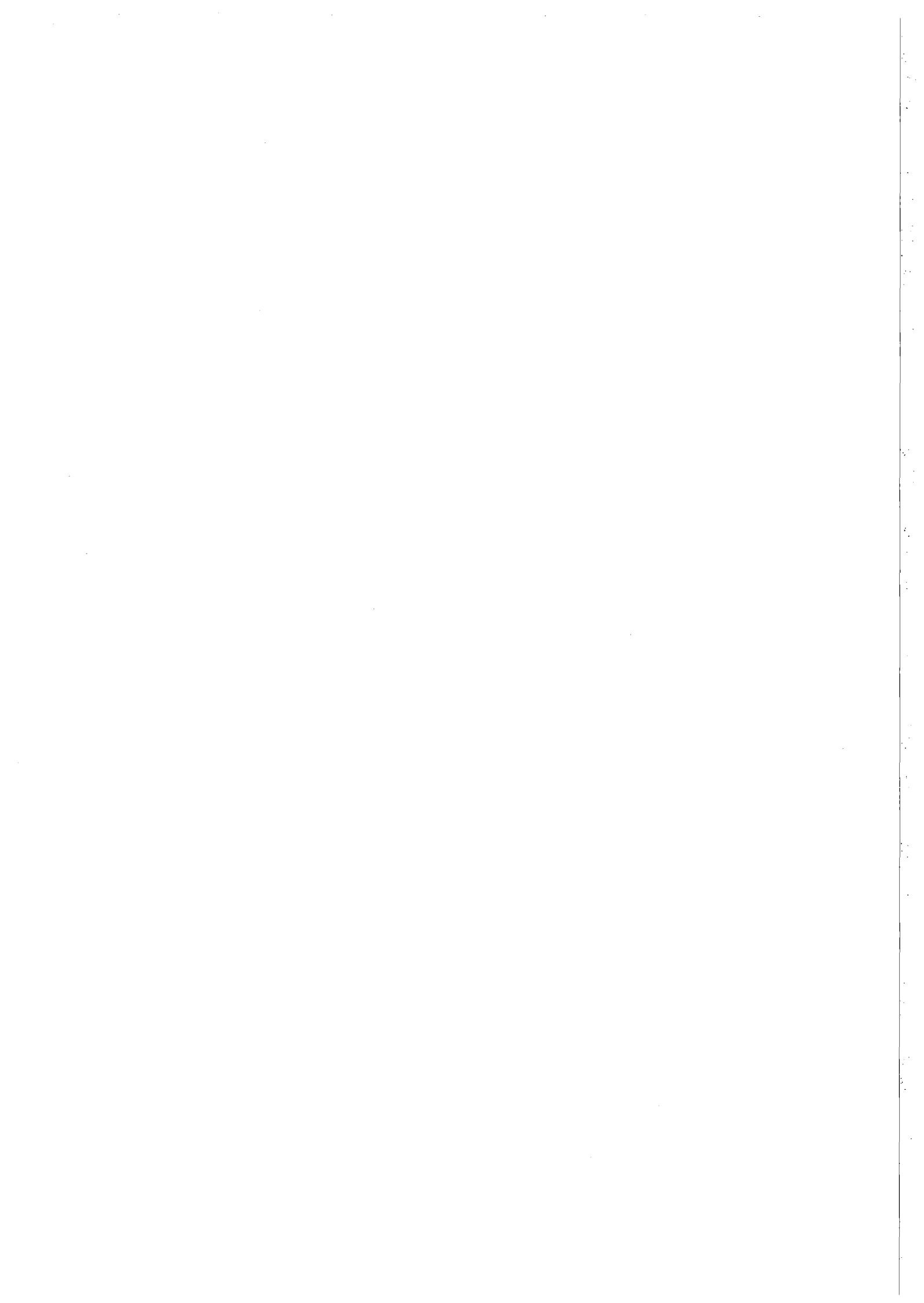
NORSAR Scientific Report No. 1-94/95

Semiannual Technical Summary

1 April - 30 September 1994

Kjeller, November 1994

APPROVED FOR PUBLIC RELEASE, DISTRIBUTION UNLIMITED



REPORT DOCUMENTATION PAGE

1a. REPORT SECURITY CLASSIFICATION Unclassified		1b. RESTRICTIVE MARKINGS Not applicable		
2a. SECURITY CLASSIFICATION AUTHORITY Not Applicable		3. DISTRIBUTION / AVAILABILITY OF REPORT Approved for public release; distribution unlimited		
2b. DECLASSIFICATION / DOWNGRADING SCHEDULE				
4. PERFORMING ORGANIZATION REPORT NUMBER(S) Scientific Rep. 1-94/95		5. MONITORING ORGANIZATION REPORT NUMBER(S) Scientific Rep. 1-94/95		
5a. NAME OF PERFORMING ORGANIZATION NFR/NORSAR.	6b. OFFICE SYMBOL (If applicable)	7a. NAME OF MONITORING ORGANIZATION HQ/AFTAC/TTS		
5c. ADDRESS (City, State, and ZIP Code) Post Box 51 N-2007 Kjeller, Norway		7b. ADDRESS (City, State, and ZIP Code) Patrick AFB, FL 32925-6001		
8a. NAME OF FUNDING / SPONSORING ORGANIZATION Advanced Research Projects Agency	8b. OFFICE SYMBOL (If applicable) NMRO	9. PROCUREMENT INSTRUMENT IDENTIFICATION NUMBER Contract No. F08606-89-C-0005		
8c. ADDRESS (City, State, and ZIP Code) 3701 N. Fairfax Dr. #717 Arlington, VA 22203-1714		10. SOURCE OF FUNDING NUMBERS		
		PROGRAM ELEMENT NO. R&D	PROJECT NO. NORSAR Phase 3	TASK NO. SOW Task 5.0
11. TITLE (Include Security Classification) Semiannual Technical Summary, 1 Apr - 30 Sep 1994				
12. PERSONAL AUTHOR(S)				
13a. TYPE OF REPORT Scientific Summary	13b. TIME COVERED FROM 1 Apr 94 TO 30 Sep 94	14. DATE OF REPORT (Year, Month, Day) 1994 November	15. PAGE COUNT 127	
16. SUPPLEMENTARY NOTATION				
17. COSATI CODES		18. SUBJECT TERMS (Continue on reverse if necessary and identify by block number) NORSAR, Norwegian Seismic Array		
FIELD	GROUP			SUB-GROUP
8	11			
19. ABSTRACT (Continue on reverse if necessary and identify by block number) This Semiannual Technical Summary describes the operation, maintenance and research activities at the Norwegian Seismic Array (NORSAR), the Norwegian Regional Seismic Array (NORESS), the Arctic Regional Seismic Array (ARCESS) and the experimental Spitsbergen Regional Array for the period for the period 1 April - 30 September 1994. Statistics are also presented for additional seismic stations, which through cooperative agreements with institutions in the host countries provide continuous data to the NORSAR Data processing Center (NDPC). These stations comprise the Finnish Experimental Seismic Array (FINESS), the German Experimental Seismic Array (GERESS), and an experimental regional seismic array in Apatity, Russia. (cont.)				
20. DISTRIBUTION / AVAILABILITY OF ABSTRACT <input type="checkbox"/> UNCLASSIFIED/UNLIMITED <input type="checkbox"/> SAME AS RPT. <input type="checkbox"/> DTIC USERS		21. ABSTRACT SECURITY CLASSIFICATION		
22a. NAME OF RESPONSIBLE INDIVIDUAL Mr. Michael C. Baker	22b. TELEPHONE (Include Area Code) (407) 494-7665	22c. OFFICE SYMBOL AFTAC/TTS		

Abstract (cont.)

This Semiannual Report also presents statistics from operation of the Intelligent Monitoring System (IMS). The IMS has been operated in an experimental mode, with continuous automatic detection and location and with analyst review of selected events of interest. Since October 1991, a new version of the IMS that accepts data from an arbitrary number of arrays and single 3-component stations has been operated.

The NORSAR Detection Processing system has been operated throughout the period with an average uptime of 99.3% as compared to 98.3% for the previous reporting period. A total of 2015 seismic events have been reported in the NORSAR monthly seismic bulletin. The performance of the continuous alarm system and the automatic bulletin transfer by telex to AFTAC has been satisfactory. The system for direct retrieval of NORSAR waveform data through an X.25 connection has been used successfully for acquiring such data by AFTAC. Processing of requests for full NORSAR and regional array data on magnetic tapes has progressed according to established schedules.

Since 1 October 1991, an effort has been undertaken to carry out a complete technical refurbishment of the NORSAR array. This project is funded jointly by AFTAC, ARPA and NFR. During the reporting period, all the new Science Horizons data acquisition hardware and software have been acquired and delivered. See NORSAR Sci. Rep. No. 2-93/94 for a system description. The data acquisition software XAVE and communication interface module CIM II were installed on 5 October 1994 at NDPC. At subarray 06C, a CIM II was installed in the Central Terminal Vault -- CTV -- and an AIM24-1 has been installed in one remote SP vault (SPV) for testing purposes. The data acquisition is running satisfactorily. Contractual arrangements for the delivery of "posthole" KS54000 seismometers have been completed.

As an intermediate step in the NORSAR Refurbishment, a modified version of the NORSAR data acquisition system was implemented on 1 January 1994. This modified version has continued to be in operation during the reporting period. The main reason for this change, which utilizes a previously established backup solution, was to circumvent some data timing problems due to deteriorating hardware. At the same time, this change has provided valuable experience in preparing the full refurbishment.

On-line detection processing and data recording at the NORSAR Data Processing Center (NDPC) of NORESS, ARCESS, FINESS and GERESS data have been conducted throughout the period. Data from two experimental small-aperture arrays at sites in Spitsbergen and Apatity, Kola Peninsula, have been recorded and processed in an experimental mode. Monthly processing statistics for the arrays as well as results of the IMS analysis for the reporting period are given.

Maintenance activities in the period comprise preventive/corrective maintenance in connection with all the NORSAR subarrays, NORESS and ARCESS. Other activities have involved testing of the NORSAR communications systems, preparations for the NORSAR refurbishment and work in connection with the experimental small-aperture arrays in Spitsbergen and Russia.

Summaries of six scientific contributions are presented in Chapter 7 of this report.

Section 7.1 is a final report on the global continuous Threshold Monitoring project, which is an effort to develop and implement a prototype, workstation-based Threshold Monitoring System for the GSETT-3 International Data Center (IDC). The main focus of this work has been to develop an environment that facilitates both real-time operation as well as testing of new ideas in the context of continuous seismic threshold monitoring. The current operational system is not fully optimized with respect to processing parameters, but the framework for a stepwise improvement exists. We can as of today demonstrate the potentials of using continuous seismic threshold monitoring as part of a global seismic verification system, but some caution has to be taken during the interpretation of the derived magnitude thresholds. Further improvements will rely heavily on the possibility of conducting extensive event analysis and associated calibration efforts.

Section 7.2 presents observations of the Lop Nor nuclear explosions of 10 June and 7 October 1994. Some comparisons are also made with the Lop Nor explosions conducted on 21 May 1992 and 5 October 1993. Most of the automatic systems at NORSAR showed good performance for these events. Particularly impressive is the high signal-to-noise ratios observed at NORESS and ARCESS. Among the available sources, the most accurate location is provided by the PDE bulletin, which uses a world-wide network for location purposes. The solutions by the Intelligent Monitoring System (IMS), both automatic and after analyst processing, are also quite satisfactory. The NORSAR automatic location was acceptable for only one of the two events, but reruns gave adequate results for both.

Section 7.3 describes the results of a study to investigate the benefits of NORSAR-NORESS joint processing. As is well known, the teleseismic NORSAR array and the regional NORESS array have to some extent overlapping capabilities as far as seismic event detection is concerned. However, when it comes to locating events, the two arrays are complementary. NORSAR has a superior location capability for teleseismic events, whereas NORESS is superior for locating local and regional events. Furthermore, NORESS has the ability to unambiguously classify an event as "regional" or "local", whereas NORSAR will usually assign a teleseismic location estimate (the "best beam") to any event, whether it is of local, regional or teleseismic origin.

The study has shown that a clear improvement in the automatic NORSAR processing can be achieved by combining NORSAR and NORESS. By a simple masking algorithm, most of the NORSAR detected local and regional events can be identified as such using NORESS data. Furthermore, NORESS complements NORSAR by giving an "independent" confirmation of the majority of teleseismic phases. Even further improvements might be possible by joint beamforming techniques, although this has not been attempted in this study.

Section 7.4 contains a study undertaken in cooperation with the Norwegian Institute of International Affairs, and addressing satellite imagery in connection with the Novaya Zemlya northern nuclear test site.

Using Landsat TM images, one craterlike feature was found close to the southwestern mountain slopes of the Matochkin Shar Strait. SPOT panchromatic 10 m resolution

images were purchased, and these revealed three features, most probably craters that were created by underground nuclear explosions. This was unexpectedly confirmed when German aerial photographs of the Matochkin Shar from the summer of 1942 became available. The craters did not show up on these and thus proved that they were formed sometime after 1942.

Three digital SPOT scenes of the Novaya Zemlya northern underground nuclear test site were purchased. The pixel and line coordinates of the crater centers were measured for each of the SPOT scenes. The three separate sets of measurements were combined with their associated ancillary SPOT data. The preliminary results of geographical coordinate determination using this method are presented.

Section 7.5 describes a study of mislocation vectors. To improve the location capabilities of the small aperture arrays (Apatity, ARCESS, FINESS, GERESS, NORESS and Spitsbergen), we compared the results of the automatic fk-analysis (i.e., slowness and azimuth) with theoretically accepted values.

In a first step, we compiled a data base for the time period from 1989 to June 30, 1994, of 157,825 reference events distributed world-wide. The following sources for reference events were used: bulletins of the ISC and NEIC (monthly and weekly), regional bulletins of the seismological institutes in Bergen and in Helsinki, a special bulletin for the Vogtland earthquake swarm region, listings of well-located mining-induced events in Poland, and confirmed quarry blasts in Russia (Kola Peninsula), the Czech Republic and in southern Germany.

For all reference events, theoretical azimuth and slowness values and onset times were calculated using the IASPEI91 tables. All theoretical onsets of local and regional P and S phases and of all teleseismic P-phases were compared with detections and results of the automatic fk-analysis of all arrays.

After carefully checking associations between theoretically expected and observed onsets, 91,290 mislocation vectors could be estimated (Apatity 1,882; ARCESS 29,738; FINESS 15,482; GERESS 17,852; NORESS 26,083; and Spitsbergen 253). Although a large scatter was observed for single mislocations, mean mislocation vectors could be defined and estimated with their standard deviations for all arrays. The mean mislocation vectors can now be used regularly to correct automatically estimated slowness and azimuth values. The corrections and the mean standard deviations of slowness and azimuth will improve the accuracy of event locations from single arrays, GBF and IMS.

Section 7.6 is a follow-up of previous studies of the promising automatic post-processing technique for extremely precise event location in mining regions (exemplified by the Khibiny Massif in the Kola Peninsula). The contribution is directed in particular toward comparing the error ellipses of various approaches, and relating the size of these ellipses to the actual location errors, using a ground-truth data base obtained from the Kola Regional Seismological Centre. The error ellipses are found to be representative both for interactive IMS processing and automatic post-processing, but not in the case of automatic IMS analysis. The main reason in the latter case seems to be that the formal calculation of error ellipses does not take into account effects of occasional erroneous phase identification.

AFTAC Project Authorization : T/9141/B/PKP
ARPA Order No. : 4138 AMD # 16
Program Code No. : 0F10
Name of Contractor : Royal Norwegian Council for Scientific and
Industrial Research (NTNF)
Effective Date of Contract : 1 Oct 1988
Contract Expiration Date : 30 Sep 1994
Project Manager : Frode Ringdal (06) 81 71 21
Title of Work : The Norwegian Seismic Array
(NORSAR) Phase 3
Amount of Contract : \$ 13,052,032
Contract Period Covered by Report : 1 April - 30 September 94

The views and conclusions contained in this document are those of the authors and should not be interpreted as necessarily representing the official policies, either expressed or implied, of the Advanced Research Projects Agency, the Air Force Technical Applications Center or the U.S. Government.

This research was supported by the Advanced Research Projects Agency of the Department of Defense and was monitored by AFTAC, Patrick AFB, FL32925, under contract no. F08606-89-C-0005 and F08650-93-C-0002.

NORSAR Contribution No. 536



Table of Contents

	<u>Page</u>
1. Summary	1
2. NORSAR Operation	4
2.1 Detection processor (DP) operation	4
2.2 Array communications	8
2.3 NORSAR event detection operation	15
3. Operation of Regional Arrays	20
3.1 Recording of NORESS data at NDPC, Kjeller	20
3.2 Recording of ARCESS data at NDPC, Kjeller	24
3.3 Recording of FINESS data at NDPC, Kjeller	27
3.4 Recording of Spitsbergen data at NDPC, Kjeller	30
3.5 Event detection operation	34
3.6 IMS operation	61
4. Improvements and Modifications	63
4.1 NORSAR	63
4.2 Regional arrays	64
5. Maintenance Activities	65
6. Documentation Developed	68
7. Summary of Technical Reports / Papers Published	69
7.1 A system for continuous global seismic threshold monitoring	69
7.2 The Lop Nor nuclear explosions of 10 June and 7 October 1994	79
7.3 Combining NORSAR and NORESS processing	91
7.4 Epicenter location and cratering at the Novaya Zemlya underground nuclear test site	96
7.5 Mislocation vectors for small aperture arrays -- a first step towards calibrating GSETT-3 stations	104
7.6 On the reliability of event location estimates from automatic and interactive processing	119

Vertical text or markings along the right edge of the page, possibly bleed-through or a margin.

1 Summary

This Semiannual Technical Summary describes the operation, maintenance and research activities at the Norwegian Seismic Array (NORSAR), the Norwegian Regional Seismic Array (NORESS), the Arctic Regional Seismic Array (ARCESS) and the experimental Spitsbergen regional array for the period 1 April - 30 September 1994. Statistics are also presented for additional seismic stations, which through cooperative agreements with institutions in the host countries provide continuous data to the NORSAR Data Processing Center (NPDC). These stations comprise the Finnish Experimental Seismic Array (FINESS), the German Experimental Seismic Array (GERESS), and an experimental regional seismic array in Apatity, Russia.

This Semiannual Report also presents statistics from operation of the Intelligent Monitoring System (IMS). The IMS has been operated in an experimental mode, with continuous automatic detection and location and with analyst review of selected events of interest. Since October 1991, a new version of the IMS that accepts data from an arbitrary number of arrays and single 3-component stations has been operated.

The NORSAR Detection Processing system has been operated throughout the period with an average uptime of 99.3% as compared to 98.3% for the previous reporting period. A total of 2015 seismic events have been reported in the NORSAR monthly seismic bulletin. The performance of the continuous alarm system and the automatic bulletin transfer by telex to AFTAC has been satisfactory. The system for direct retrieval of NORSAR waveform data through an X.25 connection has been used successfully for acquiring such data by AFTAC. Processing of requests for full NORSAR and regional array data on magnetic tapes has progressed according to established schedules.

Since 1 October 1991, an effort has been undertaken to carry out a complete technical refurbishment of the NORSAR array. This project is funded jointly by AFTAC, ARPA and NFR. During the reporting period, all the new Science Horizons data acquisition hardware and software have been acquired and delivered. See NORSAR Sci. Rep. No. 2-93/94 for a system description. The data acquisition software XAVE and communication interface module CIM II were installed on 5 October 1994 at NDPC. At subarray 06C, a CIM II was installed in the Central Terminal Vault -- CTV -- and an AIM24-1 has been installed in one remote SP vault (SPV) for testing purposes. The data acquisition is running satisfactorily. Contractual arrangements for the delivery of "posthole" KS54000 seismometers have been completed.

As an intermediate step in the NORSAR Refurbishment, a modified version of the NORSAR data acquisition system was implemented on 1 January 1994. This modified version has continued to be in operation during the reporting period. The main reason for this change, which utilizes a previously established backup solution, was to circumvent some data timing problems due to deteriorating hardware. At the same time, this change has provided valuable experience in preparing the full refurbishment.

On-line detection processing and data recording at the NORSAR Data Processing Center (NDPC) of NORESS, ARCESS, FINESS and GERESS data have been conducted throughout the period. Data from two experimental small-aperture arrays at sites in Spitsbergen and Apatity, Kola Peninsula, have been recorded and processed in an experimental mode. Monthly processing statistics for the arrays as well as results of the IMS analysis for the reporting period are given.

Maintenance activities in the period comprise preventive/corrective maintenance in connection with all the NORSAR subarrays, NORESS and ARCESS. Other activities have involved testing of the NORSAR communications systems, preparations for the NORSAR refurbishment and work in connection with the experimental small-aperture arrays in Spitsbergen and Russia.

Summaries of six scientific contributions are presented in Chapter 7 of this report.

Section 7.1 is a final report on the global continuous Threshold Monitoring project, which is an effort to develop and implement a prototype, workstation-based Threshold Monitoring System for the GSETT-3 International Data Center (IDC). The main focus of this work has been to develop an environment that facilitates both real-time operation as well as testing of new ideas in the context of continuous seismic threshold monitoring. The current operational system is not fully optimized with respect to processing parameters, but the framework for a stepwise improvement exists. We can as of today demonstrate the potentials of using continuous seismic threshold monitoring as part of a global seismic verification system, but some caution has to be taken during the interpretation of the derived magnitude thresholds. Further improvements will rely heavily on the possibility of conducting extensive event analysis and associated calibration efforts.

Section 7.2 presents observations of the Lop Nor nuclear explosions of 10 June and 7 October 1994. Some comparisons are also made with the Lop Nor explosions conducted on 21 May 1992 and 5 October 1993. Most of the automatic systems at NORSAR showed good performance for these events. Particularly impressive is the high signal-to-noise ratios observed at NORESS and ARCESS. Among the available sources, the most accurate location is provided by the PDE bulletin, which uses a world-wide network for location purposes. The solutions by the Intelligent Monitoring System (IMS), both automatic and after analyst processing, are also quite satisfactory. The NORSAR automatic location was acceptable for only one of the two events, but reruns gave adequate results for both.

Section 7.3 describes the results of a study to investigate the benefits of NORSAR-NORESS joint processing. As is well known, the teleseismic NORSAR array and the regional NORESS array have to some extent overlapping capabilities as far as seismic event detection is concerned. However, when it comes to locating events, the two arrays are complementary. NORSAR has a superior location capability for teleseismic events, whereas NORESS is superior for locating local and regional events. Furthermore, NORESS has the ability to unambiguously classify an event as "regional" or "local", whereas NORSAR will usually assign a teleseismic location estimate (the "best beam") to any event, whether it is of local, regional or teleseismic origin.

The study has shown that a clear improvement in the automatic NORSAR processing can be achieved by combining NORSAR and NORESS. By a simple masking algorithm, most of the NORSAR detected local and regional events can be identified as such using NORESS data. Furthermore, NORESS complements NORSAR by giving an "independent" confirmation of the majority of teleseismic phases. Even further improvements might be possible by joint beamforming techniques, although this has not been attempted in this study.

Section 7.4 contains a study undertaken in cooperation with the Norwegian Institute of International Affairs, and addressing satellite imagery in connection with the Novaya Zemlya northern nuclear test site.

Using Landsat TM images, one craterlike feature was found close to the southwestern mountain slopes of the Matochkin Shar Strait. SPOT panchromatic 10 m resolution images were purchased, and these revealed three features, most probably craters that were created by underground nuclear explosions. This was unexpectedly confirmed when German aerial photographs of the Matochkin Shar from the summer of 1942 became available. The craters did not show up on these and thus proved that they were formed sometime after 1942.

Three digital SPOT scenes of the Novaya Zemlya northern underground nuclear test site were purchased. The pixel and line coordinates of the crater centers were measured for each of the SPOT scenes. The three separate sets of measurements were combined with their associated ancillary SPOT data. The preliminary results of geographical coordinate determination using this method are presented.

Section 7.5 describes a study of mislocation vectors. To improve the location capabilities of the small aperture arrays (Apatity, ARCESS, FINESS, GERESS, NORESS and Spitsbergen), we compared the results of the automatic fk-analysis (i.e., slowness and azimuth) with theoretically accepted values.

In a first step, we compiled a data base for the time period from 1989 to June 30, 1994, of 157,825 reference events distributed world-wide. The following sources for reference events were used: bulletins of the ISC and NEIC (monthly and weekly), regional bulletins of the seismological institutes in Bergen and in Helsinki, a special bulletin for the Vogtland earthquake swarm region, listings of well-located mining-induced events in Poland, and confirmed quarry blasts in Russia (Kola Peninsula), the Czech Republic and in southern Germany.

For all reference events, theoretical azimuth and slowness values and onset times were calculated using the IASPEI91 tables. All theoretical onsets of local and regional P and S phases and of all teleseismic P-phases were compared with detections and results of the automatic fk-analysis of all arrays.

After carefully checking associations between theoretically expected and observed onsets, 91,290 mislocation vectors could be estimated (Apatity 1,882; ARCESS 29,738; FINESS 15,482; GERESS 17,852; NORESS 26,083; and Spitsbergen 253). Although a large scatter was observed for single mislocations, mean mislocation vectors could be defined and estimated with their standard deviations for all arrays. The mean mislocation vectors can now be used regularly to correct automatically estimated slowness and azimuth values. The corrections and the mean standard deviations of slowness and azimuth will improve the accuracy of event locations from single arrays, GBF and IMS.

Section 7.6 is a follow-up of previous studies of the promising automatic post-processing technique for extremely precise event location in mining regions (exemplified by the Khibiny Massif in the Kola Peninsula). The contribution is directed in particular toward comparing the error ellipses of various approaches, and relating the size of these ellipses to the actual location errors, using a ground-truth data base obtained from the Kola Regional Seismological Centre. The error ellipses are found to be representative both for interactive IMS processing and automatic post-processing, but not in the case of automatic IMS analysis. The main reason in the latter case seems to be that the formal calculation of error ellipses does not take into account effects of occasional erroneous phase identification.

2 NORSAR Operation

2.1 Detection Processor (DP) operation

There have been 82 breaks in the otherwise continuous operation of the NORSAR online system within the current 6-month reporting interval. The uptime percentage for the period is 99.3 as compared to 98.3 for the previous period.

Fig. 2.1.1 and the accompanying Table 2.1.1 both show the daily DP downtime for the days between 1 April and 30 September 1994. The monthly recording times and percentages are given in Table 2.1.2.

The breaks can be grouped as follows:

a)	Hardware failure	8
b)	Stops related to program work or error	0
c)	Hardware maintenance stops	0
d)	Power jumps and breaks	0
e)	TOD error correction	0
f)	Communication lines	2

The total downtime for the period was 32 hours and 52 minutes. The mean-time-between-failures (MTBF) was 16.4 days, as compared to 1.4 for the previous period.

J. Torstveit

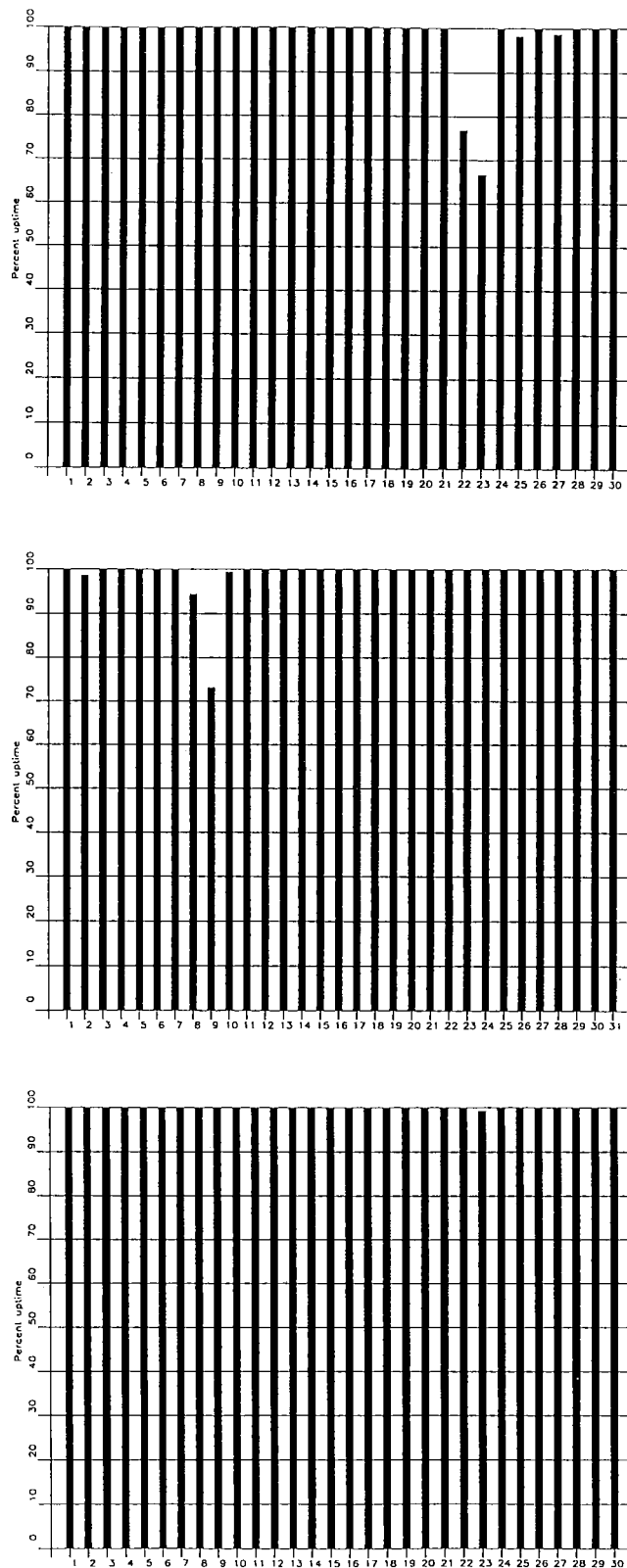


Fig. 2.1.1. Detection Processor uptime for April (top), May (middle) and June (bottom) 1994.

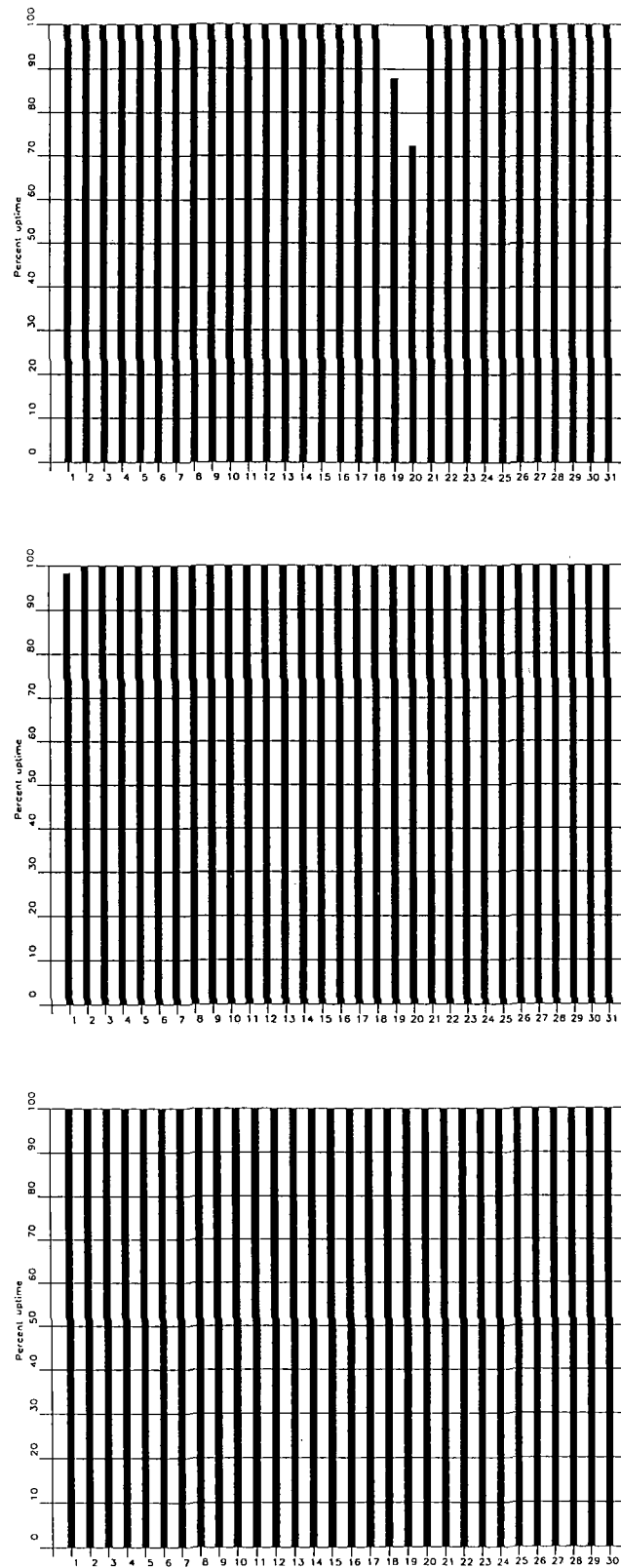


Fig. 2.1.1. Detection Processor uptime for July (top), August (middle) and September (bottom) 1994.

Date	Time	Cause
22 Apr	1827 -	Hardware failure
23 Apr	- 0801	
25 Apr	0803 - 0828	Hardware failure
27 Apr	1051 - 1110	Hardware failure
02 May	0735 - 0750	Hardware failure
02 May	1154 - 1159	Hardware failure
08 May	2239 -	Hardware failure
09 May	- 0627	
10 May	0921 - 0930	Hardware failure
23 Jun	0531 - 0542	Line failure
19 Jul	2106 -	Hardware failure
20 Jul	- 0635	
01 Aug	0948 - 1012	Line failure

Table 2.1.1. The major downtimes in the period 1 April - 30 September 1994.

Month	DP Uptime Hours	DP Uptime %	No. of DP Breaks	No. of Days with Breaks	DP MTBF* (days)
Apr 94	705.67	98.01	3	3	7.4
May 94	731.71	98.88	4	3	6.1
Jun 94	719.78	99.97	1	1	15.0
Jul 94	730.53	98.72	1	1	15.5
Aug 94	739.56	99.94	1	1	15.5
Sep 94	719.93	99.99	0	0	30.0
		99.25	98	63	16.1

*Mean-time-between-failures = total uptime/no. of up intervals.

Table 2.1.2. Online system performance, 1 April - 30 September 1994.

2.2 Array Communications

As described in the previous Semiannual Report, the Modcomp/SLEM-based communication system experienced serious problems toward the end of 1993.

As an intermediate solution, it was decided on 1 January 1994 to implement a backup version of the NORSAR recording system, thus eliminating the Modcomp/SLEM-based recording. This change succeeded in improving both the timing reliability and the individual subarray uptimes.

During the reporting period, the communication lines to all subarrays except 02B and 06C were in operation essentially 100% of the time. Subarrays 02B and 06C were inoperative during the last part of the reporting period in connection with testing and preparation for the NORSAR refurbishment.

The intermediate communication solution will remain in effect until the NORSAR Refurbishment project is completed.

A simplified daily summary of the communications performance for the seven individual subarray lines is summarized, on a month-by-month basis, in Table 2.2.1.

F. Ringdal

Table 2.2.1 (page 1 of 6)
NORSAR Communication Status Report
Month: April 1994

Day	Subarray						
	01A	01B	02B	02C	03C	04C	06C
01	X	X	X	X	X	X	X
02	X	X	X	X	X	X	X
03	X	X	X	X	X	X	X
04	X	X	X	X	X	X	X
05	X	X	X	X	X	X	X
06	X	X	X	X	X	X	X
07	X	X	X	X	X	X	X
08	X	X	X	X	X	X	X
09	X	X	X	X	X	X	X
10	X	X	X	X	X	X	X
11	X	X	I	X	X	X	X
12	X	X	I	X	X	I	X
13	X	X	I	X	X	I	X
14	X	X	I	X	X	I	X
15	X	X	I	X	X	I	X
16	X	X	I	X	X	I	X
17	X	X	I	X	X	I	X
18	X	X	I	X	X	I	X
19	X	X	I	X	X	I	X
20	X	X	I	X	X	X	X
21	X	X	I	X	X	X	X
22	X	X	I	X	X	X	X
23	X	X	X	X	X	X	X
24	X	X	X	X	X	X	X
25	X	X	X	X	X	X	X
26	X	X	X	X	X	X	X
27	X	X	X	X	X	X	X
28	X	X	X	X	X	X	X
29	X	X	X	X	X	X	X
30	X	X	X	X	X	X	X
31	X	X	X	X	X	X	X
Total hours normal operation	720	7200	443	720	720	553	720
% normal operation	100.3	1000	61.5	100	100	76.8	100

Legend :

- X : Normal operations
A : All channels masked for more than 12 hours that day
B : All SP channels masked for more than 12 hours that day
C : All LP channels masked for more than 12 hours that day
I : Communication outage for more than 12 hours

Table 2.2.1 (page 2 of 6)
NORSAR Communication Status Report
Month: May 1994

Day	Subarray						
	01A	01B	02B	02C	03C	04C	06C
01	X	X	X	X	X	X	X
02	X	X	X	X	X	X	X
03	X	X	X	X	X	X	X
04	X	X	X	X	X	X	X
05	X	X	X	X	X	X	X
06	X	X	X	X	X	X	X
07	X	X	X	X	X	X	X
08	X	X	X	X	X	X	X
09	X	X	X	X	X	X	X
10	X	X	X	X	X	X	X
11	X	X	X	X	X	X	X
12	X	X	X	X	X	X	X
13	X	X	X	X	X	X	X
14	X	X	X	X	X	X	X
15	X	X	X	X	X	X	X
16	X	X	X	X	X	X	X
17	X	X	X	X	X	X	X
18	X	X	X	X	X	X	X
19	X	X	X	X	X	X	X
20	X	X	X	X	X	X	X
21	X	X	X	X	X	X	X
22	X	X	X	X	X	X	X
23	X	X	X	X	X	X	X
24	X	X	X	X	X	X	X
25	X	X	X	X	X	X	X
26	X	X	X	X	X	X	X
27	X	X	X	X	X	X	X
28	X	X	X	X	X	X	X
29	X	X	X	X	X	X	X
30	X	X	X	X	X	X	X
31	X	X	X	X	X	X	X
Total hours normal operation	744	744	744	744	744	744	744
% normal operation	100	100	100	100	100	100	100

Legend :

- X : Normal operations
- A : All channels masked for more than 12 hours that day
- B : All SP channels masked for more than 12 hours that day
- C : All LP channels masked for more than 12 hours that day
- I : Communication outage for more than 12 hours

Table 2.2.1 (page 3 of 6)
NORSAR Communication Status Report
Month: June 1994

Day	Subarray						
	01A	01B	02B	02C	03C	04C	06C
01	X	X	X	X	X	X	X
02	X	X	X	X	X	X	X
03	X	X	X	X	X	X	X
04	X	X	X	X	X	X	X
05	X	X	X	X	X	X	X
06	X	X	X	X	X	X	X
07	X	X	X	X	X	X	X
08	X	X	X	X	X	X	X
09	X	X	X	X	X	X	X
10	X	X	X	X	X	X	X
11	X	X	X	X	X	X	X
12	X	X	X	X	X	X	X
13	X	X	X	X	X	X	X
14	X	X	X	X	X	X	X
15	X	X	X	X	X	X	X
16	X	X	X	X	X	X	X
17	X	X	X	X	X	X	X
18	X	X	X	X	X	X	X
19	X	X	X	X	X	X	X
20	X	X	X	X	X	X	X
21	X	X	X	X	X	X	X
22	X	X	X	X	X	X	X
23	X	X	X	X	X	X	X
24	X	X	X	X	X	X	X
25	X	X	X	X	X	X	X
26	X	X	X	X	X	X	X
27	X	X	X	X	X	X	X
28	X	X	X	X	X	X	X
29	X	X	X	X	X	X	X
30	X	X	X	X	X	X	X
31							
Total hours normal operation	720	720	720	720	720	720	720
% normal operation	100	100	100	100	100	100	100

Legend :

- X : Normal operations
- A : All channels masked for more than 12 hours that day
- B : All SP channels masked for more than 12 hours that day
- C : All LP channels masked for more than 12 hours that day
- I : Communication outage for more than 12 hours

Table 2.2.1 (page 4 of 6)
NORSAR Communication Status Report
Month: July 1994

Day	Subarray						
	01A	01B	02B	02C	03C	04C	06C
01	X	X	X	X	X	X	A
02	X	X	X	X	X	X	A
03	X	X	X	X	X	X	A
04	X	X	X	X	X	X	A
05	X	X	X	X	X	X	A
06	X	X	X	X	X	X	A
07	X	X	A	X	X	X	A
08	X	X	A	X	X	X	A
09	X	X	A	X	X	X	A
10	X	X	A	X	X	X	A
11	X	X	A	X	X	X	A
12	X	X	A	X	X	X	A
13	X	X	A	X	X	X	A
14	X	X	A	X	X	X	A
15	X	X	A	X	X	X	A
16	X	X	A	X	X	X	A
17	X	X	A	X	X	X	A
18	X	X	A	X	X	X	A
19	X	X	A	X	X	X	A
20	X	X	A	X	X	X	A
21	X	X	A	X	X	X	A
22	X	X	A	X	X	X	A
23	X	X	A	X	X	X	A
24	X	X	A	X	X	X	A
25	X	X	X	X	X	X	A
26	X	X	X	X	X	X	A
27	X	X	X	X	X	X	A
28	X	X	X	X	X	X	A
29	X	X	X	X	X	X	A
30	X	X	X	X	X	X	A
31	X	X	X	X	X	X	A
Total hours normal operation	744	744	290	744	744	744	0
% normal operation	100	100	39	100	100	100	0

Legend :

- X : Normal operations
- A : All channels masked for more than 12 hours that day
- B : All SP channels masked for more than 12 hours that day
- C : All LP channels masked for more than 12 hours that day
- I : Communication outage for more than 12 hours

Table 2.2.1 (page 5 of 6)
NORSAR Communication Status Report
Month: August 1994

Day	Subarray						
	01A	01B	02B	02C	03C	04C	06C
01	X	X	X	X	X	X	A
02	X	X	X	X	X	X	A
03	X	X	X	X	X	X	A
04	X	X	X	X	X	X	A
05	X	X	X	X	X	X	A
06	X	X	A	X	X	X	A
07	X	X	A	X	X	X	A
08	X	X	A	X	X	X	A
09	X	X	A	X	X	X	A
10	X	X	A	X	X	X	A
11	X	X	A	X	X	X	A
12	X	X	A	X	X	X	A
13	X	X	A	X	X	X	A
14	X	X	A	X	X	X	A
15	X	X	A	X	X	X	A
16	X	X	A	X	X	X	A
17	X	X	A	X	X	X	A
18	X	X	A	X	X	X	A
19	X	X	A	X	X	X	A
20	X	X	A	X	X	X	A
21	X	X	A	X	X	X	A
22	X	X	A	X	X	X	A
23	X	X	A	X	X	X	A
24	X	X	A	X	X	X	A
25	X	X	A	X	X	X	A
26	X	X	A	X	X	X	A
27	X	X	A	X	X	X	A
28	X	X	A	X	X	X	A
29	X	X	A	X	X	X	A
30	X	X	A	X	X	X	A
31	X	X	A	X	X	X	A
Total hours normal operation	744	744	132	744	744	744	0
% normal operation	100	71	18	100	100	100	0

Table 2.2.1 (page 6 of 6)
NORSAR Communication Status Report
Month: September 1994

Day	Subarray						
	01A	01B	02B	02C	03C	04C	06C
01	X	X	A	X	X	X	A
02	X	X	A	X	X	X	A
03	X	X	A	X	X	X	A
04	X	X	A	X	X	X	A
05	X	X	A	X	X	X	A
06	X	X	A	X	X	X	A
07	X	X	A	X	X	X	A
08	X	X	A	X	X	X	A
09	X	X	A	X	X	X	A
10	X	X	A	X	X	X	A
11	X	X	A	X	X	X	A
12	X	X	A	X	X	X	A
13	X	X	A	X	X	X	A
14	X	X	A	X	X	X	A
15	X	X	A	X	X	X	A
16	X	X	A	X	X	X	A
17	X	X	A	X	X	X	A
18	X	X	A	X	X	X	A
19	X	X	A	X	X	X	A
20	X	X	A	X	X	X	A
21	X	X	A	X	X	X	A
22	X	X	A	X	X	X	A
23	X	X	A	X	X	X	A
24	X	X	A	X	X	X	A
25	X	X	A	X	X	X	A
26	X	X	A	X	X	X	A
27	X	X	A	X	X	X	A
28	X	X	A	X	X	X	A
29	X	X	A	X	X	X	A
30	X	X	A	X	X	X	A
31							
Total hours normal operation	720	720	0	720	720	720	0
% normal operation	100	100	0	100	100	100	0

Legend :

- X : Normal operations
A : All channels masked for more than 12 hours that day
B : All SP channels masked for more than 12 hours that day
C : All LP channels masked for more than 12 hours that day
I : Communication outage for more than 12 hours

2.3 NORSAR Event Detection operation

In Table 2.3.1 some monthly statistics of the Detection and Event Processor operation are given. The table lists the total number of detections (DPX) triggered by the on-line detector, the total number of detections processed by the automatic event processor (EPX) and the total number of events accepted after analyst review (teleseismic phases, core phases and total).

	Total DPX	Total EPX	Accepted events		Sum	Daily
			P-phases	Core Phases		
Apr 94	9670	808	192	66	258	8.6
May 94	6227	751	314	56	370	11.9
Jun 94	8025	861	246	50	296	9.9
Jul 94	6734	1065	242	103	345	11.1
Aug 94	7990	1024	376	60	436	14.1
Sep 94	8970	884	262	48	310	10.3
			1632	383	2015	11.0

Table 2.3.1. Detection and Event Processor statistics, 1 April - 30 September 1994.

NORSAR Detections

The number of detections (phases) reported by the NORSAR detector during day 091, 1994, through day 273, 1994, was 46,071, giving an average of 252 detections per processed day (183 days processed). Table 2.3.2 shows daily and hourly distribution of detections for NORSAR.

B. Paulsen

Day	00	01	02	03	04	05	06	07	08	09	10	11	12	13	14	15	16	17	18	19	20	21	22	23	Sum	Date
259	20	13	23	15	9	10	18	12	5	13	11	6	14	8	13	10	12	11	10	14	9	11	12	15	294	Sep 16 Friday
260	12	18	25	22	14	20	15	20	12	17	14	12	8	17	13	13	23	13	17	16	8	15	27	15	386	Sep 17 Saturday
261	21	18	20	19	13	11	17	15	8	7	23	10	9	3	4	4	6	20	6	5	10	8	9	8	274	Sep 18 Sunday
262	7	8	6	10	3	4	4	9	2	3	2	15	5	4	16	18	1	5	12	19	14	25	16	16	224	Sep 19 Monday
263	25	13	14	14	14	9	8	7	12	7	2	20	2	7	16	7	7	4	4	15	17	11	12	10	257	Sep 20 Tuesday
264	6	10	17	11	7	3	5	2	11	6	15	13	9	6	18	9	4	9	12	15	13	14	22	21	258	Sep 21 Wednesday
265	16	30	23	21	18	23	11	15	6	8	5	18	11	14	13	8	16	13	20	25	20	18	12	24	388	Sep 22 Thursday
266	24	16	24	28	14	6	5	0	3	3	5	24	11	10	10	5	3	15	12	15	12	12	16	23	296	Sep 23 Friday
267	23	28	14	25	14	11	16	21	13	10	13	17	15	14	11	11	21	19	15	30	16	15	10	16	398	Sep 24 Saturday
268	19	18	14	17	17	16	14	18	13	13	9	13	13	6	9	12	9	11	12	14	11	15	14	13	320	Sep 25 Sunday
269	10	10	15	14	12	10	9	2	2	2	8	10	7	21	9	7	11	12	16	14	10	11	17	16	255	Sep 26 Monday
270	15	15	28	17	29	20	20	13	6	9	21	13	19	9	11	13	7	10	16	8	12	19	13	22	365	Sep 27 Tuesday
271	17	10	9	17	20	23	11	8	11	14	15	10	23	8	5	14	38	23	14	9	10	24	17	26	376	Sep 28 Wednesday
272	25	22	18	21	18	14	11	11	9	10	6	9	7	8	16	9	10	9	13	10	11	11	10	16	304	Sep 29 Thursday
273	12	10	17	21	19	10	8	11	4	5	11	8	18	10	8	8	18	14	28	31	21	15	21	21	349	Sep 30 Friday
NB2	00	01	02	03	04	05	06	07	08	09	10	11	12	13	14	15	16	17	18	19	20	21	22	23		
Sum	2281	2275	1577	1518	1748	2078	1867	1749	1783	1819	2156	2252														
	2271	2361	1982	1507	1386	1751	2053	1942	1807	1892	1879	2137	46071	Total sum												
183	12	12	13	12	11	9	8	8	8	10	10	11	11	10	11	10	10	10	10	10	10	12	12	12	252	Total average
126	13	12	13	12	10	7	6	7	6	9	9	11	11	10	10	8	9	9	10	9	9	12	11	12	235	Average workdays
57	12	14	13	13	13	13	12	12	10	11	11	11	10	10	12	12	12	10	11	11	12	12	13	13	283	Average weekends

Table 2.3.2. Daily and hourly distribution of NORSAR detections. For each day is shown number of detections within each hour of the day and number of detections for that day. The end statistics give total number of detections distributed for each hour and the total sum of detections during the period. The averages show number of processed days, hourly distribution and average per processed day. (Page 4 of 4)

3 Operation of Regional Arrays

3.1 Recording of NORESS data at NDPC, Kjeller

Table 3.1.1 lists the main outage times and reasons.

The average recording time was 94.37% as compared to 96.48% during the previous reporting period.

Date	Time	Cause
06 May	1518 -	Hardware failure
07 May	- 0843	
12 May	2007 -	Hardware failure
13 May	- 0629	
16 May	1459 -	Hardware failure
18 May	- 0602	
18 May	1125 - 1143	Hardware failure
22 May	0726 - 0956	Hardware failure
31 May	0237 - 0622	Hardware failure
31 May	0849 - 0904	Hardware failure
13 Jun	1316 - 1329	Hardware failure
27 Jun	1329 -	Continuous gaps of length from 1 sec to several minutes
29 Jun	- 1300	
08 Jul	0746 - 0902	Power failure due to thunderstorm
18 Jul	0501 - 0604	Hardware failure
26 Jul	1858 - 2047	Hardware failure
27 Jul	1342 - 1619	Power failure due to thunderstorm
27 Jul	2100 -	Power failure due to thunderstorm
29 Jul	- 0145	
10 Aug	0914 - 1047	Hardware maintenance
10 Aug	1109 - 1122	Hardware maintenance
02 Sep	1550 -	Hardware failure
05 Sep	- 0617	
22 Sep	0349 - 0620	Hardware failure
25 Sep	0100 - 0200	Software failure

Table 3.1.1. Interruptions in recording of NORESS data at NDPC, 1 April - 30 September 1994.

Monthly uptimes for the NORESS on-line data recording task, taking into account all factors (field installations, transmissions line, data center operation) affecting this task were as follows:

April 94	:	99.21
May	:	88.12
June	:	95.79
July	:	95.42
August	:	98.25
September	:	89.42

Fig. 3.1.1 shows the uptime for the data recording task, or equivalently, the availability of NORESS data in our tape archive, on a day-by-day basis, for the reporting period.

J. Torstveit

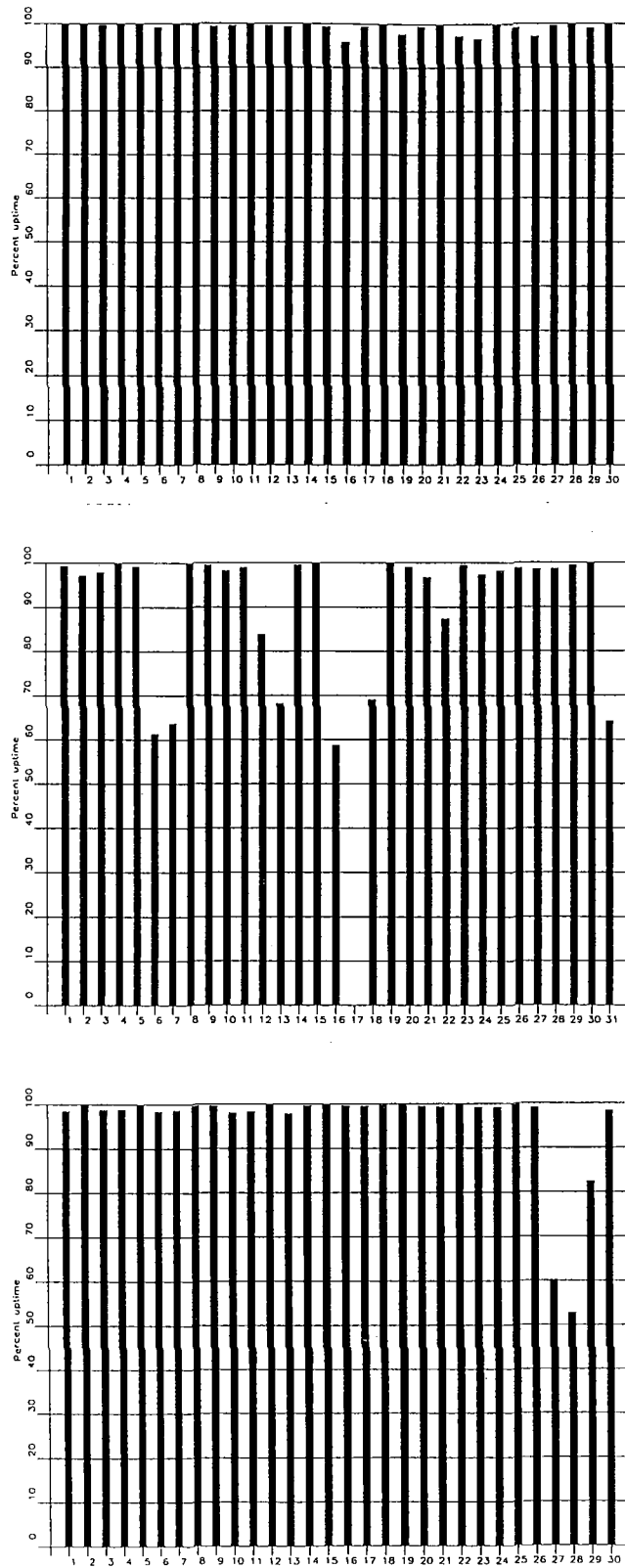


Fig. 3.1.1. NORESS data recording uptime for April (top), May (middle) and June (bottom) 1994.

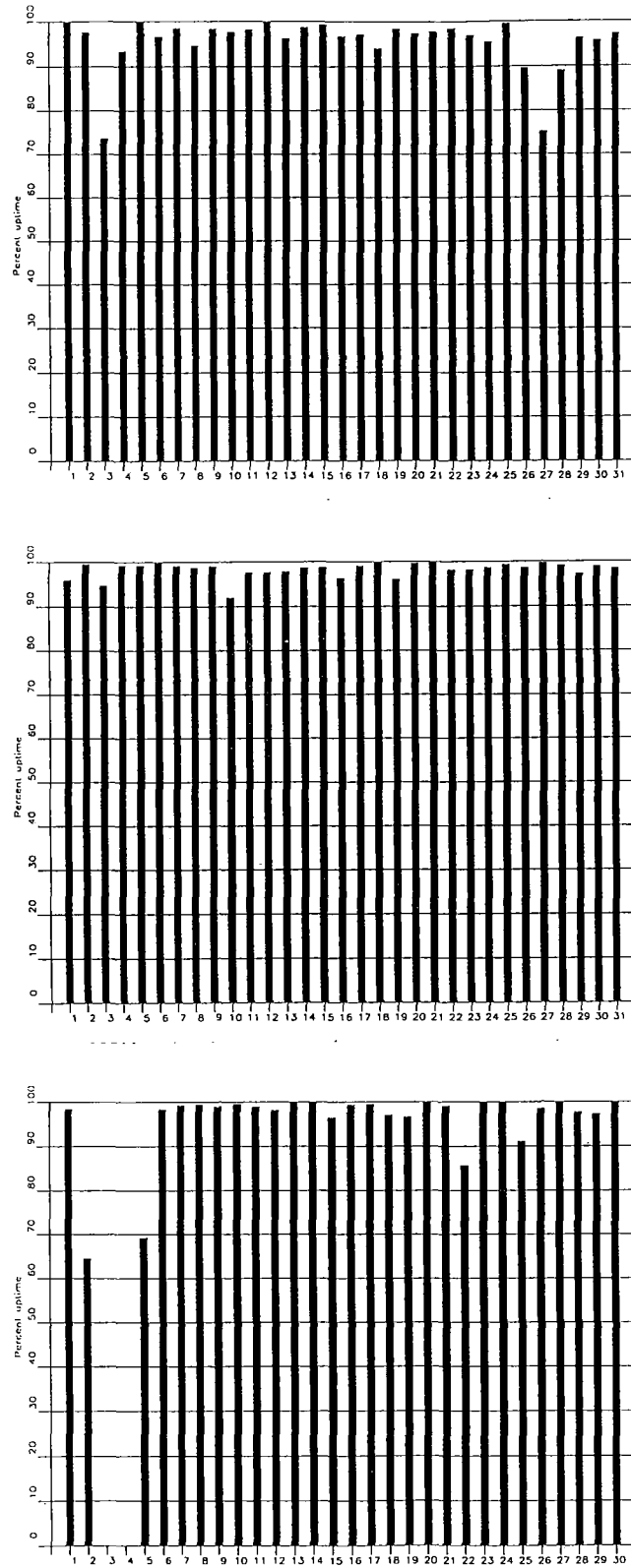


Fig. 3.1.1. (cont.) NORESS data recording uptime for July (top), August (middle) and September (bottom) 1994.

3.2 Recording of ARCESS data at NDPC, Kjeller

Table 3.2.1 lists the main outage times and reasons.

The average recording time was 99.28% as compared to 99.19% for the previous reporting period.

Date	Time	Cause
16 Jun	2239 -	Satellite link failure
17 Jun	- 0406	
07 Jul	0743 - 1446	Work on power line to Hub
10 Jul	0537 - 2202	Transmission line failure
13 Aug	1341 - 1450	Hardware failure
13 Aug	1504 - 1541	Hardware failure
23 Aug	0634 - 0919	Power failure Hub
28 Aug	1556 -	Hardware failure
29 Aug	- 0700	

Table 3.2.1. The main interruptions in recording of ARCESS data at NDPC, 1 April - 30 September 1994.

Monthly uptimes for the ARCESS on-line data recording task, taking into account all factors (field installations, transmissions line, data center operation) affecting this task were as follows:

April 94	:	100.00%
May	:	99.94%
June	:	99.23%
July	:	96.49%
August	:	98.72%
September	:	97.89%

Fig. 3.2.1. shows the uptime for the data recording task, or equivalently, the availability of ARCESS data in our tape archive, on a day-by-day basis, for the reporting period.

J. Torstveit

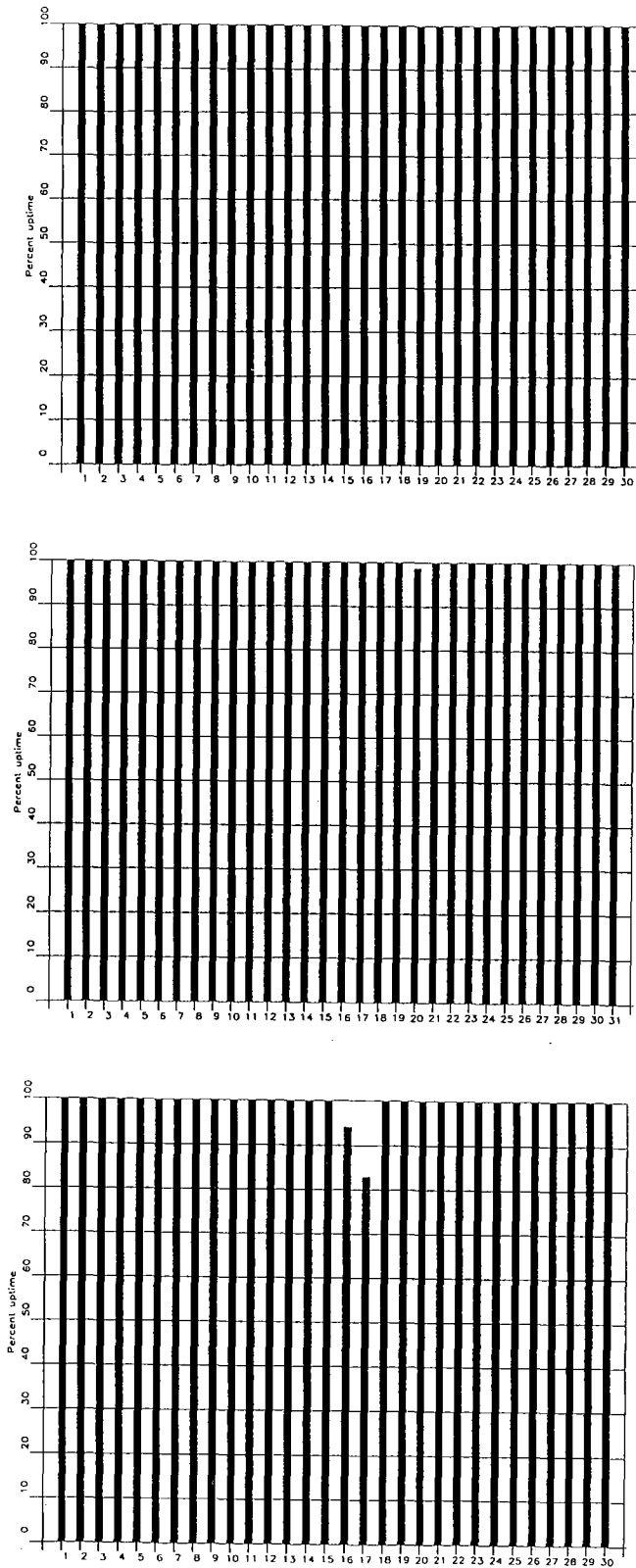


Fig. 3.2.1. ARCESS data recording uptime for April (top), May (middle) and June (bottom) 1994.

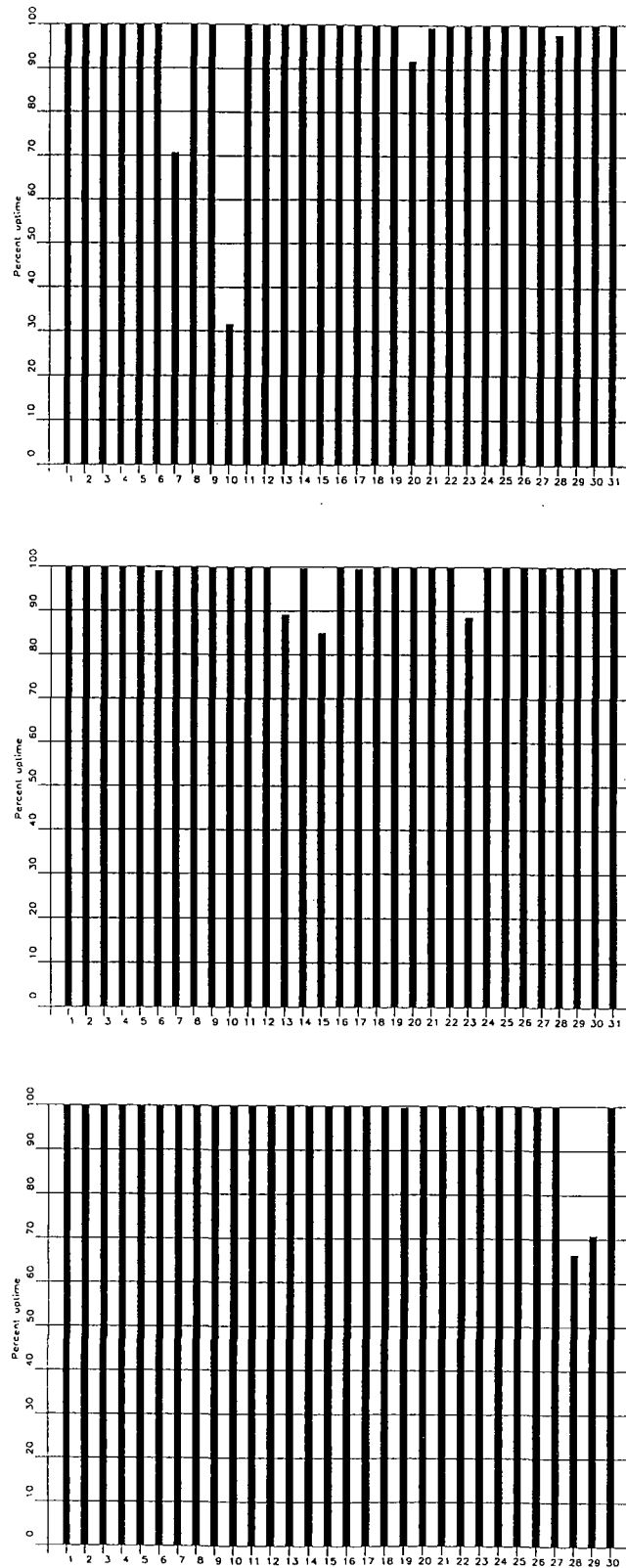


Fig. 3.2.1. ARCESS data recording uptime for July (top), August (middle) and September (bottom) 1994.

3.3 Recording of FINESS data at NDPC, Kjeller

The average recording time was 95.7%.

Date	Time	Cause
11 May	1916 - 2312	Transmission line failure
12 May	1450 - 2214	Transmission line failure
08 Jun	1306 -	Transmission line failure
09 Jun	- 0638	
21 Jul	0416 - 1022	Transmission line failure
12 Aug	1940 -	Transmission line failure
15 Aug	- 0632	
27 Aug	0459 -	Transmission line failure
29 Aug	- 0551	
30 Aug	1014 - 2017	Transmission line failure
09 Sep	0513 - 1012	Hub failure
16 Sep	1553 -	Problems in Finland
17 Sep	- 1300	

Table 3.3.1. The main interruptions in recording of FINESS data at NDPC, 1 April - 30 September 1994.

Monthly uptimes for the FINESS on-line data recording task, taking into account all factors (field installations, transmission lines, data center operation) affecting this task were as follows:

April 94	:	99.95%
May	:	98.44%
June	:	97.55%
July	:	99.17%
August	:	84.31%
September	:	96.40%

Fig. 3.3.1 shows the uptime for the data recording task, or equivalently, the availability of FINESS data in our tape archive, on a day-by-day basis, for the reporting period.

J. Torstveit

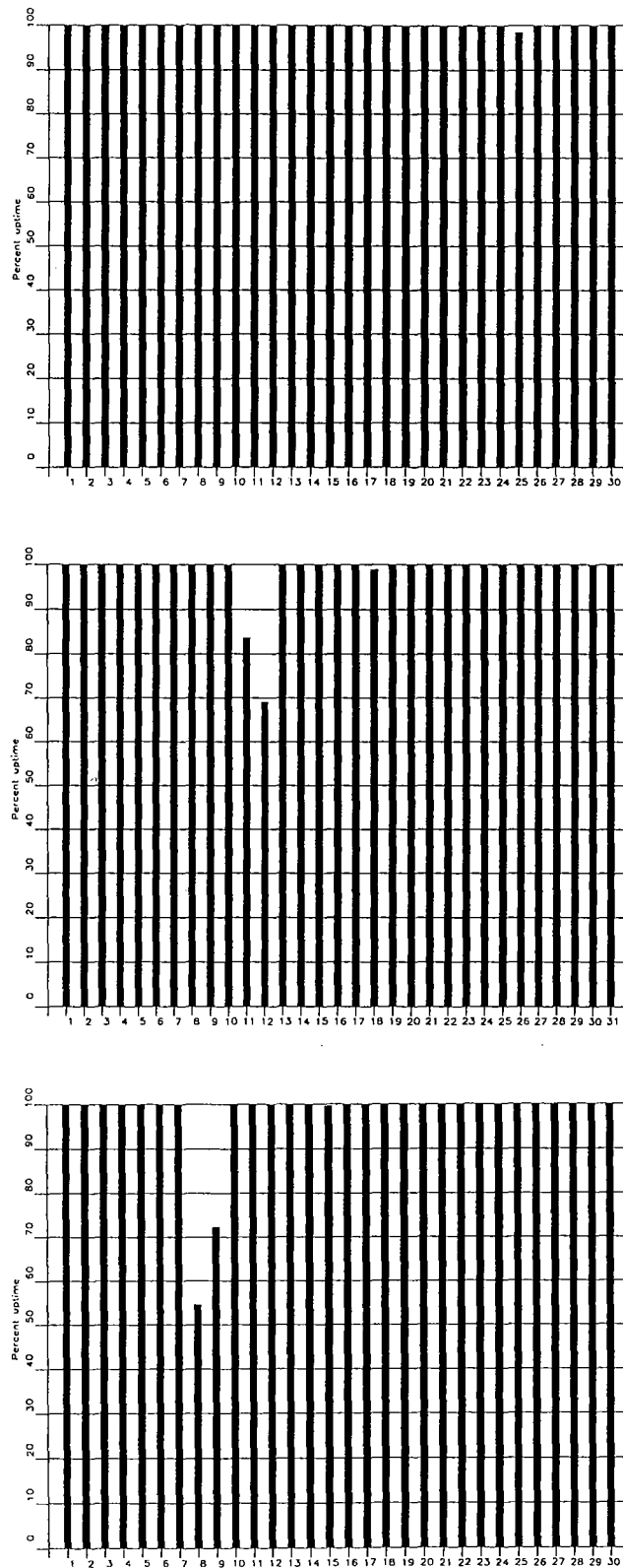


Fig. 3.3.1. FINESS data recording uptime for April (top), May (middle) and June (bottom) 1994.

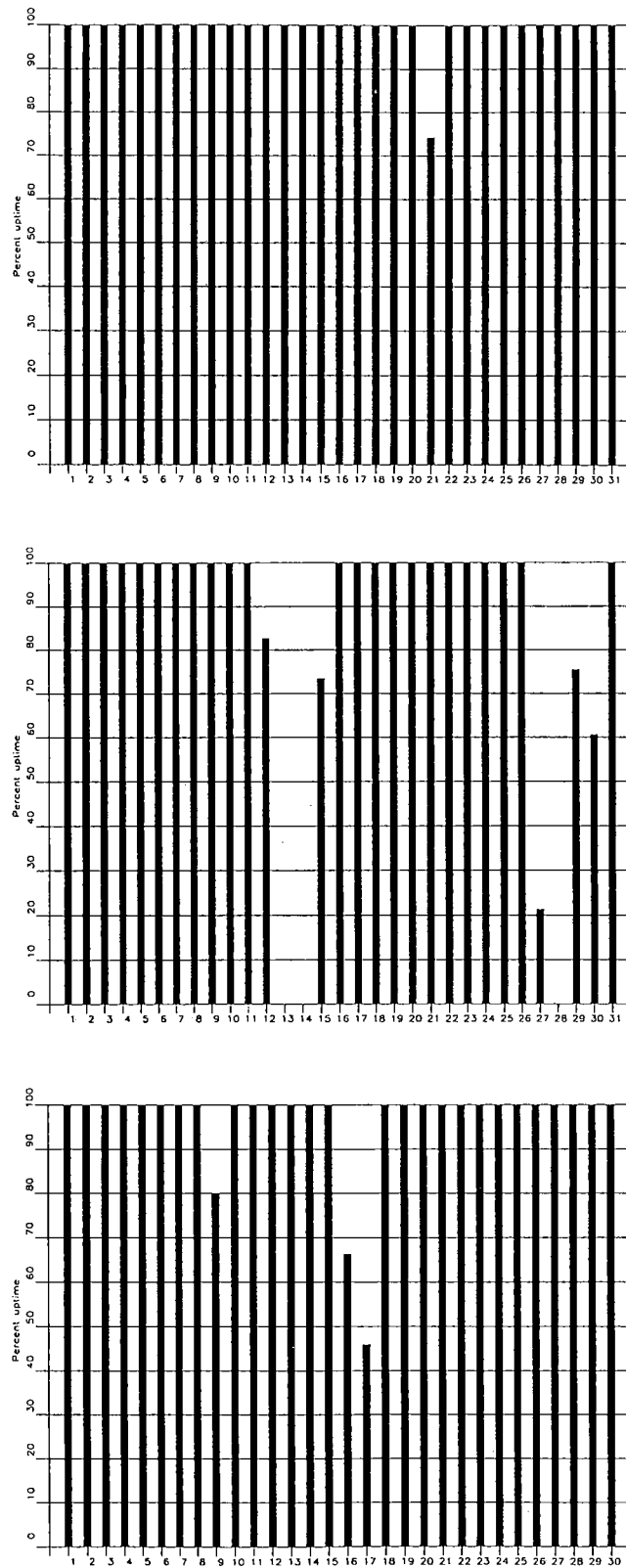


Fig. 3.3.1. FINESS data recording uptime for July (top), August (middle) and September (bottom) 1994.

3.4 Recording of Spitsbergen data at NDPC, Kjeller

The average recording time was 91.8% as compared to 88.39% for the previous reporting period.

The main reasons for downtime follow:

Date	Time	Cause
08 Apr	2216 - 2300	Communication line failure
09 Apr	0034 - 0134	Communication line failure
22 Apr	2217 - 2245	Communication line failure
29 Apr	0400 - 0432	Communication line failure
05 May	0849 - 1250	Radio link problems
07 Jun	0619 -	Communication line failure
10 Jun	- 0738	
04 Jul	1612 -	Communication line failure
05 Jul	- 0804	
08 Jul	1016 - 1322	Maintenance communication line
12 Jul	0913 - 1051	Communication line failure
20 Jul	1749 -	Communication line failure
21 Jul	- 1128	
02 Aug	1450 -	Communication line failure
03 Aug	- 0735	
13 Aug	1019 -	Maintenance communication line
15 Aug	- 0908	
22 Aug	1406 -	Maintenance and site construction work
26 Aug	- 1741	
26 Aug	2219 -	Maintenance and site construction work
28 Aug	- 2050	
29 Aug	0955 - 1833	Maintenance and site construction work
31 Aug	1625 - 2214	Maintenance and site construction work
01 Sep	0639 - 1001	Maintenance and site construction work
15 Sep	0056 - 0408	Communication line failure

Monthly uptimes for the Spitsbergen online data recording task, taking into account all factors (field installations, transmission line, data center operation) affecting this task were as follows:

April 94	:	99.51%
May	:	98.45%
June	:	89.81%
July	:	94.42%
August	:	69.48%
September	:	99.12%

Fig. 3.4.1 shows the uptime for the data recording task, or equivalently, the availability of Spitsbergen data in our tape archive, on a day-by-day basis for the reporting period.

J. Torstveit

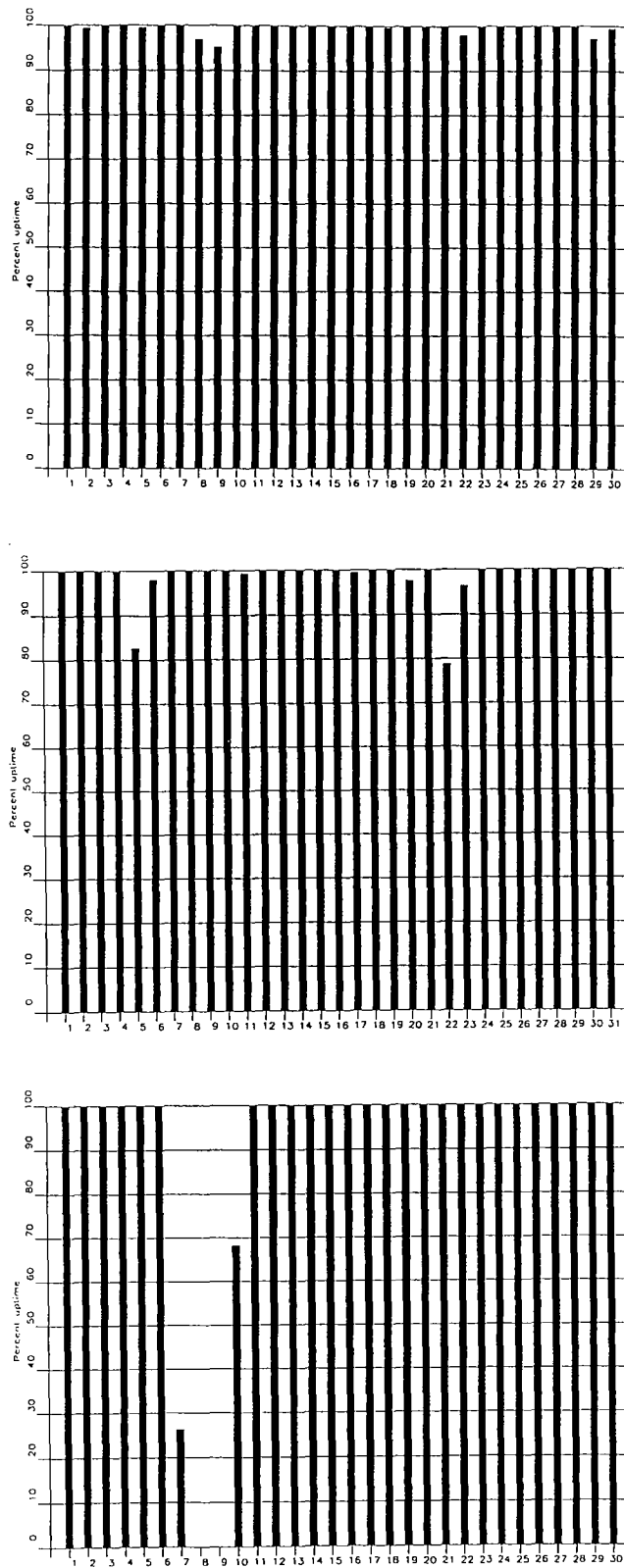


Fig. 3.4.1. Spitsbergen data recording uptime for April (top), May (middle) and June (bottom) 1994.

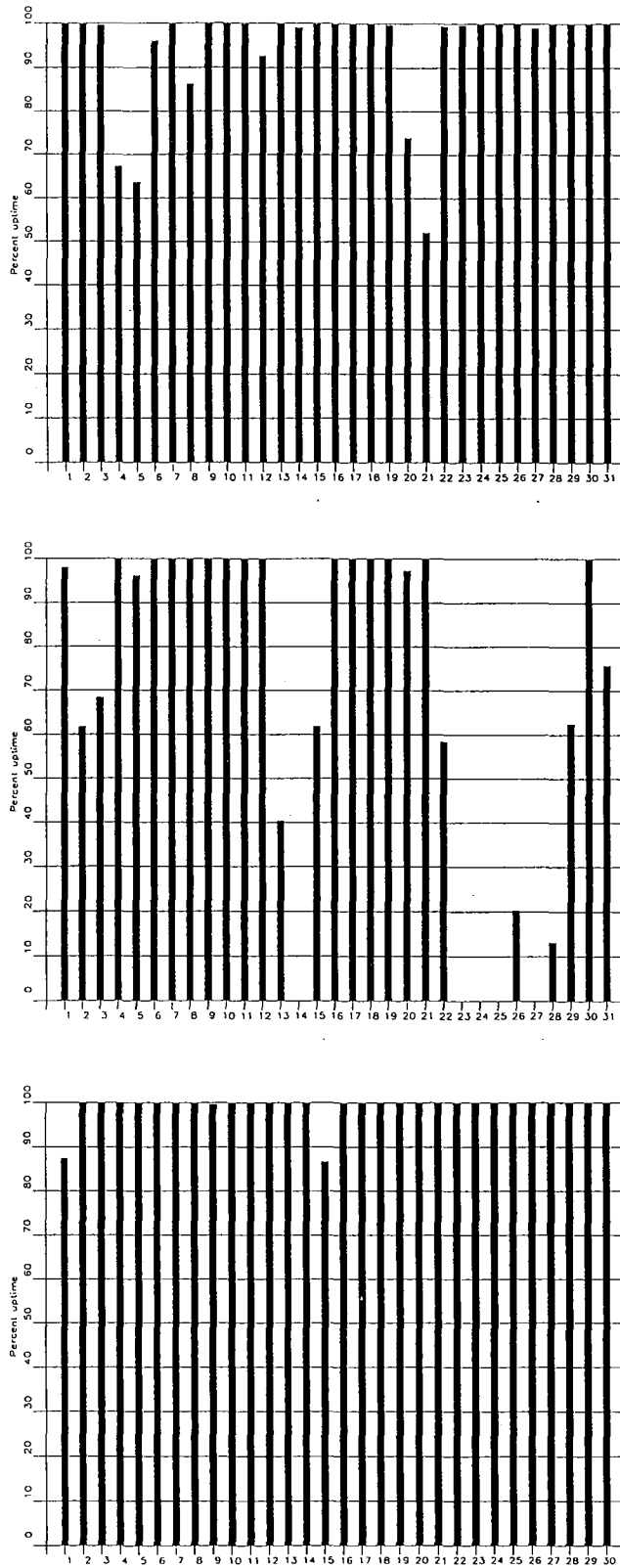


Fig. 3.4.1. Spitsbergen data recording uptime for July (top), August (middle) and September (bottom) 1994.

3.5 Event detection operation

This section reports results from one-array automatic processing using signal processing recipes and "ronapp" recipes for the ep program (NORSAR Sci. Rep. No 2-88/89).

Three systems are in parallel operation to associate detected phases and locate events:

1. The ep program with "ronapp" recipes is operated independently on each array to obtain simple one-array automatic solutions.
2. The Generalized Beamforming method (GBF) (see F. Ringdal and T. Kværna (1989), A multichannel processing approach to real time network detection, phase association and threshold monitoring, BSSA Vol 79, no 6, 1927-1940) processes the four arrays jointly and presents locations of regional events.
3. The IMS system is operated on the same set of arrivals as ep and GBF and reports also teleseismic events in addition to regional ones.

IMS results are reported in section 3.6.

In addition to these three event association processes, we are running test versions of the so-called Threshold Monitoring (TM) process. This is a process that monitors the seismic amplitude level at the four regional arrays continuously in time to estimate the upper magnitude limit of an event that might go undetected by the network. The current TM process is beamed to several sites of interest, including the Novaya Zemlya test site. Simple displays of so-called threshold curves reveal instants of particular interest; i.e., instants when events above a certain magnitude threshold may have occurred in the target region. Results from the three processes described above are used to help resolve what actually happened during these instances.

NORESS detections

The number of detections (phases) reported from day 091, 1994, through day 273, 1994, was 36,245, giving an average of 202 detections per processed day (179 days processed).

Table 3.5.1 shows daily and hourly distribution of detections for NORESS.

Events automatically located by NORESS

During days 091, 1994, through 273, 1994, 2267 local and regional events were located by NORESS, based on automatic association of P- and S-type arrivals. This gives an average of 12.7 events per processed day (179 days processed). 71% of these events are within 300 km, and 89% of these events are within 1000 km.

ARCESS detections

The number of detections (phases) reported during day 091, 1994, through day 273, 1994, was 70,784, giving an average of 387 detections per processed day (183 days processed).

Table 3.5.2 shows daily and hourly distribution of detections for ARCESS.

Events automatically located by ARCESS

During days 091, 1994, through 273, 1994, 4328 local and regional events were located by ARCESS, based on automatic association of P- and S-type arrivals. This gives an average 23.7 events per processed day (183 days processed). 56% of these events are within 300 km, and 87% of these events are within 1000 km.

FINESS detections

The number of detections (phases) reported during day 091, 1994, through day 273, 1994, was 40,602, giving an average of 226 detections per processed day (180 days processed).

Table 3.5.3 shows daily and hourly distribution of detections for FINESS.

Events automatically located by FINESS

During days 091, 1994, through 273, 1994, 2265 local and regional events were located by FINESS, based on automatic association of P- and S-type arrivals. This gives an average of 12.6 events per processed day (180 days processed). 77% of these events are within 300 km, and 92% of these events are within 1000 km.

GERESS detections

The number of detections (phases) reported from day 091, 1994, through day 273, 1994, was 41,905, giving an average of 235 detections per processed day (178 days processed).

Table 3.5.4 shows daily and hourly distribution of detections for GERESS.

Events automatically located by GERESS

During days 091, 1994, through 273, 1994, 3743 local and regional events were located by GERESS, based on automatic association of P- and S-type arrivals. This gives an average of 21.0 events per processed day (178 days processed). 72% of these events are within 300 km, and 89% of these events are within 1000 km.

Apatity array detections

The number of detections (phases) reported from day 091, 1994, through day 273, 1994, was 124,718, giving an average of 931 detections per processed day (134 days processed).

As described in earlier reports, the data from the Apatity array are transferred by one-way (simplex) radio links to Apatity city. The transmission suffers from radio disturbances that

occasionally result in a large number of small data gaps and spikes in the data. In order for the communication protocol to correct such errors by requesting retransmission of data, a two-way radio link would be needed (duplex radio). However, it should be noted that noise from cultural activities and from the nearby lakes cause most of the unwanted detections. These unwanted detections are "filtered" in the signal processing, as they give seismic velocities that are outside accepted limits for regional and teleseismic phase velocities.

Table 3.5.5 shows daily and hourly distribution of detections for the Apatity array.

Events automatically located by the Apatity array

During days 091, 1994, through 273, 1994, 1489 local and regional events were located by the Apatity array, based on automatic association of P- and S-type arrivals. This gives an average of 11.1 events per processed day (134 days processed). 34% of these events are within 300 km, and 70% of these events are within 1000 km.

Spitsbergen array detections

The number of detections (phases) reported from day 091, 1994, through day 273, 1994, was 66,989, giving an average of 381 detections per processed day (176 days processed).

Table 3.5.6 shows daily and hourly distribution of detections for the Spitsbergen array.

Events automatically located by the Spitsbergen array

During days 091, 1994, through 273, 1994, 1792 local and regional events were located by the Spitsbergen array, based on automatic association of P- and S-type arrivals. This gives an average of 10.2 events per processed day (176 days processed). 46% of these events are within 300 km, and 78% of these events are within 1000 km.

U. Baadshaug

Day	00	01	02	03	04	05	06	07	08	09	10	11	12	13	14	15	16	17	18	19	20	21	22	23	Sum	Date	
259	3	0	3	11	4	0	14	2	5	6	15	3	12	4	5	11	12	18	22	33	32	31	27	34	307	Sep 16 Friday	
260	30	36	27	26	26	34	7	12	11	5	7	6	6	5	13	11	9	11	13	12	10	5	11	8	341	Sep 17 Saturday	
261	5	4	8	10	2	1	10	8	4	8	8	2	6	8	11	5	5	11	9	3	7	5	3	3	146	Sep 18 Sunday	
262	1	2	3	5	5	1	2	5	2	3	3	14	3	2	15	16	9	19	3	12	3	8	7	8	151	Sep 19 Monday	
263	8	2	7	4	3	6	4	3	6	2	4	14	2	8	7	9	7	7	6	7	10	10	4	3	143	Sep 20 Tuesday	
264	3	12	2	6	1	3	2	2	3	3	6	18	16	3	8	7	4	7	3	10	2	11	1	2	135	Sep 21 Wednesday	
265	1	12	21	1	0	0	1	11	1	3	2	17	7	7	12	12	9	10	8	7	3	1	11	2	159	Sep 22 Thursday	
266	3	3	9	8	9	6	1	3	1	3	6	15	12	7	10	2	11	4	1	12	8	23	2	4	163	Sep 23 Friday	
267	8	6	9	9	11	8	7	4	7	14	13	15	4	5	3	10	2	11	8	9	3	2	10	4	182	Sep 24 Saturday	
268	15	0	2	6	7	2	3	7	8	7	9	10	7	12	5	3	9	4	5	8	5	11	8	14	167	Sep 25 Sunday	
269	8	11	12	11	6	3	2	2	3	3	9	7	4	18	5	15	10	14	8	4	6	11	4	14	190	Sep 26 Monday	
270	5	4	2	2	11	0	12	1	12	6	20	4	15	10	9	10	6	8	7	2	4	4	14	6	174	Sep 27 Tuesday	
271	2	1	3	12	2	7	2	5	9	8	20	7	14	5	8	6	14	22	4	4	10	8	11	3	187	Sep 28 Wednesday	
272	4	13	5	11	4	7	4	4	7	9	4	13	6	14	18	11	10	13	2	5	7	2	8	5	186	Sep 29 Thursday	
273	8	5	3	16	3	7	3	6	5	15	14	8	10	6	15	15	11	13	0	6	19	4	10	11	213	Sep 30 Friday	
NRS	00	01	02	03	04	05	06	07	08	09	10	11	12	13	14	15	16	17	18	19	20	21	22	23			
Sum	1382	1432	1122	1288	1531	1815	1862	1638	1539	1818	1813	1344															
	1308	1398	1255	1312	1314	1560	1896	1774	1549	1478	1391	1426	36245	Total sum													
179	7	8	8	8	7	6	7	7	7	9	9	10	11	10	10	9	9	9	8	10	8	10	8	8	202	Total average	
125	7	7	7	7	6	5	7	6	7	9	9	11	11	11	10	9	9	9	8	11	8	11	8	7	199	Average workdays	
54	9	10	9	9	9	10	9	9	8	9	8	8	9	8	9	10	8	9	8	8	8	8	8	9	9	211	Average weekends

Table 3.5.1. Daily and hourly distribution of NORESS detections. For each day is shown number of detections within each hour of the day, and number of detections for that day. The end statistics give total number of detections distributed for each hour and the total sum of detections during the period. The averages show number of processed days, hourly distribution and average per processed day.

Day	00	01	02	03	04	05	06	07	08	09	10	11	12	13	14	15	16	17	18	19	20	21	22	23	Sum	Date	
259	10	8	8	8	12	5	11	9	24	17	44	30	13	26	12	22	24	22	22	25	13	13	7	13	398	Sep 16 Friday	
260	8	11	27	16	12	10	13	18	13	13	18	9	19	23	8	5	8	15	11	13	6	10	10	10	306	Sep 17 Saturday	
261	3	13	8	12	4	8	7	7	10	3	7	11	15	17	37	35	25	28	11	2	7	7	12	10	299	Sep 18 Sunday	
262	10	13	7	10	10	8	16	19	14	13	12	19	20	28	30	37	26	16	28	9	7	10	14	13	389	Sep 19 Monday	
263	18	0	4	12	15	28	31	36	38	41	45	56	60	13	17	26	17	36	18	34	11	17	18	14	605	Sep 20 Tuesday	
264	9	7	8	11	16	20	30	32	39	36	47	27	28	30	23	23	6	10	15	10	15	20	11	12	485	Sep 21 Wednesday	
265	4	9	4	5	15	24	20	22	35	20	27	17	14	14	22	27	35	16	32	20	26	8	18	13	447	Sep 22 Thursday	
266	7	5	17	12	16	43	25	31	30	9	24	24	25	5	2	10	4	13	10	7	5	11	10	11	356	Sep 23 Friday	
267	1	6	13	10	7	4	6	4	25	15	13	22	14	20	8	21	13	10	22	10	9	16	16	12	297	Sep 24 Saturday	
268	15	12	11	7	9	8	18	9	7	9	5	6	12	8	10	11	8	10	11	6	12	8	9	10	231	Sep 25 Sunday	
269	13	2	8	11	15	89	49	10	15	70	86	86	30	37	7	62	11	16	14	20	24	11	11	13	710	Sep 26 Monday	
270	14	3	1	7	5	28	44	62	86	45	40	26	52	7	14	44	21	23	18	11	8	12	7	13	591	Sep 27 Tuesday	
271	16	4	6	14	20	29	24	33	33	74	30	64	64	43	23	15	0	0	0	0	0	0	0	0	0	492	Sep 28 Wednesday
272	0	0	0	0	0	0	0	68	72	40	20	20	39	26	16	62	42	8	6	7	2	4	7	8	447	Sep 29 Thursday	
273	11	3	3	12	18	73	10	60	27	26	37	55	12	22	15	9	29	6	7	24	8	10	5	17	499	Sep 30 Friday	
ARC	00	01	02	03	04	05	06	07	08	09	10	11	12	13	14	15	16	17	18	19	20	21	22	23			
Sum	1804	2026	2244	3403	3863	4857	3301	3324	2828	2567	2325	1973															
	1910	1949	2367	2916	3506	4393	3879	2857	3104	3194	2583	3611	70784	Total sum													
183	10	10	11	11	13	12	16	19	19	21	24	27	21	18	16	18	17	15	17	14	14	13	20	11	387	Total average	
126	10	9	10	11	14	14	18	21	21	23	27	30	24	19	16	20	18	16	19	15	15	13	20	11	414	Average workdays	
57	11	11	11	10	11	9	11	13	14	17	18	19	15	15	14	13	14	15	14	12	13	12	20	11	323	Average weekends	

Table 3.5.2. Daily and hourly distribution of ARCESS detections. For each day is shown number of detections within each hour of the day, and number of detections for that day. The end statistics give total number of detections distributed for each hour and the total sum of detections during the period. The averages show number of processed days, hourly distribution and average per processed day.

Day	00	01	02	03	04	05	06	07	08	09	10	11	12	13	14	15	16	17	18	19	20	21	22	23	Sum	Date	
259	11	5	10	7	8	3	8	2	15	13	12	10	17	14	17	17	0	0	0	0	0	0	0	0	0	169	Sep 16 Friday
260	0	0	0	0	0	0	0	0	0	0	0	0	0	1	7	7	7	9	6	3	3	6	4	2	55	Sep 17 Saturday	
261	7	4	3	16	3	2	5	7	11	6	9	3	5	6	6	4	6	16	9	6	8	7	6	3	158	Sep 18 Sunday	
262	4	6	4	6	2	1	3	7	2	9	0	9	9	5	11	12	3	4	4	8	8	8	7	9	141	Sep 19 Monday	
263	9	7	4	2	3	4	4	2	11	7	16	16	9	7	8	13	6	3	6	11	7	10	7	9	181	Sep 20 Tuesday	
264	5	8	12	5	1	7	3	4	6	2	15	20	18	12	12	8	5	2	8	9	5	8	6	7	188	Sep 21 Wednesday	
265	6	4	10	3	4	7	7	6	7	11	13	14	9	12	8	11	5	5	4	10	6	11	3	10	186	Sep 22 Thursday	
266	8	10	9	7	3	3	4	4	10	9	10	19	13	3	4	4	0	4	5	3	7	2	8	2	151	Sep 23 Friday	
267	5	3	5	10	6	7	3	0	3	10	14	5	4	8	3	9	6	16	24	11	11	20	32	10	225	Sep 24 Saturday	
268	2	6	11	12	16	9	9	4	6	11	18	8	4	3	0	2	5	4	13	6	13	6	13	11	192	Sep 25 Sunday	
269	7	13	7	10	8	4	1	1	4	10	9	5	10	26	9	5	0	6	6	6	10	6	2	3	168	Sep 26 Monday	
270	3	9	13	4	6	2	3	8	2	7	12	12	17	6	13	7	1	9	4	3	5	6	2	10	164	Sep 27 Tuesday	
271	9	8	6	10	4	4	1	8	3	11	10	16	23	12	12	8	11	10	3	6	5	7	1	3	191	Sep 28 Wednesday	
272	4	10	4	8	3	8	9	6	12	13	5	12	10	12	11	6	6	4	0	5	6	5	7	11	177	Sep 29 Thursday	
273	7	5	12	9	2	1	1	6	0	10	15	6	15	15	7	4	3	4	4	6	5	10	4	10	161	Sep 30 Friday	
FIN	00	01	02	03	04	05	06	07	08	09	10	11	12	13	14	15	16	17	18	19	20	21	22	23			
Sum	1921	1393	924	1481	1939	2552	1898	1605	1472	1684	1701	1599															
	1808	1927	1098	1238	1841	2317	2284	1698	1350	1662	1562	1648	40602	Total sum													
180	10	11	11	8	6	5	7	8	10	11	13	14	13	11	9	9	8	8	9	9	9	9	9	9	9	226	Total average
126	11	11	12	8	5	5	6	8	11	12	15	17	14	11	10	10	8	8	9	9	8	9	9	9	9	234	Average workdays
54	8	10	9	8	8	6	8	9	8	8	9	8	8	9	8	7	6	9	9	9	9	9	9	8	199	Average weekends	

Table 3.5.3. Daily and hourly distribution of FINESS detections. For each day is shown number of detections within each hour of the day, and number of detections for that day. The end statistics give total number of detections distributed for each hour and the total sum of detections during the period. The averages show number of processed days, hourly distribution and average per processed day.

Day	00	01	02	03	04	05	06	07	08	09	10	11	12	13	14	15	16	17	18	19	20	21	22	23	Sum	Date
259	3	1	6	4	7	7	18	7	17	24	21	19	21	5	10	16	7	7	1	3	1	1	0	5	211	Sep 16 Friday
260	7	0	11	6	5	2	2	8	4	12	14	16	10	5	4	2	5	6	2	1	1	2	10	3	138	Sep 17 Saturday
261	0	7	0	0	0	1	2	14	10	10	10	9	12	13	8	6	4	3	4	0	1	4	4	2	124	Sep 18 Sunday
262	4	6	7	2	0	12	9	9	7	17	26	24	7	11	15	8	4	5	3	5	5	1	5	7	199	Sep 19 Monday
263	8	10	8	4	3	7	4	11	17	16	21	24	20	31	24	15	4	5	5	12	4	5	5	1	264	Sep 20 Tuesday
264	5	5	6	6	3	10	7	22	21	18	15	31	17	15	8	18	12	5	3	3	6	3	1	4	244	Sep 21 Wednesday
265	5	4	8	7	12	5	4	16	11	23	13	24	18	14	17	16	7	0	10	3	2	1	1	2	223	Sep 22 Thursday
266	3	9	7	3	3	1	9	16	18	17	31	29	11	7	5	8	5	5	2	3	0	2	1	2	197	Sep 23 Friday
267	1	5	2	6	9	1	11	8	5	17	8	11	8	8	7	3	7	7	2	4	5	4	1	5	145	Sep 24 Saturday
268	3	2	0	6	1	2	2	10	2	5	13	8	8	13	6	9	18	4	0	2	1	8	5	4	132	Sep 25 Sunday
269	7	5	3	10	5	6	3	5	12	15	20	18	19	21	16	8	13	9	6	5	6	5	0	2	219	Sep 26 Monday
270	6	2	5	3	5	0	7	9	8	27	26	16	33	9	10	10	12	6	8	3	3	6	5	9	228	Sep 27 Tuesday
271	1	4	6	10	7	4	6	2	16	16	23	23	29	16	9	5	14	13	6	1	9	13	1	2	236	Sep 28 Wednesday
272	1	1	6	10	1	5	6	4	12	25	28	21	17	11	8	17	17	4	5	3	4	3	3	3	215	Sep 29 Thursday
273	6	8	3	9	8	2	11	15	18	24	27	21	19	10	12	6	20	3	6	7	3	1	9	4	252	Sep 30 Friday
GER	00	01	02	03	04	05	06	07	08	09	10	11	12	13	14	15	16	17	18	19	20	21	22	23		
Sum	928	954	1536	2306	3558	3317	2403	2442	1143	905	759	795														
	966	986	1075	1888	2955	3349	2614	2525	1785	1030	885	801	41905	Total sum												
178	5	5	6	5	6	9	11	13	17	20	19	19	15	14	14	14	10	6	6	5	5	4	5	4	235	Total average
123	6	6	7	6	6	10	12	15	20	24	22	22	17	15	17	16	12	8	7	6	6	4	5	4	271	Average workdays
55	3	4	3	5	5	6	6	8	10	12	12	12	9	9	9	8	5	4	4	3	3	4	4	5	151	Average weekends

Table 3.5.4. Daily and hourly distribution of GERESS detections. For each day is shown number of detections within each hour of the day, and number of detections for that day. The end statistics give total number of detections distributed for each hour and the total sum of detections during the period. The averages show number of processed days, hourly distribution and average per processed day.

Day	00	01	02	03	04	05	06	07	08	09	10	11	12	13	14	15	16	17	18	19	20	21	22	23	Sum	Date	
259	0	0	0	0	0	0	0	0	0	0	0	0	0	0	0	0	0	0	0	0	0	0	0	0	0	0 Sep 16	Friday
260	0	0	0	0	0	0	0	0	0	0	0	0	0	0	0	0	0	0	0	0	0	0	0	0	0	0 Sep 17	Saturday
261	0	0	0	0	0	0	0	0	0	0	0	0	0	0	0	0	0	0	0	0	0	0	0	0	0	0 Sep 18	Sunday
262	0	0	0	0	0	0	0	0	0	0	0	0	0	0	0	0	0	0	0	0	0	0	0	0	0	0 Sep 19	Monday
263	0	0	0	0	0	0	0	0	0	0	0	0	0	0	0	0	0	0	0	0	0	0	0	0	0	0 Sep 20	Tuesday
264	0	0	0	0	0	0	0	0	0	0	0	0	0	0	0	0	0	0	0	0	0	0	0	0	0	0 Sep 21	Wednesday
265	0	0	0	0	0	0	0	0	0	0	0	0	0	0	0	0	0	0	0	0	0	0	0	0	0	0 Sep 22	Thursday
266	0	0	0	0	0	0	0	0	0	0	0	0	0	0	0	0	0	0	0	0	0	0	0	0	0	0 Sep 23	Friday
267	0	0	0	0	0	0	0	0	0	0	0	0	0	0	0	0	0	0	0	0	0	0	0	0	0	0 Sep 24	Saturday
268	0	0	0	0	0	0	0	0	0	0	0	0	0	0	0	0	0	0	0	0	0	0	0	0	0	0 Sep 25	Sunday
269	0	0	0	0	0	0	0	0	0	0	0	0	0	0	0	0	0	0	0	0	0	0	0	0	0	0 Sep 26	Monday
270	0	0	0	0	0	0	0	0	0	0	0	0	0	0	0	0	0	0	0	0	0	0	0	0	0	0 Sep 27	Tuesday
271	0	0	0	0	0	0	0	0	0	0	0	0	0	0	0	0	0	0	0	0	0	0	0	0	0	0 Sep 28	Wednesday
272	0	0	0	0	0	0	0	0	0	0	0	0	0	0	0	0	0	0	0	0	0	0	0	0	0	0 Sep 29	Thursday
273	0	0	0	0	0	0	0	0	0	0	0	0	0	0	0	0	0	0	0	0	0	0	0	0	0	0 Sep 30	Friday
APA	00	01	02	03	04	05	06	07	08	09	10	11	12	13	14	15	16	17	18	19	20	21	22	23			
Sum	2762	6301	9195	8203	7334	7794	6688	4249	3655	2157	1854	1722															
	2041	4343	7148	9195	8055	7785	7839	5718	4220	2546	2240	1674	124718	Total sum													
134	15	21	32	47	53	69	69	61	60	55	58	58	59	50	43	32	31	27	19	16	17	14	12	13	931	Total average	
91	16	22	39	56	64	85	85	76	75	67	70	71	71	60	49	38	36	31	22	18	19	15	13	13	1111	Average workdays	
43	14	18	18	29	30	34	33	29	28	28	32	31	32	27	30	18	21	20	13	12	13	11	11	12	544	Average weekends	

Table 3.5.5. Daily and hourly distribution of Apatity array detections. For each day is shown number of detections within each hour of the day, and number of detections for that day. The end statistics give total number of detections distributed for each hour and the total sum of detections during the period. The averages show number of processed days, hourly distribution and average per processed day.

Day	00	01	02	03	04	05	06	07	08	09	10	11	12	13	14	15	16	17	18	19	20	21	22	23	Sum	Date	
259	30	17	36	30	34	26	24	18	25	22	28	33	14	14	20	30	17	12	19	34	16	36	20	34	589	Sep 16	Friday
260	26	23	31	20	27	43	29	22	31	38	34	22	30	24	17	21	36	31	31	32	36	31	27	41	703	Sep 17	Saturday
261	31	28	24	47	23	31	24	42	32	28	37	34	34	33	39	39	45	34	34	38	35	45	69	62	888	Sep 18	Sunday
262	61	76	57	57	71	45	63	49	50	40	40	44	36	52	34	37	50	39	41	44	34	69	53	31	1173	Sep 19	Monday
263	33	37	37	33	26	40	40	19	20	18	37	38	31	13	14	38	11	30	19	28	25	37	30	27	681	Sep 20	Tuesday
264	23	16	38	26	37	12	35	49	33	48	14	43	28	23	41	34	20	24	28	28	53	24	28	30	735	Sep 21	Wednesday
265	33	24	24	41	30	29	15	39	34	29	29	35	41	36	16	19	30	20	17	21	21	36	19	34	672	Sep 22	Thursday
266	35	39	34	31	35	38	42	40	94	31	48	70	29	68	26	29	39	27	28	40	30	31	59	37	980	Sep 23	Friday
267	52	42	21	15	28	14	21	25	25	20	14	23	15	19	22	27	19	26	16	7	17	27	34	28	557	Sep 24	Saturday
268	25	24	34	31	20	34	41	31	46	25	41	39	41	24	31	33	23	26	37	24	33	21	34	37	755	Sep 25	Sunday
269	26	51	25	28	25	21	26	20	24	25	29	39	27	24	26	33	16	35	27	37	54	28	21	18	685	Sep 26	Monday
270	29	11	33	34	21	16	40	45	126	58	13	25	21	14	27	22	38	29	27	28	26	12	12	29	736	Sep 27	Tuesday
271	25	12	24	20	19	20	21	18	6	12	10	12	6	9	24	18	20	20	17	19	57	20	20	17	446	Sep 28	Wednesday
272	17	8	10	45	52	14	209	95	17	76	152	18	65	187	154	117	74	49	14	38	41	28	40	26	1546	Sep 29	Thursday
273	32	27	13	15	25	104	29	26	15	16	14	23	21	29	18	22	17	31	40	26	21	33	35	39	671	Sep 30	Friday
SPI	00	01	02	03	04	05	06	07	08	09	10	11	12	13	14	15	16	17	18	19	20	21	22	23			
Sum	2438	2744	2733	2964	2454	2842	2946	2843	2896	2782	2816	2580															
	2583	2587	2763	2901	3364	2688	2666	3143	2807	3017	2790	2642	66989	Total sum													
176	15	14	15	16	16	16	16	17	19	14	15	16	15	17	18	16	16	16	17	16	16	16	15	15	381	Total average	
121	14	12	13	14	17	16	16	18	22	15	15	17	16	17	18	17	15	16	16	17	15	15	14	14	378	Average workdays	
55	15	17	18	18	12	13	16	12	13	11	14	13	13	15	16	14	18	18	19	14	17	19	18	16	369	Average weekends	

Table 3.5.6. Daily and hourly distribution of Spitsbergen array detections. For each day is shown number of detections within each hour of the day, and number of detections for that day. The end statistics give total number of detections distributed for each hour and the total sum of detections during the period. The averages show number of processed days, hourly distribution and average per processed day.

3.6 IMS operation

The Intelligent Monitoring System (IMS) was installed at NORSAR in December 1989 and was operated at NORSAR from 1 January 1990 for automatic processing of data from ARCESS and NORESS. A second version of IMS that accepts data from an arbitrary number of arrays and single 3-component stations was installed at NORSAR in October 1991, and regular operation of the system comprising analysis of data from the 4 arrays ARCESS, NORESS, FINESS and GERESS started on 15 October 1991. As opposed to the first version of IMS, the one in current operation also locates events at teleseismic distance.

Data from the Apatity array were included on 14 December 1992, and from the Spitsbergen array on 12 January 1994. Due to missing calibration information for the new Guralp SP sensors installed in the Spitsbergen array in late August, detections from the Spitsbergen array were not used in the automatic phase association after 1 September 1994, but the detections were available to the analysts and could be added manually during analysis.

The operational stability of IMS has been very good during the reporting period. In fact the IMS event processor (pipeline) has had no downtime of its own; i.e., all data available to IMS have been processed by IMS.

Phase and event statistics

Table 3.6.1 gives a summary of phase detections and events declared by IMS. From top to bottom the table gives the total number of detections by the IMS, the number of detections that are associated with events automatically declared by the IMS, the number of detections that are not associated with any events, the number of events automatically declared by the IMS, the total number of events defined by the analyst, and finally the number of events accepted by the analyst without any changes (i.e., from the set of events automatically declared by the IMS)

Due to reductions in the FY94 funding for IMS activities (relative to previous years), new criteria for event analysis, effective from January 1, 1994 were introduced. Since that date, only regional events in areas of special interest (e.g, Spitsbergen, since it is necessary to acquire new knowledge in this region) or other significant events (e.g, felt earthquakes and large industrial explosions) have been thoroughly analyzed. Teleseismic events are analyzed as before.

	Apr 94	May 94	Jun 94	Jul 94	Aug 94	Sep 94	Total
Phase detections	67287	61976	70465	72409	47220	44911	364268
- Associated phases	8139	8394	8661	7677	9229	7262	49362
- Unassociated phases	59148	53582	61804	64732	37991	37649	314906
Events automatically declared by IMS	2354	2406	2549	2227	2846	2336	14718
No. of events defined by the analyst	384	455	410	386	556	359	2550
No. of events accepted without modifications	1	0	46	11	6	3	67

Table 3.6.1. IMS phase detections and event summary.

U. Baadshaug
B. Ferstad
B.Kr. Hokland
L.B. Loughran
B. Paulsen

4 Improvements and Modifications

4.1 NORSAR

NORSAR data acquisition

The current NORSAR data acquisition system was described in NORSAR Sci. Rep. No. 2-93/94, and is functioning as a backup system until the refurbishment of NORSAR array is finished. The system has been running satisfactorily during the whole reporting period.

NORSAR detection processing

The NORSAR detection processor has been running satisfactorily. To maintain consistent detection capability, the NORSAR beam tables have not been changed.

Detection statistics for the NORSAR array are given in section 2.

NORSAR event processing

The routine processing of NORSAR events was described in NORSAR Sci. Rep No 2-93/94. The process continues to use a data base with time delay corrections and slowness corrections for location calibration that was established in 1974 (Berteussen, 1974). This data base still gives valuable corrections for the NORSAR array, but the data base itself is technically based on old IBM architecture disk files. The correction subroutines and disk file access routines have been converted to give identical results on SUN and the old IBM system. However, this data base is in today's technology outdated, and an effort to create a new data base is given high priority.

NORSAR refurbishment

All the new Science Horizons data acquisition hardware and software have been acquired and delivered. See NORSAR Sci. rep. No. 2-93/94 for a system description. The data acquisition software XAVE and communication interface module CIM II were installed on October 5, 1994 at NDPC. At subarray 06C, a CIM II was installed in the Central Terminal Vault - CTV, and an AIM24-1 has been installed in one remote SP vault (SPV) for testing purposes. The data acquisition is running satisfactorily.

Between every SPV and CTV, the data will be transmitted using ADCCP protocol and asynchronous modems. These modems require DC power, and together with one AIM24-1 and one GPS clock, this equipment consumes almost all the power we can deliver at the remote sites. To give DC power out to the remote sites and to get data back, we now need to use additional pairs from the buried cables as compared to the old analog data transmission. This means that cable pairs that used to be spares, will now be used as power cables, and cable problems earlier not detected will now be exposed. The consequence is that many more cable repairs than initially predicted will be needed.

Boreholes in the seven LPVs for the KS5400P seismometers have been drilled. Contractual arrangements for the delivery of "posthole" KS54000 seismometers have been completed.

Although several technical problems have delayed the refurbishment, we are still planning to send NORSAR data to IDC during the GSETT-3 experiment.

4.2 Regional Arrays

DP - Detection processing

The routine detection processing of the arrays is running satisfactorily on each of the arrays' SUN-3/280 or Sparcstation 1 acquisition systems. The same program is used for NORSAR, NORESS, ARCESS, FINESA, GERESS, Apatity and Spitsbergen, but with different "recipes". The beam table for NORESS and ARCESS is found in NORSAR Sci. Rep. No. 1-89/90. The beam table for FINESA and GERESS is found in NORSAR Sci. Rep. No. 1-90/91. The beam table for Apatity is found in NORSAR Sci. Rep. No. 1-92/93, and that for Spitsbergen is found in NORSAR Sci. Rep. No. 2-92/93.

Detection statistics are summarized in section 3.

EP_SigPro - Signal processing. Phase estimation

This process performs f-k and polarization analysis for each detection to determine phase velocity, azimuth and type of phase, and the results are stored in the ORACLE detection and arrival tables for use by the IMS.

Some modifications have been done as a result of IDC testing.

EP_Ronapp - Event Processing. Plot and epicenter determination

A description of single-array event processing is found in NORSAR Sci. Rep. No. 2-88/89, and NORSAR Sci. Rep. No. 2-89/90.

J. Fyen

Reference:

Berteussen, K.A. (1974): NORSAR Location calibrations and time delay corrections, NORSAR Scientific Report No. 2-73/74, Kjeller, Norway.

5 Maintenance Activities

Activities in the field and at the Maintenance Center

This section summarizes the activities at the Maintenance Center (NMC) Hamar, and includes activities related to monitoring and control of the NORSAR teleseismic array, as well as the NORESS, ARCESS, FINESS, GERESS, Apatity and Spitsbergen small-aperture arrays.

Activities involve preventive and corrective maintenance, planning and activities related to the refurbishment of the NORSAR teleseismic array.

NORSAR

Visits to subarrays in connection with:

- Adjusted gain and offset, SP/LP channels
- Demounted equipment in the 06C CTV
- Power failures at 01A and 02B
- Construction of concrete floor and painting work at 06C CTV

NMC

- Continued the NORSAR refurbishment preparations
- Prepared for the Spitsbergen expedition

NORESS

- Repaired damage caused by lightning

ARCESS

- Replaced fiber optical transmitters and adjusted optical link

Spitsbergen

- Replaced decoder in Longyearbyen
- Buried all cables between the HUB and remote sites (approx. 5 km of cables)
- Installed wellhead vaults at all remote sites
- Replaced old battery bank with new NiCa batteries
- Replaced Teledyne S-500 seismometers with Guralp CMG-3V instruments
- Installed a 3-component broadband instrument in borehole at site B4
- Expanded the station "hut" with two "storerooms"
- Replaced a defective windmill

Additional details for the reporting period are provided in Table 5.1.

Subarray/ area	Task	Date
NORSAR		April
02C	Adjusted DC offset and gain on SP channels Adjusted SP and LP channels	12 Apr
NMC	NORSAR refurbishment work continued.	April
		May
ARCESS	B4, C2, C4, D2 and D3: Replaced fiber optical transmitters Adjusted optical link, all channels	2-5 May
Spitsbergen	Replaced decoder, Longyearbyen	6 May
NMC	Continued NORSAR refurbishment work Began preparations for expedition to Spitsbergen	May
		June
NORSAR		June
06C	Demounted the equipment in the CTV Began preparations for making new concrete floor	27-28 Jun
NMC	Continued NORSAR refurbishment work Continued preparations for the expedition to Spitsbergen	June
		July
NORSAR		July
01A	Subarray visited due to power failure	19 Jul
02B	Subarray visited due to failure on the 1000 V AC powerline.	19 Jul
02B	Bad insulators found at two different places.	21 Jul
02B	Replaced RD6 due to failure on the power supply card, damaged by lightning.	25 Jul
06C	Made new concrete floor in CTV.	1 Jul
06C	Replaced RD6 due to failure on power supply card. Replaced modem, which had been damaged by lightning Adjusted gain on all SP channels. Checked MP and FP, LP-Z.	12 Jul

Subarray/ area	Task	Date
NORESS	Replaced Hub 10 processor card because of spike problems after thunderstorm	4 Jul
	Repaired Hub power system, damaged by lightning	8 Jul
	Repaired Hub 14 digital interface card, damaged by lightning Restarted the UPS system	27 Jul
NMC	Continued NORSAR refurbishment work Continued preparations for the expedition to Spitsbergen	July
NORSAR		August
06C	Painted the floor and walls of the CTV	15 Aug
Spitsbergen	All cables between the Hub and the remote sites were buried (approx. 5 km), as required by local authorities. Wellhead vaults were installed at all remote sites. The old battery bank was replaced with new NiCa batteries. The Teledyne S-500 seismometers were replaced with Guralp CMG-3V instruments. A 3-component broadband instrument (Guralp CMG-3T) was installed on top of the SP-vertical instrument in borehole 4. The station hut was expanded with two "storerooms".	22 Aug - 2 Sep
NMC	Continued NORSAR refurbishment work.	August
NORSAR	Preparations were made for installation of Science Horizons equipment in the subarray vaults. Experimental testing of VSAT-transmission from one subarray was carried out.	September
NMC	Continued the NORSAR refurbishment work.	September

Table 5.1. Activities in the field and the NORSAR Maintenance Center, including NDPC activities related to monitoring and control of the NORSAR array, as well as the NORESS, ARCESS, FINESS, GERESS, Apatity and Spitsbergen small-aperture arrays during 1 April - 30 September 1994.

P.W. Larsen

K.A. Løken

6 Documentation Developed

Fyen, J. and B. Paulsen (1994): Combining NORSAR and NORESS processing, in *Semiann. Tech. Summ. 1 Apr - 30 Sep 94*, NORSAR Sci. Rep. 1-94/95, Kjeller, Norway.

Kværna, T. (1994): Automatic processing of data from small-aperture arrays and seismograph networks in the context of seismic verification, Doctoral thesis, University of Oslo, Norway.

Kværna, T. and F. Ringdal (1994): A system for continuous seismic threshold monitoring, final report, in *Semiann. Tech. Summ. 1 Apr - 30 Sep 94*, NORSAR Sci. Rep. 1-94/95, Kjeller, Norway.

Mykkeltveit, S., U. Baadshaug, J. Fyen and B.Kr. Hokland (1994): The Lop Nor nuclear explosions of 10 June and 7 October 1994, in *Semiann. Tech. Summ. 1 Apr - 30 Sep 94*, NORSAR Sci. Rep. 1-94/95, Kjeller, Norway.

Ringdal, F. and T. Kværna (1994): On the reliability of event location estimates from automatic and interactive processing, in *Semiann. Tech. Summ. 1 Apr - 30 Sep 94*, NORSAR Sci. Rep. 1-94/95, Kjeller, Norway.

Schweitzer, J. (1994): Mislocation vectors for small aperture arrays -- a first step towards calibrating GSETT-3 stations, in *Semiann. Tech. Summ. 1 Apr - 30 Sep 94*, NORSAR Sci. Rep. 1-94/95, Kjeller, Norway.

Semiannual Tech. Summary, 1 Oct 93 - 31 Mar 94, NORSAR Sci. Rep. 2-93/94, NORSAR, Kjeller, Norway.

Skorve, J. (1994): Epicenter location and cratering at the Novaya Zemlya underground nuclear test site, in *Semiann. Tech. Summ. 1 Apr - 30 Sep 94*, NORSAR Sci. Rep. 1-94/95, Kjeller, Norway.

7 Summary of Technical Reports / Papers Published

7.1 A system for continuous seismic threshold monitoring, final report

Introduction

In the previous NORSAR Semiannual Technical Summary, we outlined the general approach and the implementation considerations of the continuous seismic threshold monitoring (CSTM) system (Kværna et al, 1994a). We have now completed the development, and we will in this report describe the automatic processing flow, outline the key functions of the interactive analysis, discuss the output produced by this system, and finally outline possible future modifications and extensions.

Processing flow

The CSTM system is logically divided into two parts; the continuous processing modules and the interactive analysis modules. A flowchart of the processing modules is given in Fig. 7.1.1, and comments on the different steps are given in the following.

The basis for all calculations are the diskloops with continuous seismic data from the network stations. Following the recording onto the diskloops, the seismic data for each station is subjected to beamforming (arrays only), bandpass filtering and short-term-average (STA) calculations. The continuous STA data are then stored onto new diskloops with a typical sampling rate of 1 Hz.

The STA data for each station is subsequently used for calculation of the network upper magnitude thresholds. In our previous report (Kværna et al, 1994a), we showed that the term $\log(A/T)$ in the magnitude relation can be well approximated by $\log(\text{STA})$ multiplied by a constant that is specific for each instrument and bandpass filter. These constants are found from analysis of representative event segments, and for standard short-period instruments, these constants are often very close to the displacement response value at 1 Hz.

The calculation of network magnitude thresholds from a large number of stations (~50) is a computer intensive task. Using a sampling interval of 10 s and a global grid of 2562 targets, it took about 50 minutes to process 60 minutes of data on a Sparcstation 20 (60 MHz). In comparison, the computational load of the STA calculations for each station is rather low. The continuous network magnitudes for each of the nodes of the global grid system is written onto a new diskloop. These data are stored in demultiplexed form to facilitate fast read access for plotting of time series.

The final step in the processing flow is to interpolate and reformat the magnitude thresholds to multiplexed form. This makes reading of the threshold data for a given time very fast, and enables us to rapidly update displays of magnitude thresholds onto different types

of map sections. The computational load of this module is modest compared to the calculation of the actual magnitude thresholds.

Interactive analysis

A detailed description of and examples from the different interactive analysis options are given in the Continuous Seismic Threshold Monitoring User's Guide (Kværna et al, 1994b), that is available from NORSAR upon request. A schematic overview of the functionality of and the interaction between the different interactive analysis modules is shown in Fig. 7.1.2.

- **The TM trace displayer:** The main function of this module is to display time-series of magnitude thresholds for given target regions. The selection of targets can be done from the trace displayer itself, or alternatively, from interactive selection of targets using the TM map overlay module. The traces can be plotted normalized or on a fixed scale, such that time intervals with high thresholds stand out clearly.

Events from various bulletins can also be shown. The main purpose of this option is to associate increased thresholds with signals from actual events.

For a quantitative assessment of the magnitude thresholds, displays of both peak statistics and cumulative distributions are available.

- **The TM map overlay module:** In order to show how the magnitude thresholds vary as a function of geographical position, we have the possibility to display colored snapshots of the magnitude thresholds onto various map sections. A large selection of predefined map sections are already available, and new sections can easily be generated.

The time of the snapshot can be set from the TM map overlay module itself, or alternatively, from interactive cursor control using the TM trace displayer. This interaction allows us to investigate the time-space variation of the magnitude thresholds, and is therefore a valuable tool for identifying time intervals and regions with increased thresholds. To further investigate the cause of the increased thresholds, located events can be plotted onto the maps for a predefined time interval around the origin time of the events.

An example of global magnitude threshold variations during the occurrence of a major earthquake is given in Fig. 7.1.3.

After interactively selecting a time interval on the trace displayer, we also have the possibility to sequentially update the colored magnitude thresholds within the selected time interval. This kind of animation can be very instructive to understand how increased noise levels and seismic events influence the global magnitude thresholds.

Another option of the TM map overlay module is to update the colored thresholds at regular intervals, with a given lag behind real-time (e.g., one hour). This lag is necessary to accommodate the arrival of phases with the largest travel-times, as well as

the time needed to process the data. With a modification to the algorithm for threshold calculations, this function can be used for a continuous assessment of the detection capability of the network.

- **The World Map:** One purpose with this module is to show the station distribution of the network used in the calculation of the magnitude thresholds. Another application is to display the location of events in the available bulletins. On the TM trace displayer we may interactively select events and by using inter-process communication we may plot the events onto the world map.

Interpretation of derived magnitude thresholds

We have noticed that there have been some misunderstandings on the interpretation of the magnitude thresholds computed by the CSTM system. It is important **not** to consider the values as a 90 per cent network detection threshold, since we have not taken into account a signal-to-noise ratio which would be required in order to detect an event.

However, if we exclude the time intervals where our network actually detected and located an event in the target region, we may use the following interpretation:

“We are confident (at the 90 per cent level) that no events larger than the calculated thresholds occurred in the area”.

Practical monitoring of a given target region (e.g., of a 24 hour time interval) should be done in the following way:

- Check to see if the network bulletin has reported any events located in the target region. If so, identify the threshold peaks associated with the located events.
- Attempt to associate the largest peaks in the threshold trace to events located outside the target area. In theory, it may have been possible that an explosion in the target area could have been hidden in the coda of the interfering event, but this requires that the origin time of the explosion coincided with the time of the threshold peak. However, due to the short time periods with significant threshold peaks, the probability of such a coincidence is very small. For further discussion on this topic, see Kværna (1992).
- Use the threshold trace to determine a magnitude reference level for which all exceedances are caused by signals from known events. We may then conclude: We are confident (at the 90 per cent level) that no events larger than the magnitude reference level occurred in the target region during this time period.

In this way, the analyst can rapidly get an assessment of the possible seismic activity in the target region during the given time interval. This will also enable him to focus his analysis on the short time intervals when “real” evasion opportunities exist.

Uncertainty considerations

Generic global attenuation and travel-time curves form the basis for the network magnitude calculations (see Figs. 7.1.4a and 7.1.4b). As is well known, the attenuation curves are accompanied with significant uncertainties. E.g., the studies made on P-wave amplitude variability (Veith and Clawson, 1972; Lilwall, 1986; Ringdal and Fyen, 1979) indicate a standard deviation of 0.35-0.40 magnitude units. If reliable regional corrections are available, the uncertainty can be reduced somewhat. In the calculation of the network magnitude thresholds, these uncertainties are taken into account.

There are also other factors in the calculation of magnitude thresholds that are associated with uncertainties. These are:

- The use of $\log(\text{STA})$ as a representation of $\log(A/T)$
- The effect of beamforming, filtering and different instrument responses on the seismic amplitude
- Instrument calibration
- The effect of each target point representing a finite geographical area.

We have during our development of the CSTM system used the strategy of being conservative with respect to the estimation of upper magnitude thresholds. Missing information on the exact values of the different parameters are therefore compensated for by assuming conservative values or by increasing the uncertainty. With this in mind, it is obvious that the quality of the output from the CSTM system can be significantly improved. By conducting additional studies, more precise estimates of the parameters and their associated uncertainties can be obtained, and we can thereby lower the derived magnitude thresholds and/or increase the degree of confidence.

Future improvements

The by far largest uncertainties involved in the magnitude threshold calculations are associated with the use of generic global attenuation relations. Ideally, one would for each network station like to derive regionalized attenuation curves for the entire globe, but this is an extremely complex undertaking that is unlikely to be done in the near future. There are, however, some improvements that can be made without such extensive efforts.

First of all, known station biases should be taken into account. We are especially worried about stations with large negative biases, because this may give rise to unrealistically low magnitude thresholds. Along the same lines, we would for each station like to identify and introduce corrections to regions with very extreme amplitude anomalies. Also in this case, the large negative biases cause the largest problems.

It should be emphasized that the calculation of network magnitude thresholds is not an averaging process, but is very sensitive to outliers in the population of individual station magnitude estimates. For a large network of more than 50 stations it may often happen

that some of the stations are not operating properly, e.g., due to low gain. For such a large network it may be necessary to introduce an additional outlier rejection algorithm before calculating the actual magnitude thresholds.

On the other hand, this sensitivity to outliers can be used as a quality control of the stations in the network, and this application should be explored further.

The program module calculating the STA data for each station is a modified version of the detector program (DP) program developed at NORSAR. When intervals with bad data occur (spikes, gaps, clipped data, calibration signals), we have already procedures in place that take actions that are sufficient for operating a detector. However, for computing of threshold magnitudes, we should not allow any bad data to be included at all. It is therefore necessary to implement additional routines that identify all time intervals with bad data for any given station, such that all these intervals can be discarded from further processing for that station.

Both the relation between $\log(\text{STA})$ and $\log(A/T)$ and the signal loss due to beamforming and filtering have turned out to vary among the different seismic stations. In order to obtain precise estimates of the relations, we have to analyze a representative number of events for each station in the network. In the current version of the CSTM system, we have only used conservative generic relations, and even a limited effort of analyzing only 3-5 events per station would significantly improve the precision of the magnitude threshold estimates.

As explained earlier in this report, the derived magnitude thresholds should not be interpreted as a 90 per cent network detection threshold. But by modifying the algorithm to take into account a predefined signal-to-noise ratio (SNR) as well as the number of stations required to detect an event, the maps generated by the CSTM system can be made very similar to the standard capability maps produced by programs like SNAP/D or Network.

Conclusions

The main focus during the development of the CSTM system has been to develop an environment that facilitates both real-time operation as well as testing of new ideas in the context of continuous seismic threshold monitoring. The current operational system is not fully optimized with respect to processing parameters, but the framework for a stepwise improvement exists. We can as of today demonstrate the potentials of using continuous seismic threshold monitoring as a part of a global seismic verification system, but some caution has to be taken during the interpretation of the derived magnitude thresholds. Further improvements will rely heavily on the possibility of conducting extensive event analysis and associated calibration efforts.

T. Kværna
F. Ringdal
H. Iversen
N.H.K. Larsen

References

- Kværna, T. 1992: Continuous seismic threshold monitoring of the northern Novaya Zemlya test site: Long-term operational characteristics, Sci. Rep. No. 12, PL-TR-92-2118, Phillips Lab., Mass., USA.
- Kværna, T., F. Ringdal, H. Iversen and N.H.K. Larsen (1994a): A system for continuous global seismic threshold monitoring, Semiannual Tech. Summary, 1 Oct 93 - 31 Mar 94, NORSAR Sci. Rep. No. 2-93/94, Kjeller, Norway.
- Kværna, T., H. Iversen and N.H.L. Larsen (1994b): Continuous Seismic Threshold Monitoring User's Guide, NORSAR, Kjeller, Norway.
- Lilwall (1986): Empirical amplitude-distance / depth curves for short-period P waves in the distance range 20 to 180°, AWRE Report No. O 30/86.
- Ringdal, F. and J. Fyen (1979): Analysis of Global P-wave Attenuation Characteristics using ISC data files, Semiannual Tech. Summary, 1 Apr - 30 Sep 1979, NORSAR Sci. Rep. No. 1-79/80, Kjeller, Norway.
- Veith, K.F. and G.E. Clawson (1972): Magnitude from short-period P-wave data, *Bull. Seism. Soc. Am.*, 62, 435-453

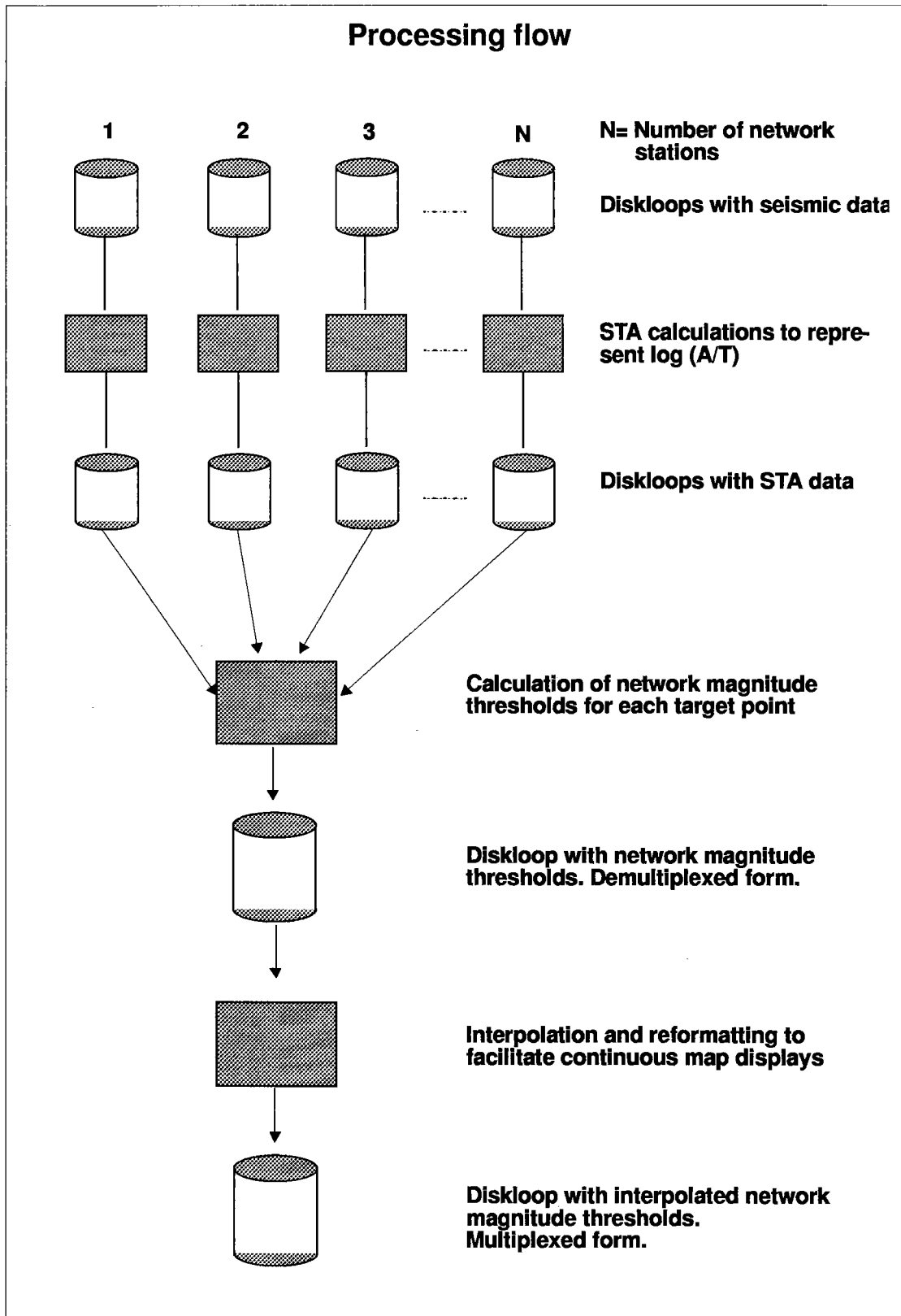


Fig. 7.1.1: Flowchart showing the structure of the continuous processing flow of the CSTM system

Interactive Analysis

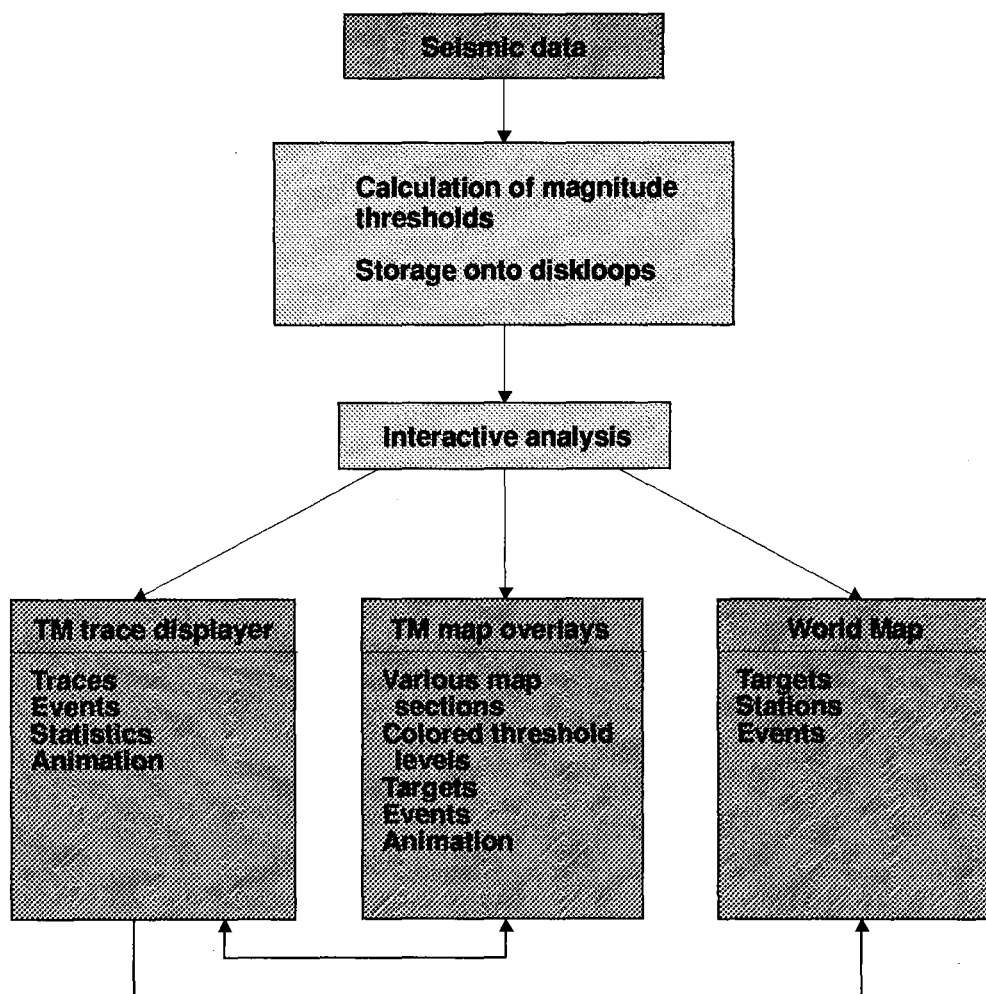
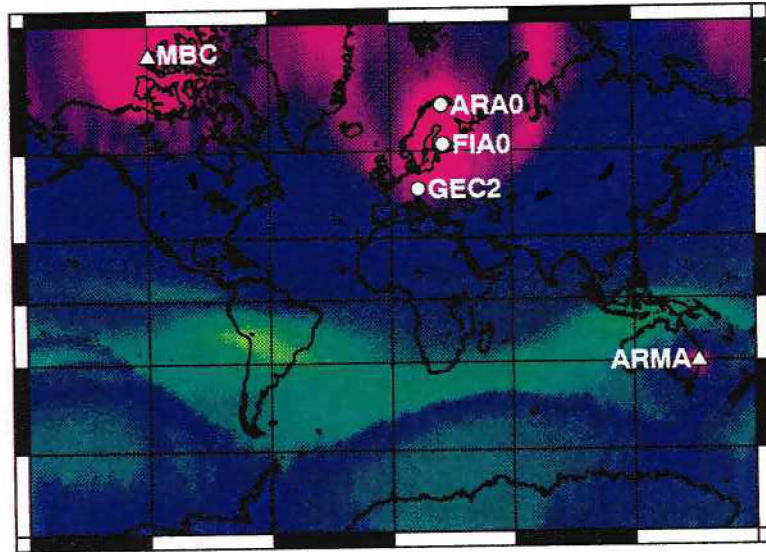
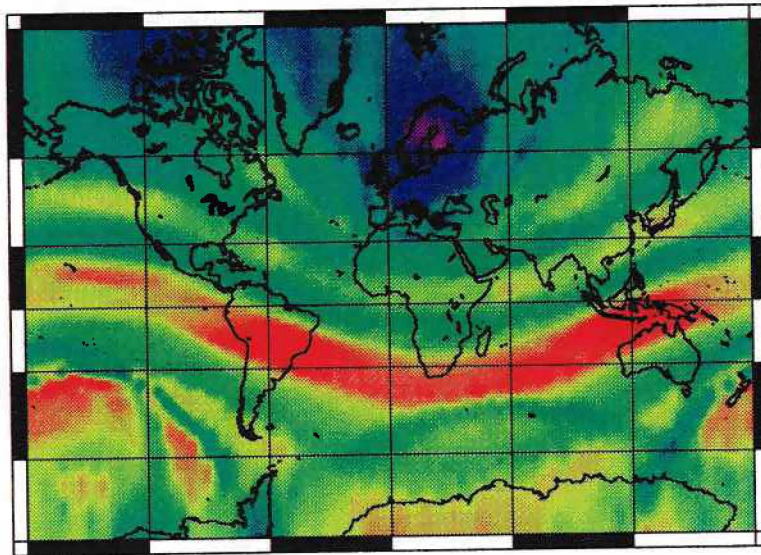


Fig. 7.1.2: Flowchart describing the functions of and interaction between the interactive modules of the CSTM system.

Noise



Coda



Event

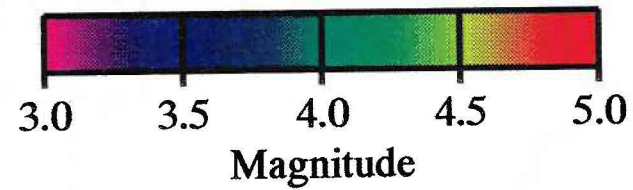
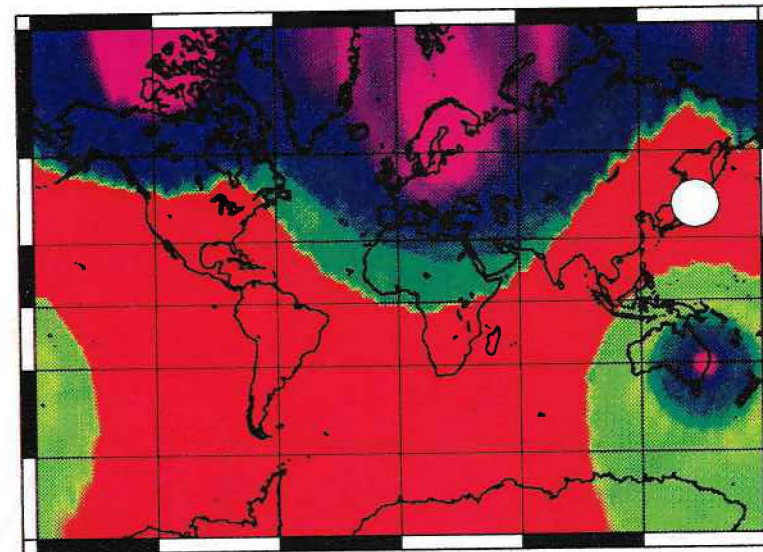


Fig. 7.1.3: Example of global magnitude threshold variations before, during and in the coda of the large Kurile Island event (Oct. 4, 1994, m_b 7.5). Data from the five stations plotted onto the upper left map section have been used to calculate the thresholds. During noise conditions (upper left map section) the thresholds vary from below 3.0 in the vicinity of the stations, to 4.5 in South America.

At the origin time of the event (the event location is shown in the upper right map section), the magnitude thresholds strongly exceed 5.0 in large parts of the world.

During the coda of the event (lower left map section), the thresholds start to fall back to normal (e.g., in Northern Europe).

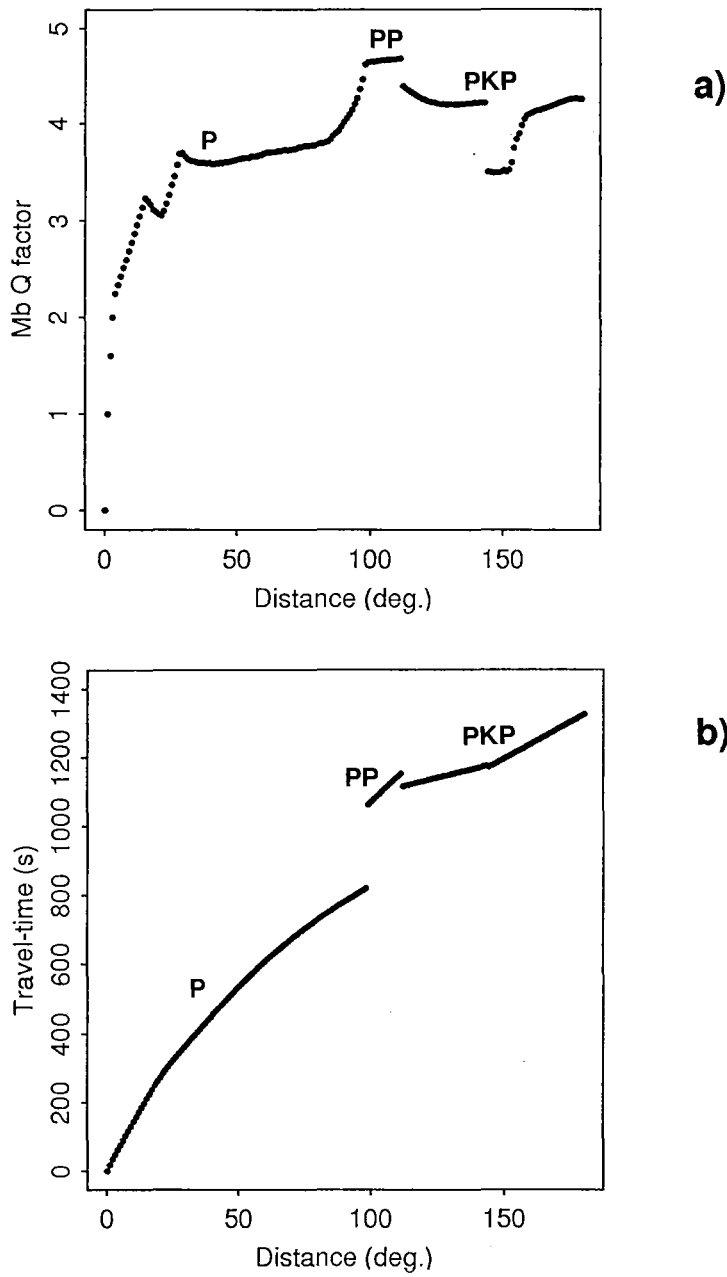


Fig. 7.1.4

- a) Global m_b attenuation relations used to calculate the magnitude thresholds. Notice that relations for three different phases (P, PP and PKP) have been used to span the 0 - 180 degrees distance range.
- b) Travel-times of the phases used for magnitude threshold calculations.

7.2 The Lop Nor nuclear explosions of 10 June and 7 October 1994

Introduction

This contribution describes observations made at our institution for the two Lop Nor nuclear explosions on 10 June and 7 October this year. Some comparisons are also made with the Lop Nor explosions conducted on 21 May 1992 and 5 October 1993.

The Lop Nor nuclear explosion of 10 June 1994

The explosion took place on 10 June 1994, with origin time 0626 GMT. Table 7.2.1 lists the basic parameters of the event as provided by various sources. The m_b magnitudes range from 5.68 to 5.84. The most accurate location is provided by the PDE bulletin, which uses a world-wide network for location purposes. The solutions by the Intelligent Monitoring System (IMS) (Bache et al, 1993), both automatic (IMS) and after analyst processing (ARS), are also listed. The NORSAR automatic and reprocessed solutions are included in the table. The NORSAR automatic detection/event processor output is shown in Fig. 7.2.1, whereas the plot associated with the reprocessed solution is shown in Fig. 7.2.2.

Figs. 7.2.3 and 7.2.4 show plots of the interactive IMS processing results. The trace plots of Fig. 7.2.4 are based on array beams for the four arrays FINESS, ARCESS, NORESS and GERESS, and a single channel (Z9, broad-band channel) for Apatity. The Spitsbergen array had a communication line problem at the time of this explosion.

Table 7.2.2 summarizes the automatic processing results for the six arrays. The NORESS, ARCESS and NORSAR arrays show outstanding SNR. The velocity/azimuth estimates are within the expected uncertainty for all arrays.

The Lop Nor nuclear explosion of 7 October 1994

The explosion took place on 7 October 1994, with origin time 0326 GMT. Table 7.2.3 lists the basic parameters of the event as provided by various sources. The m_b magnitudes range from 5.67 to 5.90. The most accurate location is again provided by the PDE bulletin, but the NORSAR Rerun solution is very close to the PDE solution. The solutions by the Intelligent Monitoring System, both automatic (IMS) and after analyst processing (ARS), are also listed. The NORSAR reprocessed solution is included in the table. The automatic NORSAR solution was wrong for this event. Although the EP-SigPro-estimated onset time and slowness for this event are precise, the event processing tried to associate coda detections, and in this case a bad coda detection was used for event definition.

Figs. 7.2.5 and 7.2.6 show plots of the interactive IMS processing results. The trace plots of Fig. 7.2.6 are based on array beams for the five arrays Apatity, ARCESS, NORESS, FINESS and GERESS, and a single channel (A0) for Spitsbergen.

Table 7.2.4 summarizes the automatic processing results for the six arrays. The NORESS array has the best signal-to-noise ratio (1231.1) for this event, and by extrapolation, this array would be expected to have a detectable signal for an event about 2.5 magnitude units lower.

Comparison with previous events

In the following we make a brief comparison between the two 1994 Lop Nor explosions dealt with above and the tests conducted at Lop Nor on 21 May 1992 and 5 October 1993.

Table 7.2.5 summarizes the PDE parameters for these four events. The 21 May 1992 explosion was significantly larger than the other three. The 1993 and 1994 explosions have very similar magnitudes, especially when estimated by IMS and the NORSAR array data. This similarity is illustrated in Fig. 7.2.7, which shows the NORESS P-wave recordings (AOZ seismometer) for the four events.

As seen in Tables 7.2.2 and 7.2.4, the NORESS STA/LTA values are, on the other hand, different by a factor of more than 2 for the two 1994 events, with the October event having the highest value. Since the signal amplitudes are very similar, this means that the NORESS noise level varied between the two 1994 events. The ARCESS STA/LTA values for the two 1994 events also differ by a factor of more than 2, but with the June event having the largest STA/LTA value. This finding is consistent with previous investigations about diurnal and seasonal noise variations at NORESS and ARCESS. These investigations have shown that NORESS is more exposed to cultural noise sources and also has an increased noise level during May-June due to snow melting. The June explosion occurred during working hours in Norway, while the October event occurred at 0426 a.m. local time in Norway. The STA/LTA variations for the other arrays are smaller.

**S. Mykkeltveit
U. Baadshaug
J. Fyen
B. Kr. Hokland**

Reference

Bache, T.C., S.R. Bratt, H.J. Swanger, G.W. Beall and F.K. Dashiell (1993): Knowledge-based interpretation of seismic data in the Intelligent Monitoring System, *Bull. Seism. Soc. Am.*, 83, 1507-1526.

Ref.	Origin time	Lat	Lon	m_b
IMS (automatic)	06.26.13.2	42.242	87.940	5.68
ARS	06.25.55.1	41.220	89.928	5.68
NORSAR (automatic)	06.25.47.3	40.540	91.870	5.84
NORSAR Rerun	06.25.59.7	41.600	88.600	5.82
PDE	06.25.58.0	41.570	88.702	5.70

Table 7.2.1. Location estimates by various systems of the 10 Jun 1994 Lop Nor nuclear explosion. Two of the estimates were made automatically (indicated in the table).

Array	Onset time	Res	STA/LTA	Vel	Res	Azi	Res
NORESS	161:06.34.46.7	0.6	538.2	18.0	3.5	80.4	4.2
ARCESS	161:06.33.56.4	0.1	893.6	13.8	0.1	91.2	-6.0
GERESS	161:06.35.06.4	-0.3	95.9	15.3	2.0	66.4	-1.7
Apatity	161:06.33.31.0	0.4	57.2	11.1	-2.2	85.6	-16.9
FINESS	161:06.33.50.5	0.6	160.0	13.7	-0.1	90.5	1.8
NORSAR	161:06.34.47.0	0.6	333.3	14.7	0.2	77.1	0.9

Table 7.2.2. Automatic detection list for the Lop Nor nuclear explosion 10 June 1994. The columns show array name, automatic EP-SigPro onset time, onset residual relative to PDE origin time, maximum signal-to-noise ratio (STA/LTA), apparent velocity (km/sec), residual in km/sec, back-azimuth in degrees, back-azimuth residual. All residuals are relative to predictions using IASPEI91 tables and PDE origin time and location.

Ref.	Origin time	Lat	Lon	m_b
IMS (automatic)	03.26.10.2	42.070	88.336	5.67
ARS	03.25.55.3	41.018	89.500	5.67
NORSAR Rerun	03.25.59.3	41.600	88.600	5.79
PDE	03.25.57.8	41.574	88.680	5.90

Table 7.2.3. Location estimates by various systems of the 7 October 1994 Lop Nor nuclear explosion. Two of the estimates were made automatically (indicated in the table).

Array	Onset time	Res	STA/LTA	Vel	Res	Azi	Res
NORESS	280:03.34.46.1	1.1	1231.1	16.1	1.6	77.8	1.6
ARCESS	280:03.33.56.0	0.4	418.1	15.0	1.3	78.9	18.3
GERESS	280:03.35.06.1	-0.1	122.8	16.1	1.3	67.3	0.8
FINESS	280:03.33.50.2	0.8	218.4	14.0	0.4	80.2	8.5
Apatity	280:03.33.30.3	1.0	194.9	13.5	0.3	95.7	-6.8
Spitsbergen	280:03.34.25.3	0.1	97.4	7.8	-6.3	95.0	-1.9
NORSAR	280:03.34.46.7	1.1	277.5	14.7	0.2	75.9	-0.3

Table 7.2.4. Automatic detection list for the Lop Nor nuclear explosion 7 October 1994.

The columns show array name, automatic EP-SigPro onset time, onset residual relative to PDE origin time, maximum signal-to-noise ratio (STA/LTA), apparent velocity (km/sec), residual in km/sec, back-azimuth in degrees, back-azimuth residual. All residuals are relative to predictions using IASPEI91 tables and PDE origin time and location.

Event	PDE parameters				IMS m_b	NORSAR Rerun m_b
	Origin time	Lat	Lon	m_b		
Lop Nor 92	21 May 92 04.59.57.5	41.604	88.813	6.5		
Lop Nor 93	05 Oct 93 01.59.56.5	41.647	88.681	5.9	5.65	5.83
Lop Nor 94a	10 Jun 94 06.25.58.0	41.570	88.702	5.7	5.68	5.82
Lop Nor 94b	07 Oct 94 03.25.57.8	41.574	88.680	5.9	5.67	5.79

Table 7.2.5. PDE parameters for four events discussed in the text.

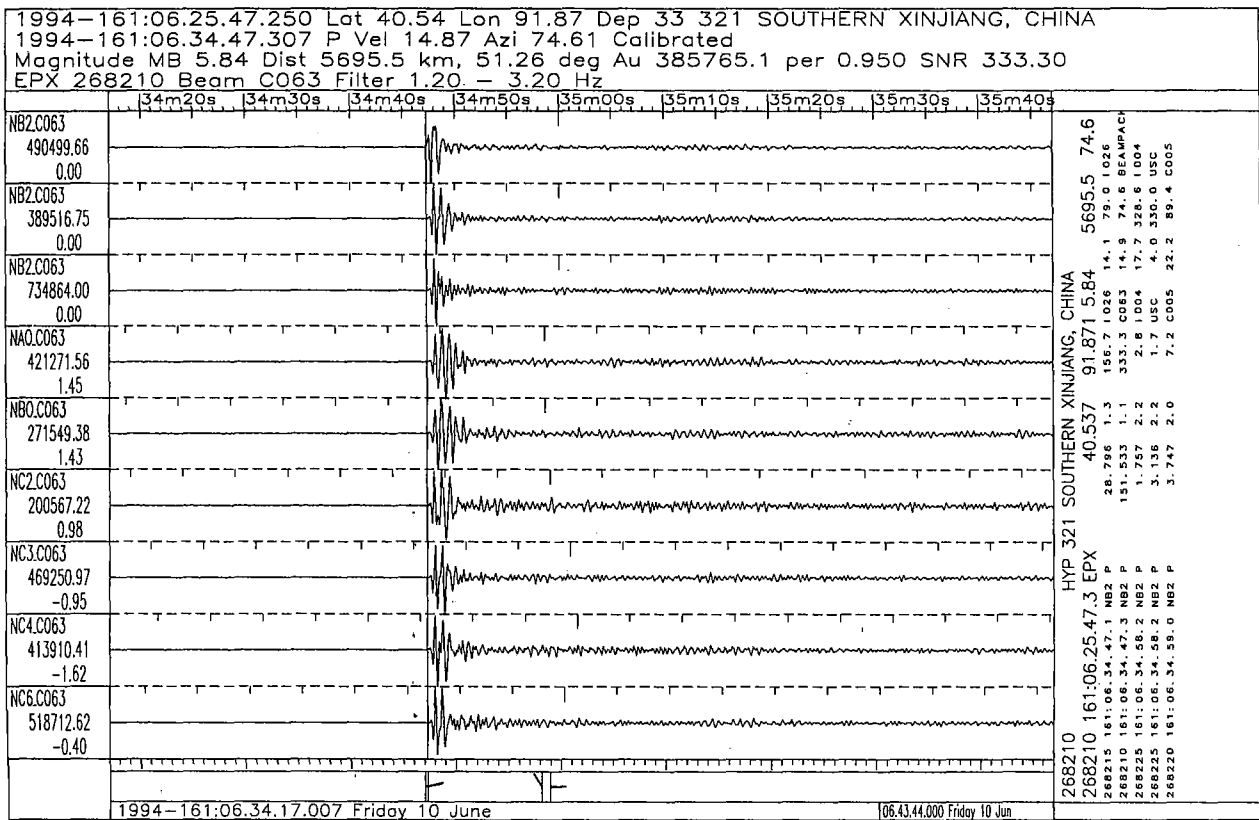


Fig. 7.2.1. Plot of the automatic NORSAR detection/event processor output for the Lop Nor nuclear explosion of 10 June 1994.

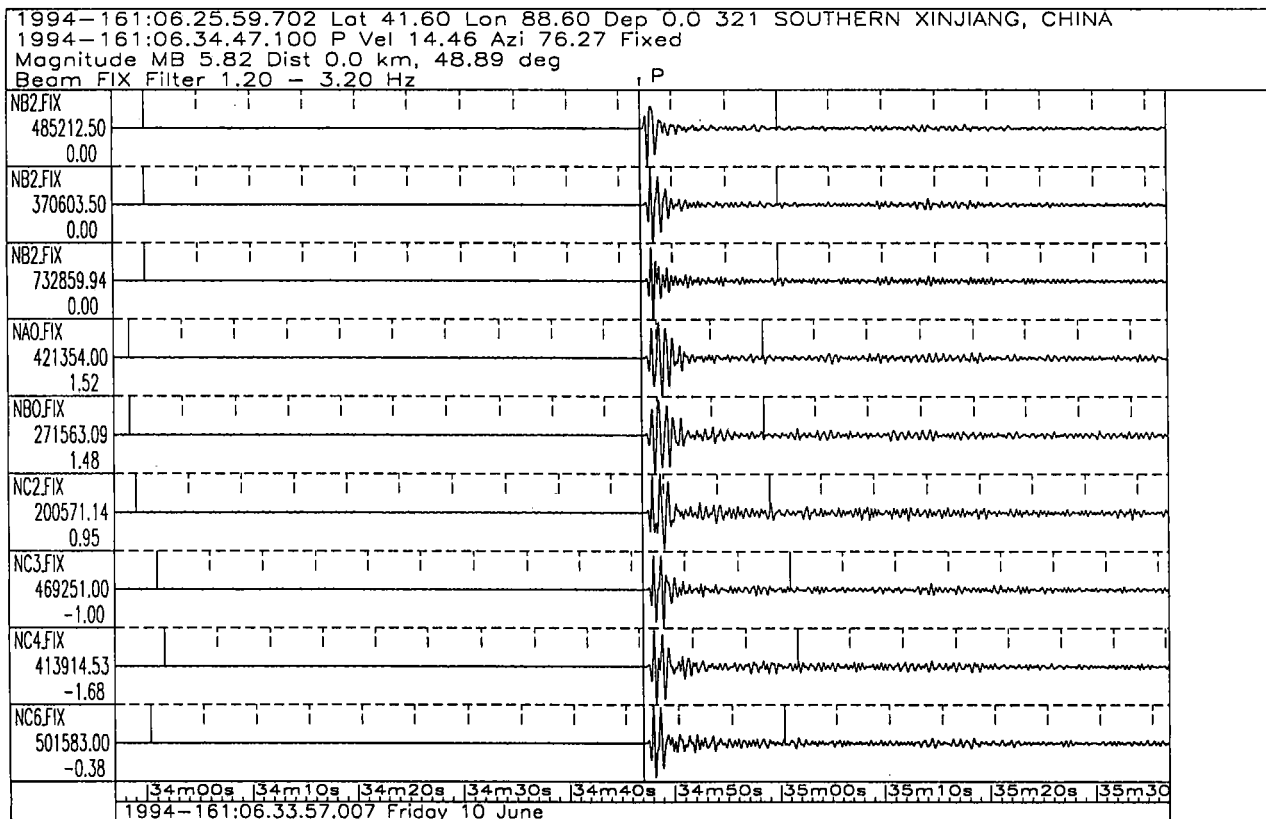


Fig. 7.2.2. Plot of the NORSAR reprocessed solution for the Lop Nor explosion of 10 June 1994.

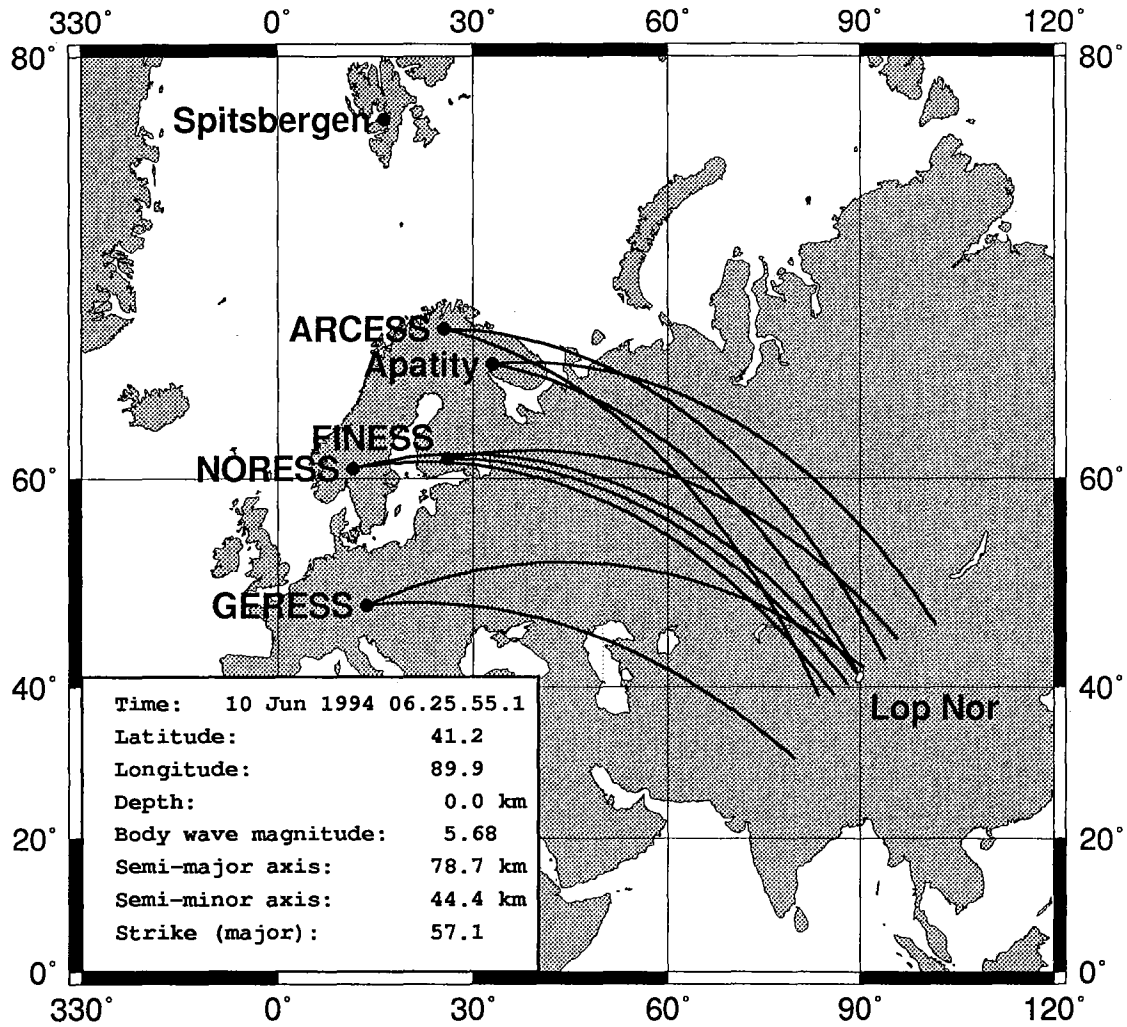


Fig. 7.2.3. Map showing the IMS solution (after analyst review) of the 10 June 1994 Lop Nor explosion. The great circle paths for the detecting arrays (based on P and PcP estimated azimuths) are also shown.

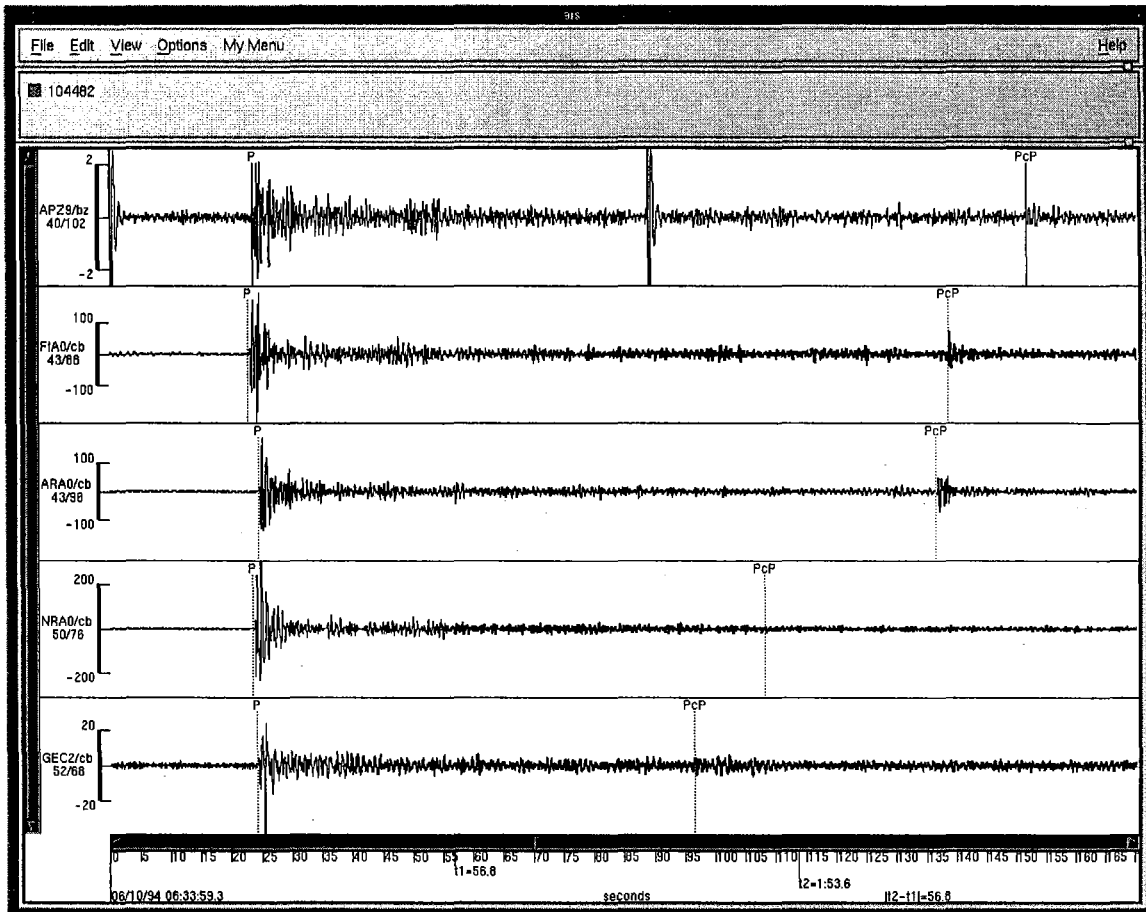


Fig. 7.2.4. P-phase waveforms of the 5 array traces (single sensor for Apatity, otherwise array beams) for the 10 June 1994 Lop Nor explosion.

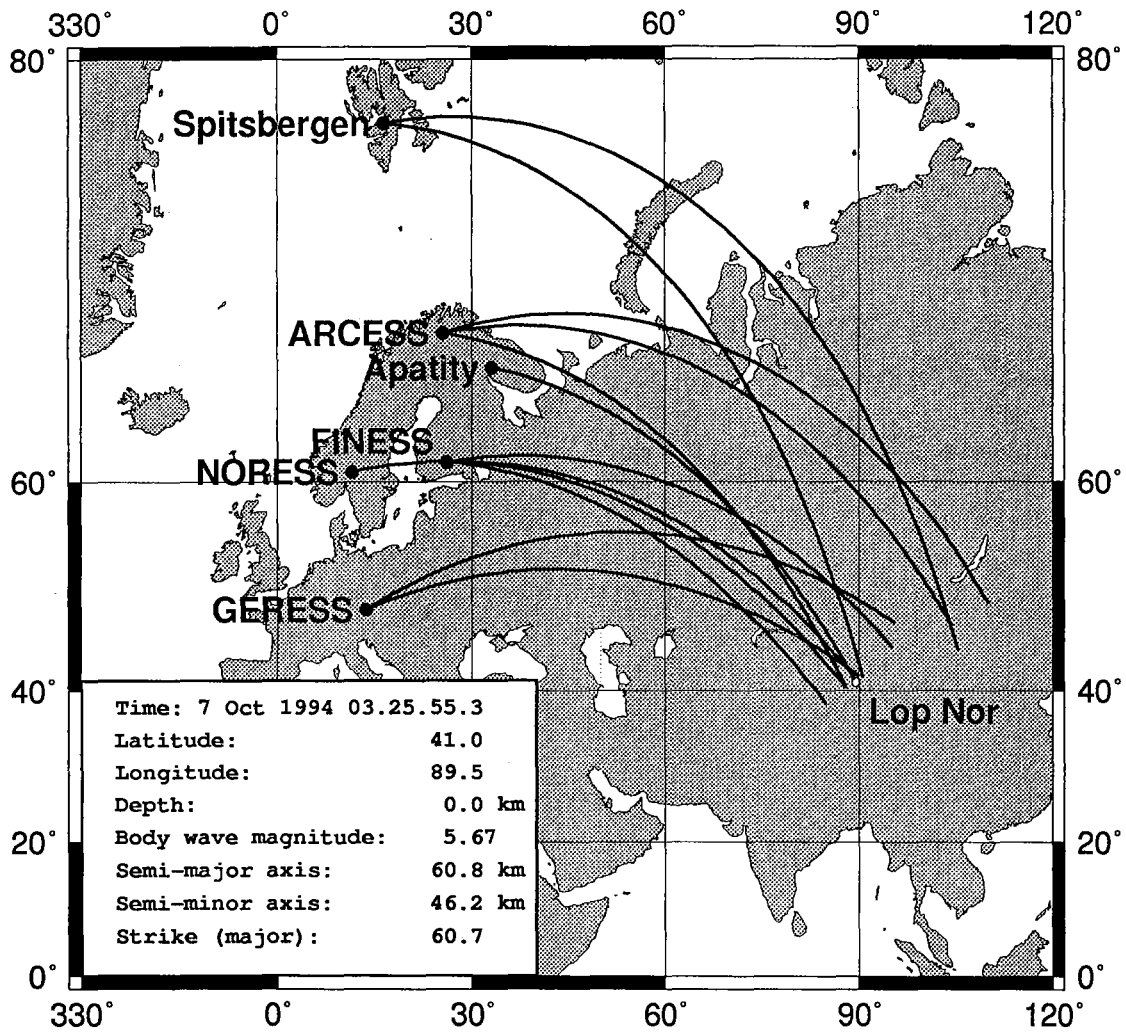


Fig. 7.2.5. Map showing the IMS solution (after analyst review) of the 7 October 1994 Lop Nor explosion. The great circle paths for the detecting arrays (based on P and PcP estimated azimuths) are also shown

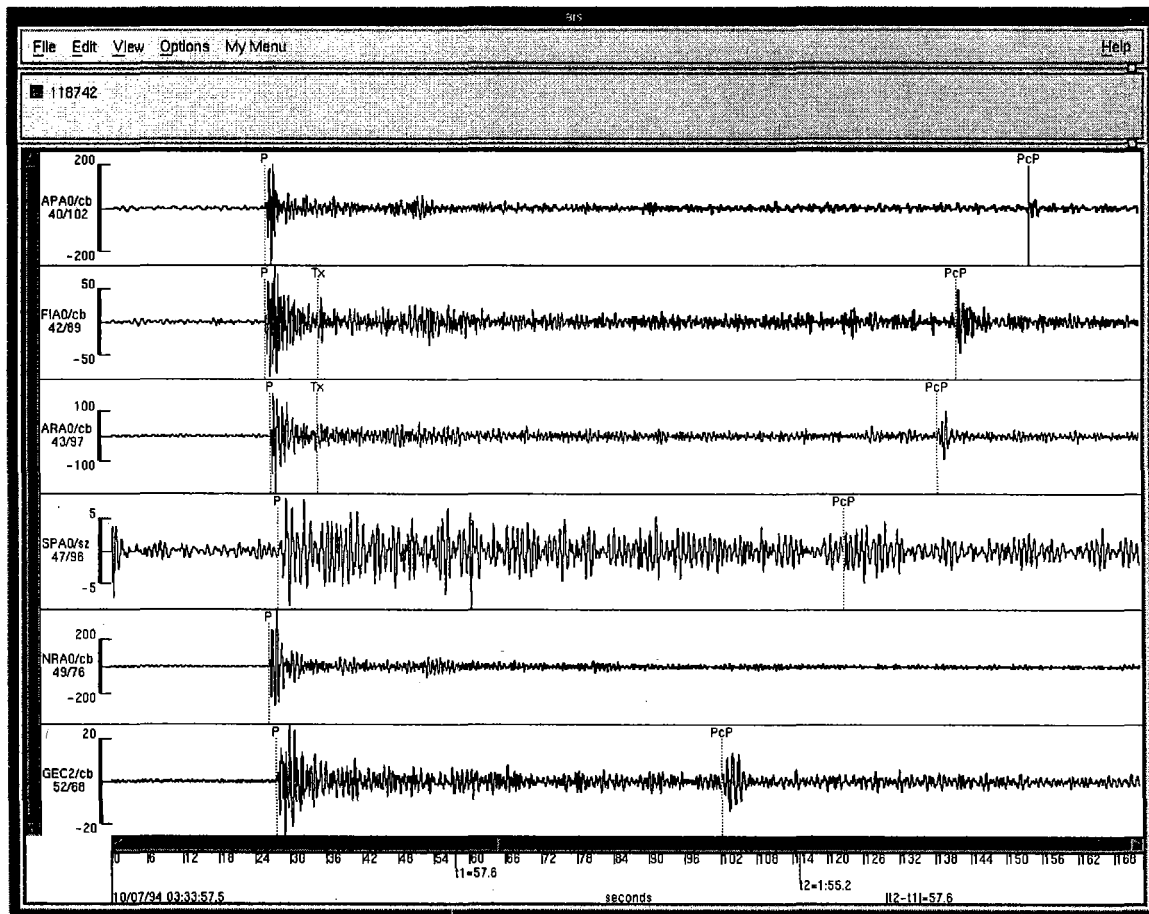


Fig. 7.2.6. P-phase waveforms of the six array traces (single sensor for Spitsbergen, otherwise array beams) for the 7 October 1994 Lop Nor explosion.

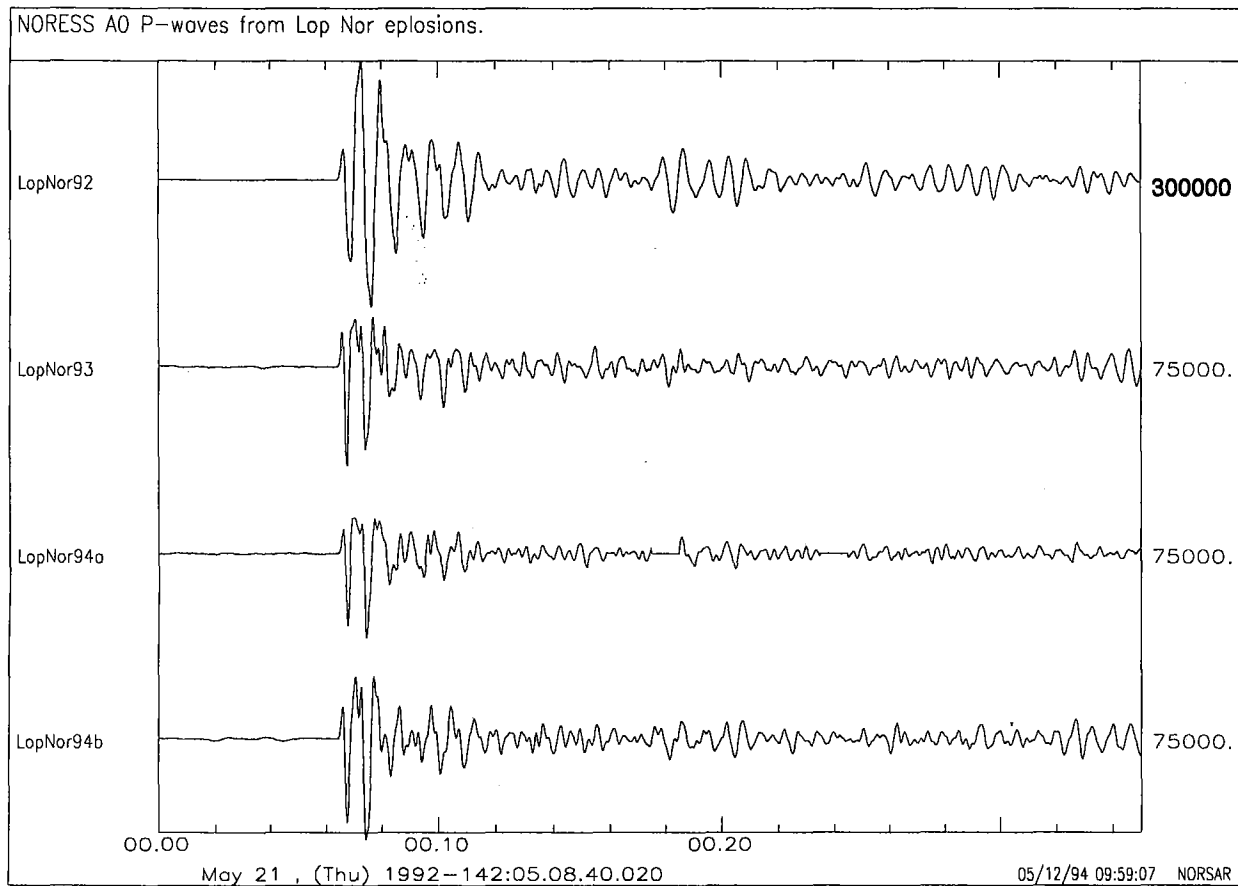


Fig. 7.2.7. NORESS P-waves (A0Z seismometer) for the four events discussed in the text. Note that the three lower traces are in the same scale, whereas the LopNor92 trace has a scaling factor that is different from the others. See Table 7.2.5 for magnitude estimates.

7.3 Combining NORSAR and NORESS processing

Introduction

The large aperture NORSAR array started operations in 1970 with 22 subarrays distributed over a diameter of 100 km. On October 1, 1976, the array was reduced to 7 subarrays with aperture about 60 km. Each subarray has 6 short period seismometers and the subarray aperture is about 8 km. During the years 1980-1981, experiments were performed with different subarray geometries to design a smaller array with good detection and location capabilities for local and regional events. As a consequence of this research, the NORESS array was constructed, and it became operational in 1984. The NORESS array has a diameter of 3 km and it is colocated with NORSAR subarray 06C. Figure 7.3.1 shows the geometry of the co-located arrays.

Throughout many years the NORSAR array has shown excellent detection and location capability. The analyst reviewed bulletin for the NORSAR array has been a significant contribution to the seismic community. The NORESS array has also shown very good detection capability for teleseismic events, as well as excellent detection and location capability for local and regional events. Moreover, automatic methods work very well for producing a bulletin of local and regional events. (Mykkeltveit and Bungum, 1984).

In this report we will demonstrate how to combine the two different processing techniques used for NORSAR and NORESS to improve the quality of an automatic teleseismic bulletin.

The method for detection of signals is identical for the two arrays. For slowness observations, f/k analysis can be used for the smaller array, due to the high correlation of the signals. For a large aperture array f/k analysis without time corrections does not work, and a beamforming (beampacking) method is used for slowness observation. (See NORSAR Sci. Rep. No 2-93/94).

In automatic detection procedures, many uninteresting signals are usually detected. For the NORESS array, it turns out that the f/k method normally gives apparent velocity values that are lower than R_g phase velocities for such detections, and these detections can therefore be classified as "noise detections", and do not represent real seismic phases from local, regional or teleseismic events. For the NORSAR array, the automatic method is based on a teleseismic beam deployment, and consequently always gives a resulting teleseismic slowness both for non-seismic disturbances and for local events.

An automatically produced bulletin of teleseismic events by this method is therefore less reliable than a corresponding local/regional automatic procedure using NORESS.

In the report mentioned earlier we discussed additional methods based on the NORSAR array alone to identify local events. In this report we will consider methods where NORESS automatic results are used to try to automatically identify false events in the automatic NORSAR bulletin.

NORESS automatic bulletin

An automatic NORESS bulletin with local and regional events is produced using the "EP_Ronapp" process (Fyen, 1987, 1989). For each event in the NORESS bulletin, we can predict arrivals in the NORSAR array. A simple rule is for each event to pick the first P-phase and the last S-phase arrival time and then define this as a time window. We then extend each end of the window with 20 seconds. For each such time window, we inspect the NORSAR detection list, and mark each phase arrival within the list as a potential local/regional phase.

In addition to definition of local/regional events, the NORESS automatic bulletin identifies teleseismic phase arrivals. A related issue is therefore to investigate the potential for using a NORESS defined teleseismic phase as basis for beamforming of the NORSAR and NORESS array. Another interesting aspect is to try to enhance a NORSAR defined teleseismic location by including NORESS in the process.

Data analysis

For selected data days during the period 4 August - 18 September 1994, we carefully inspected the automatic and reviewed bulletin for the NORSAR array together with the automatic bulletin for the NORESS array.

NORSAR events that the analyst do not include in the reviewed bulletin are routinely classified into the three classes 1) probable local event, 2) clear spike or non-seismic noise on one or more subarrays, and 3) ambiguous event with low SNR or secondary teleseismic phase.

By comparing the automatic NORESS bulletin with the automatic NORSAR bulletin, we "masked" all probable local/regional phases, using the simple time window rule defined above. Then we calculated statistics on:

- 1a) How many NORSAR defined events are correctly masked as probable local?
- 1b) How many NORSAR defined events are in-correctly masked as probable local?
- 1c) How many NORSAR defined events that are probably local are not masked?

In addition we looked at NORESS defined teleseismic phases and counted:

- 2a) How many are connected with NORSAR-defined teleseismic events?
- 2b) How many are not connected with NORSAR-defined teleseismic events?
- 2c) How many NORSAR teleseismic events are not connected with NORESS teleseismic phases?

Results

Table 7.3.1 shows the results of the bulletin analysis. We see that 36% of the automatically defined events are accepted as teleseismic events by the analyst. The remaining 64% of the events are either due to triggering from local disturbances within one subarray, or due to bad data conditions (spikes), or due to real local/regional events (but falsely detected as teleseismic by the automatic process).

64% of the local events are correctly identified by this simple masking rule, using the NORESS automatic bulletin. In this analysis we have not counted events where the Lg phase alone has been detected by NORESS. Only events that have been formed by association of a Pn/Pg phase and an Sn/Lg phase at NORESS have been used.

By combining the identified local events and the confirmed teleseismic events, we find that 42% of the NORSAR automatic detections are correctly classified. The remaining detections are mostly of low SNR or "spike" detections.

The analysis shows that 64% of the local events falsely reported as teleseismic events by the NORSAR automatic processor, can be masked automatically by inspecting the NORESS automatic bulletin.

Two real teleseismic events are masked out by this method. Both were in the coda of regional events.

75% of the real teleseismic events reported by NORSAR are also confirmed as such by the NORESS array. Thus, by combining NORESS and NORSAR defined teleseismic events, 75% of the NORSAR events can be confirmed automatically.

In addition, NORESS reports a significant number of teleseismic phases that are not detected with the current NORSAR beam deployment. This indicates a significant potential for improvement both by adjusting the NORSAR time delay corrections and by joint NORSAR/NORESS processing.

Conclusions

This study has shown that a clear improvement in the automatic NORSAR processing can be achieved by combining NORSAR and NORESS. By a simple masking algorithm, most of the NORSAR detected local and regional events can be identified as such using NORESS data. Furthermore, NORESS complements NORSAR by giving an "independent" confirmation of the majority of teleseismic phases. Even further improvements might be possible by joint beamforming techniques, although this has not been attempted in this study.

J. Fyen
B. Paulsen

References:

- Mykketveit, S. and H. Bungum (1984): Processing of regional events using data from small-aperture arrays, *Bull. Seism. Soc. Am.*, 74, 2313-2333.
- Fyen, J. (1987): Improvements and modifications, *NORSAR Semiannual Technical Summary, 1 Oct 1986 - 31 Mar 1987*, NORSAR Sci. rep. No. 2-86/87, Kjeller, Norway.
- Fyen, J. (1989): Event processor program package, *NORSAR Semiannual Technical Summary, 1 Oct 1988 - 31 Mar 1989*, NORSAR Sci. rep. No. 2-88/89, Kjeller, Norway.

Day #	1A Local	1B Local	1C Local	2A NRS	2B NRS	2C NB2	3A NB2	3B NB2	3C NB2	Number
1994	Masked	Error	NRS miss	Tele OK	Tele -	Tele	Accepted	Low SNR	False	EPX
209										
216	9	1	3	10	2	3	14	7	2	35
219	0	0	0	8	4	2	10	1	1	12
225	0	0	0	9	4	2	11	10	2	23
228	9	0	5	14	3	5	19	1	9	43
234	7	0	5	15	3	1	16	3	8	39
237	0	0	15	6	2	3	9	2	9	35
243	16	0	2	7	3	2	9	1	14	42
253	1	0	0	4	4	3	7	1	8	17
255	9	0	4	11	0	3	14	4	3	34
256	9	0	0	11	3	1	12	5	5	31
257	9	0	3	5	1	0	5	7	10	34
258	0	0	1	5	4	3	8	8	6	23
259	3	0	0	3	2	2	5	14	3	25
260	4	0	0	7	0	3	10	10	3	27
261	1	0	0	8	2	2	10	3	4	18
264	4	0	3	4	6	6	9	4	6	26
265	1	1	5	5	2	3	8	3	13	30
267	2	0	1	5	8	0	5	8	6	22
269	5	0	2	2	3	2	4	7	5	23

Sum 89 2 49 139 56 46 185 99 117 539

- 1A NORSAR defined events correctly marked as local 64.5% of local events
- 1B NORSAR accepted events that are in-correctly marked as probable local 1.1% of accepted events
- 1C NORSAR defined events that are probable local, but not marked as such 35.5% of local events
- 2A NORESS teleseismic phases connected with NORSAR accepted events 75.1% of accepted events
- 2B NORESS teleseismic phases that are not connected with NORSAR accepted events 30.3% of accepted events
- 2C NORSAR accepted events not connected with NORESS teleseismic phases 24.9% of accepted events
- 3A Total number of NORSAR accepted events 34.3% of all NORSAR events
- 3B Number of NORSAR defined events not reported due to low SNR or secondary phases 18.4% of all NORSAR events
- 3C Number of false NORSAR defined events due to noisy subarray(s) or spikes 21.7% of all NORSAR events
- Percentage of events that are correctly classified by combining NORESS and NORSAR 42.3% of all NORSAR events

Table 7.3.1. Results of the bulletin analysis.

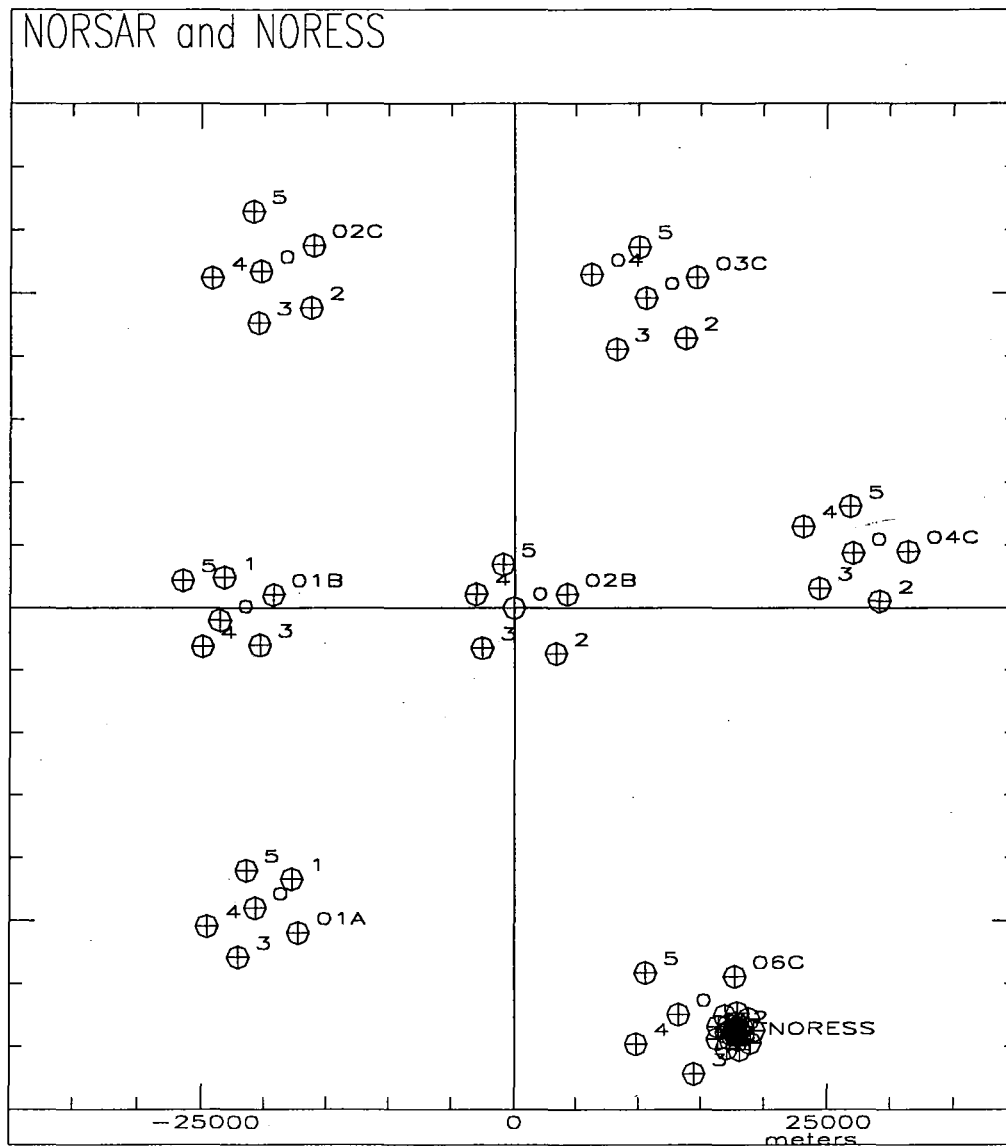


Fig. 7.3.1 The NORSAR and NORESS arrays.

7.4 Epicenter location and cratering at the Novaya Zemlya underground nuclear test site

In 1989 the Norwegian Institute of International Affairs (NUPI) started a satellite study of the northern underground nuclear test area on Novaya Zemlya. Results from this study were published in Skorve and Skogan (1992). Early in this work, using Landsat TM images, one craterlike feature was found close to the southwestern mountain slopes of the Matochkin Shar Strait. SPOT panchromatic 10 m resolution images were purchased, and these revealed three features, most probably craters that were created by underground nuclear explosions. This was unexpectedly confirmed when German aerial photographs of the Matochkin Shar from the summer of 1942 became available. The craters did not show up on these and thus proved that they were formed sometime after 1942. Fig. 7.4.1 is a spot photo from 1989 of the test area, showing the three craters. The aerial photo taken in 1942 is shown in Fig. 7.4.2.

The craters are lined up in a row approximately parallel to the Matochkin Shar coast. The northernmost crater ("N" in Fig. 7.4.1) is very well defined, being nearly circular and about 100 m in diameter. The middle one ("M" in Fig. 7.4.1) is by far the largest and appears roughly elliptical, measuring about 220 x 270 m. The reason for its irregular shape is probably that the epicenter is very close to the crest of the steep mountain slope down toward the Matochkin Shar coast. Following the underground explosion, parts of the mountain above the detonation center, big blocks of rock and boulders, slid down the slope. The crater to the south ("S" in Fig. 7.4.1) is about 75 m in diameter and is situated on a quite level mountain slope, not steep, facing the Shumilikha river. The obvious question was which underground explosions created these three craters. To check this, we plotted the locations of underground nuclear explosions on a map of the area. For underground tests made before the TTBT-agreement became effective in 1976, the epicenter locations were taken from Lilwall and Marshall (1986), while for the later ones, NORSAR provided the data. However, the uncertainty involved proved to be too large to make it possible to connect the craters to specific underground nuclear explosions in that area.

The Joint Epicenter Determination (JED) method, described in Lilwall and Marshall (1986) paper, that was used to improve location of epicenters, attracted our attention. The JED-method requires that at least one of the epicenters in the test area be restrained to predetermined values. The difficulty on Novaya Zemlya is that there is no information on true locations. The explosion on 29 September 1976 (event 14 in Lilwall and Marshall (1986)) was chosen as the constrained epicenter for the northern test site. It is well recorded and centrally placed with respect to the distribution of epicenters. Since the true location of event 14, "the origo point", is also uncertain, we thought the location of the craters found close to the Matochkin Shar could be used as new constrained epicenters for the northern test site to obtain more accurate location of the underground nuclear explosions on Novaya Zemlya. Two requirements have then to be met: determination of the exact coordinates of the crater centers and identification of which explosions caused the formation of the three craters. As mentioned earlier, the seismic location is too inaccurate to relate specific epicenters to the three craters. However, some time after the NUPI study (Skorve and Skogan, 1992) was published in 1992, collateral information emerged with information on which specific nuclear explosions caused the formation of the three craters. Additional

information is found in Matzko (1993), as it contains data on scaled depth of burial (SDOB) for the underground nuclear explosions on Novaya Zemlya. For all the three explosions that caused the formation of craters, SDOB was 90 m according to Matzko (1993).

The approximate depth of explosion can be calculated from the formula: $D = mY^{1/3}$, where D = approximate depth of explosion in meters, m = the scale depth in meters (=90 m) and Y = yield in kilotons (TNT equivalent). Measurements and calculated data on the Novaya Zemlya craters and their associated explosions are collected in Table 7.4.1. The yields given in this table are from Matzko (1993).

The location of the crater centers on SPOT satellite images can be measured with an accuracy of 2-3 pixels (20-30 meters). Unfortunately, it is presently not possible to transform this to the same degree of cartographical accuracy. This is due to the total lack of good topographical maps of the Matochkin Shar area. The best available map is at the scale of 1:500,000, which is clearly inadequate.

One alternative way to improve the geographical location of the craters is now being tried. The method uses the pixel and line coordinates measured on SPOT satellite images combined with ancillary data that is available on the leaderfile on SPOT digital data tapes. These are measurements made during the imaging process and include satellite position, satellite velocity, satellite attitude velocity, look angle of the imaging instrument and observation time.

Three digital SPOT scenes of the Novaya Zemlya northern underground nuclear test site were purchased. The pixel and line coordinates of the crater centers were measured for each of the SPOT scenes. The three separate sets of measurements were combined with their associated ancillary SPOT data. This procedure is illustrated for two of the SPOT scenes in Figs. 7.4.3 and 7.4.4. The preliminary results of geographical coordinate determination using this method are presented in Table 7.4.2.

The pixel/line measurements were made by Masahiro Etaya of TRIC, Tokyo, and Johnny Skorve, NUPI, while calculation of the crater center coordinates was made by Pål Bjerke, researcher at the Norwegian Defence Establishment (NDRE). The crater center coordinates can be derived by calculating the middle values of the three data sets.

The average inaccuracy of SPOT in this context is about 500 m and relates to uncertainties in satellite position and the look angle of the imaging instrument. Additional inaccuracy is added to this by the perspective effect when doing off-nadir imaging. The size of the effect is determined by the off-nadir look angle and the attitude above the sea level of the area or spot of interest.

J. Skorve, Norwegian Institute of International Affairs

References

- Lilwall, R.C. and P.D. Marshall (1986): Body Wave Magnitudes and Locations of Soviet Underground Explosions at the Novaya Zemlya Test Site. Atomic Weapons Research Establishment Rep. No. O 17/86, HM Stationary Office, London, England.
- Matzko, J.R. (1993): Physical environment of the underground nuclear test site on Novaya Zemlya, Russia. USGS Open-File Rep. 93-501, Reston, VA, USA.
- Skorve, J. and J.K. Skogan (1992): The NUPI Satellite Study of the Northern Underground Nuclear Test Area on Novaya Zemlya. NUPI Research Rep. No. 165, Oslo, Norway.

Crater	Approximate Dimension	Date of Detonation	Approximate Yield of Explosion	Approximate Depth of Explosion
Northern	Circular Diam.=100 m	28 Aug 1972	330 kt	620 m
Middle	Irregular 220x270 m	21 Oct 1967	95 kt	410 m
Southern	Nearly Circular Diam.=70 m	27 Oct 1966	420 kt	680 m

Table 7.4.1. Measurements and calculated data for the explosions associated with three craters described in the text. The approximate depth of explosion is calculated from the scaled depth of burial and yields given in Matzko (1993).

Crater	Pixel No.	Line No.	Crater Center Location	
SPOT Image 24 August 1989				
Northern	2263	1363	54:50:56 40 8146334	73:23:58 431423
Middle	2257	1425	54:50:08 40 8145892	73:23:45 450982
Southern	2230	1518	54:48:40 40 8245343	73:23:26 430176
SPOT Image 29 July 1990				
Northern	5031	4794	54:50:26 40 8146433	73:24:82 431157
Middle	5024	4854	54:49:42 40 8145978	73:23:47 430757
Southern	4989	4945	54:48:15 40 8145425	73:23:28 429948
SPOT Image 17 August 1992				
Northern	1861	3247	54:52:21 40 8145085	73:23:20 432127
Middle	1860	3309	54:51:36 40 8144624	73:23:05 431712
Southern	1831	3401	54:50:03 40 8144127	73:22:48 430874

Table 7.4.2. Crater center locations for the three craters described in the text. The coordinates are estimated from three SPOT scenes, from 1989, 1990 and 1992, respectively. The crater locations are given in geographical coordinates (degrees: minutes: seconds) and in the Universal Transverse Mercator (UTM) grid.



Fig. 7.4.1. This enlargement of a SPOT photo taken in August of 1989 covers the Matochkin Shar strait of Novaya Zemlya from the Shumlikha delta and about 8 km north-eastward. The Severny Base is seen in the middle of the lower part of the picture. The craters found on this picture (denoted "N" for northern, "M" for middle, and "S" for southern) are seen as white or partly white spots because of snow left inside their boundaries. (PHOTO: SPOT IMAGE; IMAGE PRODUCTION: TRIC: TOKYO)



Fig. 7.4.2. The area shown on this mosaic of two Luftwaffe aerial photos from 1942 is the same as that of Fig. 7.4.1. There is no trace of the three craters seen on Fig. 7.4.1. (PHOTOS: GERMAN LUFTWAFFE)

SPOT IMAGE, AUGUST 24 1989

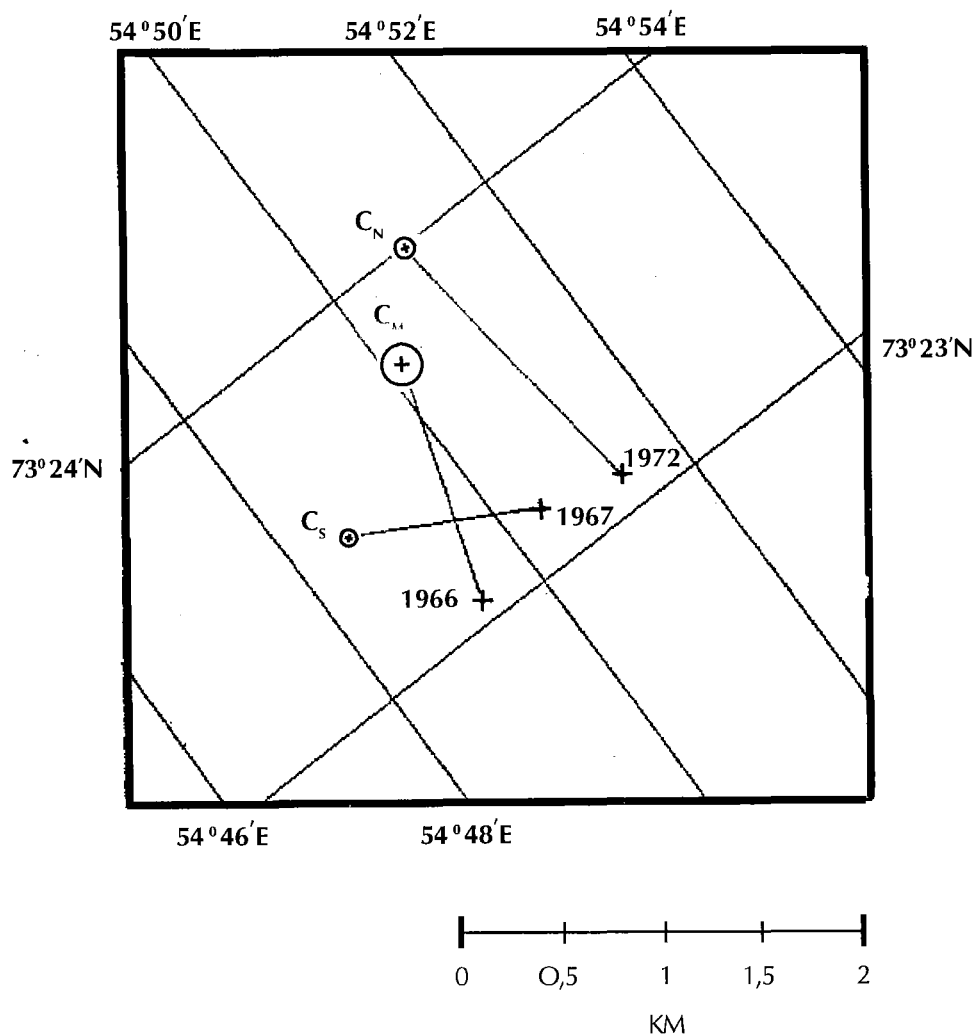


Fig. 7.4.3. Crater center locations based on the SPOT scene from 24 August 1989. The position of the coordinate grid is based on ancillary data available on the SPOT digital data tape, as explained in the text. The epicenters of the associated explosions are from Lilwall and Marshall (1986). Note that the southernmost epicenter location (1966) does not correspond to the southernmost crater.

SPOT IMAGE, JULY 26 1990

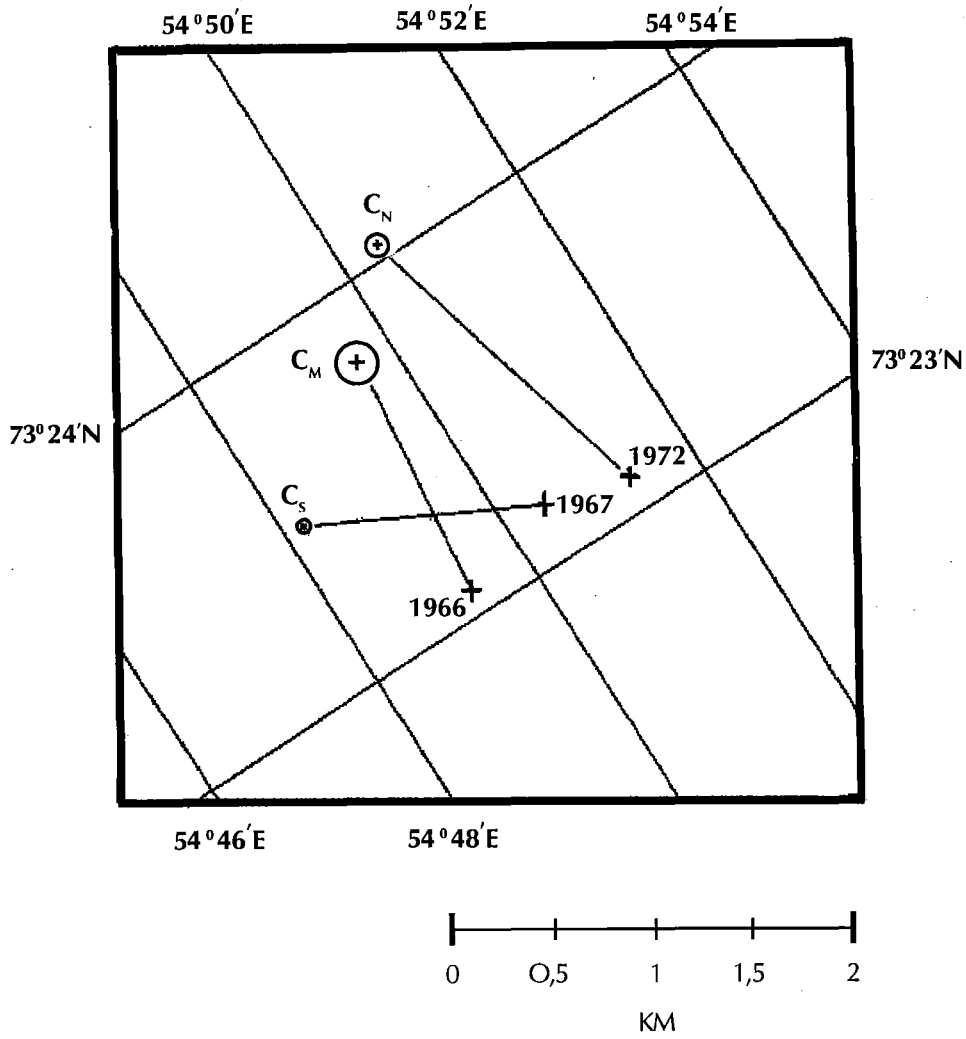


Fig. 7.4.4. Same as Fig. 7.4.3, but here based on the SPOT scene from 26 July 1990.

7.5 Mislocation vectors for small aperture arrays - a first step towards calibrating GSETT-3 stations

Introduction

At NORSAR small aperture arrays have been used for many years to locate seismic events either with onsets at single arrays or with a common interpretation of detections from all available arrays. In this context automatically calculated ray parameter and azimuth values play an important role. It is well known that some observed data show systematic deviations from theoretically expected values, and it is also well known that single data from known source regions show a large scatter. Whatever the reason is for these deviations, they influence the quality of all event locations based on automatically estimated parameters. In this study the phrase "slowness" is always used for the total length of the slowness vector derived from ray parameter and azimuth. Estimation of systematic slowness deviations and statistical information about the scatter of individually measured slowness values are part of the generally needed calibration of all seismic stations of the GSETT-3 network to correct the input to the location procedures. Therefore the data base of all detected phases from all six small aperture arrays for which data are recorded and processed at NORSAR, was investigated to search for systematic patterns in slowness deviations.

Data bases used

At NORSAR the earliest automatically estimated fk-results are available since Jan 1, 1989. To obtain deviations from theoretically expected values a list of reference events is needed. Therefore such a list was compiled for the time period Jan 1, 1989 to June 30, 1994, which was chosen as the end time of this study. Main sources for this list were the bulletins of ISC and PDE. But because these bulletins are not complete for all observable smaller events in Europe, the following local and regional catalogues from Europe were added: for Scandinavia the bulletins of the Seismological Institutes in Helsinki and Bergen, a list of confirmed quarry blasts from the Kola peninsula, for Central Europe a local Bulletin of the Vogtland / Western Bohemian region of earthquake swarms, a list of precisely located events from the Polish mining areas, and a list of confirmed quarry blasts in Bavaria / Germany and in the Czech Republic (for details see Table 7.5.1). All these event lists were merged together, and double entries were carefully eliminated. Table 7.5.1 also gives information about the amount of contributions from each source to the final list of 157 825 reference events.

For all these events, their theoretical onset times as well as predicted slowness values were calculated and compared with automatically estimated values from detections at the arrays investigated. The availability of the fk-results is not the same for all arrays and reflects mostly the successive extension of the European array network (Table 7.5.2).

Association of observed onsets with theoretically estimated onsets

To get reliable mislocation vectors the association criteria must be carefully defined. In this study the following procedure was chosen:

- a) For each event in the list of reference events azimuth and distance were calculated with respect to the observing arrays.
- b) To get an optimum coverage of the slowness space it is of interest to compare all theoretical arrivals with detected onsets. Using distance, depth, and event origin time, the absolute onset times of all seismic phases as included in the IASP91 tables (Kennett and Engdahl, 1991) were calculated for all arrays considered. To reduce the number of erroneous associations some restrictions related to epicentral distance and event magnitude were introduced, some secondary onsets were only associated if an earlier phase of the same event was also associable, and additionally, all theoretical phases to be considered for comparison with observed ones must be separated in time by at least 3 seconds. The list of used phases with the restrictions that apply is given in Table 7.5.3.
- c) These list of onsets for every event was then compared with detections and SigPro-results for each array. For GERESS, the SigPro-results from the processing in Bochum since November 9, 1990 were used instead of the results at NORSAR because of completeness and data quality. To define a theoretically expected phase as observed the residual between detected and theoretically estimated onset time must be less than 10 seconds and the absolute slowness residual must be less than 10 s/deg. In the case of more than one detection in this time interval of +/- 10 seconds around the theoretical onset, the onset with the smallest travel time residual and an acceptable slowness residual was associated. Sometimes, onsets of two or more events have approximately the same arrival time at a seismic station and the list of associations had to be checked for such situations. In such cases all associations were discarded from further use.
- d) In a final step, the quality of associations was increased by applying even more restrictive criteria. For P-type onsets no association was used with a larger travel time residual than 4 seconds or a slowness residual of more than 4 s/deg. For the investigated crustal S-type onsets these values were increased to 8 seconds and 8 s/deg respectively, because of larger uncertainty of onset time estimates and larger scatter of observed slowness values for S-type onsets. High frequent noise is often interpreted by the automatic fk-analysis as a teleseismic P-phase. To eliminate these errors high frequency (> 4 Hz) onsets with a ray parameter less than 10 s/deg were not used.

Especially the arrays with a smaller aperture (Apatity, FINESS, and Spitsbergen) had a remarkable number of onsets with large slowness residuals due to lower slowness resolution and less redundancy in the data. In contrast, the array with the largest aperture (GERESS) had the smallest loss of associations due to this point. The influence of high frequency noise was relatively equal for all Scandinavian arrays but neglectable for GERESS due to differences in the detector/SigPro recipes at NORSAR and in Bochum. The restriction to smaller travel time residuals reduced the data for all arrays only slightly.

In summary, these restrictions led to a smaller but more stable set of observed mislocation vectors (compare first and second column in Table 7.5.4). Figure 7.5.1 shows for NORESS all 26 083 used slowness values and gives an impression of the coverage of the slowness space and the scatter of the data. On the top all observed slowness values are seen and at the bottom all corresponding theoretical values are plotted. The circular pattern for large slowness values for the theoretical case (bottom part of figure) is associated with the crustal layering in the IASP91 model.

Mean mislocation vectors

Because of the scatter in single observations it became necessary to calculate mean mislocation vectors. For that the slowness space was divided into 1849 bins and all mislocation vectors were averaged per bin. To divide the slowness space into approximately equally sized areas, the size of the bins varied for different ray parameters between 1 s/deg times 30 deg and 2 s/deg times 5 deg. In this study only mislocation vectors are shown which are based on at least 3 observations in one bin (compare Figs. 7.5.1 and Fig. 7.5.6 which show single observations and mean mislocation vectors for NORESS, respectively). Besides the mean mislocation vectors also corresponding standard deviations were calculated for the observed azimuth and ray parameter values. These standard deviations can be used to weight single observations in further studies. Table 7.5.4 gives for all arrays the mean values of the single mislocation vectors and the mean scatter of the ray parameter and azimuth values before and after applying the slowness corrections. This slowness correction amounts to subtracting the mean mislocation vectors from the observed slowness values within each bin. In comparing columns 3 and 6 of Table 7.5.4 one can see the significant reduction of between 25% and 40% for the mean values of the single mislocation vectors after slowness corrections have been applied.

No explicit relation can be given between observation and theory. So two different types of mislocation vectors can be calculated depending on which slowness value was used as reference for defining the corresponding bin. The first type of vector points from the observations (e.g. as in Fig. 7.5.1 on the top) to the most likely "true" value (the theoretical slowness values shown e.g. in Fig 7.5.1 at the bottom) and the second type points from the theoretical slowness (as in Fig. 7.5.1 at the bottom) to the most likely observed value (i.e. the expected slowness value at the array; see, e.g., Fig 7.5.1 on the top). The latter can predict systematic mislocation errors but not the scatter which is caused by too low slowness resolution or noise. The two types of mislocation vectors are useful for different applications. Figs. 7.5.2 - 7.5.7 show the mislocation vectors for each array. For each figure, the top part shows the observed mislocations (first type) and the bottom part the predicted (second type) mislocations. The symbol size corresponds to the number of single mislocation vectors which were observed per bin and the vectors plotted have to be added to the reference value to get the corrected azimuth and ray parameter.

The figures clearly show that for a sufficient coverage of the slowness space with mislocation vectors a long observing period is needed. This is not only because the seismicity distribution of the Earth is changing by time but also gaps due to station problems must be filled. For the two arrays at Apatity and Spitsbergen which have suffered from problems with data quality and data acquisition, an operation period of about 2.5 years is not long

enough. Unfortunately, these two arrays also have the largest problems with low slowness resolution due to their very small aperture. So the estimation of a sufficient set of mislocation vectors will need several more years of data for these arrays. However, the results for the Apatity array can be used as a first approximation and the results for the Spitsbergen array are shown here for completeness.

Finally, the following question was investigated: How relevant are mislocation vectors that are based on automatically estimated slowness values? At the Institute of Geophysics at Bochum many results of the automatic fk-analysis are reviewed by seismologists, and the values are recomputed following inspection of the data. Such reviewed results are available since April 1991 mostly for P-type onsets with a ray parameter less than 10 s/deg (see Table 7.5.2). For this set of data mislocation vectors can also be estimated and compared with the results for the automatic computations. Fig. 7.5.8 shows these mislocation vectors at the bottom for the reviewed data and on top for the corresponding subset of the automatically estimated data from Fig. 7.5.5. The scatter in the reviewed data is about 8% less (see Table 7.5.4 last two rows). But the main features are very similar in the two plots and the differences between the two mislocation sets are mostly for bins with a small number of observations (smaller symbols). This confirms the use of automatically estimated slowness values in location procedures and shows that the mislocation vectors demonstrated in this paper for small aperture arrays are not the result of some arbitrary processes.

Conclusion

Although a large scatter was observed for single mislocations, mean mislocation vectors could be defined and estimated with their standard deviations for all arrays. These mislocation vectors can now be used regularly to correct automatically estimated slowness and azimuth values. A reduction of the scatter for single observations and a correction for mean mislocation errors is especially needed for single array location routines and for IMS like location algorithms. The predicted mislocation vectors are helpful for estimating better values for the GBF-method. These vectors can also be used to investigate systematic deviations between the used velocity model IASP91 and the velocity structure under the arrays.

J. Schweitzer

References

- Kennett, B. L. N. and E. R. Engdahl (1991): Travel times for global earthquake location and phase identification, *Geophys. Journ. Int.*, 105, 429-466.
- Mykkeltveit, S (1992): Mining explosions in the Khibiny Massif (Kola peninsula of Russia) recorded at the Apatity three-component station, Report PL-TR-92-2253, Phillips Laboratory, Hanscom AFB, Ma, USA.

Bulletin	Time period	Number of events	Remarks
ISC	Jan 1, 1989 - Jul 31, 1992	120 716	
PDE monthly	Mar 1, 1990 - Dec 31, 1993	26 484	
PDE weekly	Jan 1, 1994 - Jun 30, 1994	4 905	
Helsinki	Jan 1, 1989 - Jun 30, 1994	3 429	
Bergen	Jan 1, 1989 - Mar 31, 1994	1 319	
Polish mines	Jun 27, 1990 - Jun 12, 1992	418	P. Wiejacz and J. Niewiadomski (both Polish Academy of Sciences, Warsaw) several pers. communications in 1991 and 1992
Bavarian & Czech quarries	Jan 9, 1991 - Oct 14, 1992	285	Compiled at the Institute of Geophysics at Ruhr-University Bochum, supported by several pers. communications with J. Zednik (Czech Academy of Sciences, Praha) in 1992
Kola quarries	Jun 15, 1991 - Oct 23, 1992	195	Mykkeltveit (1992)
Vogtland	Jan 31, 1991 - Nov 16, 1992	74	Bulletin of the Vogtland / Western Bohemian earthquakes, ed. by H. Neunhoefer, University of Jena
Sum	Jan 1, 1989 - Jun 30, 1994	157 825	

Table 7.5.1: Contributions of the different bulletins to the list of reference events.

Array	Analyzed time period
Apatity	May 31, 1992 - Jun 30, 1994
ARCESS	Jan 1, 1989 - Jun 30, 1994
FINESS	Nov 23, 1989 - Jun 30, 1994
GERESS	Oct 17, 1990 - Jun 30, 1994
GERESSr	Apr 22, 1991 - Jun 30, 1994
NORESS	Jan 28, 1989 - Jun 30, 1994
Spitsbergen	Nov 23, 1992 - Jun 30, 1994

Table 7.5.2: Time periods of investigated fk-results for the various small aperture arrays. Additionally, for GERESS a data set of analyst-reviewed fk results could be investigated (GERESSr).

Phase	Restrictions
Pg, Sg	del < 10 deg
PgPg, SgSg	4 deg ≤ del < 10 deg; *
Pb, Sb	del < 15 deg
PbPb, SbSb	4 deg ≤ del < 15 deg; *
Pn, Sn	---
PnPn, SnSn	4 deg ≤ del < 18 deg; (SnSn *)
P, pP, sP	---
PcP, ScP	10 deg ≤ del; mag; *
Pdiff	110 deg ≤ del
pPdiff, sPdiff	110 deg ≤ del; if magnitude < 4.0 then *
PKiKP	del ≥ 80 deg
pPKiKP, sPKiKP	del ≥ 80 deg; if magnitude < 4.0 then *
PKP, pPKP, sPKP, SKP	---
PKKP	del ≥ 30 deg; mag; * P'P' mag; *

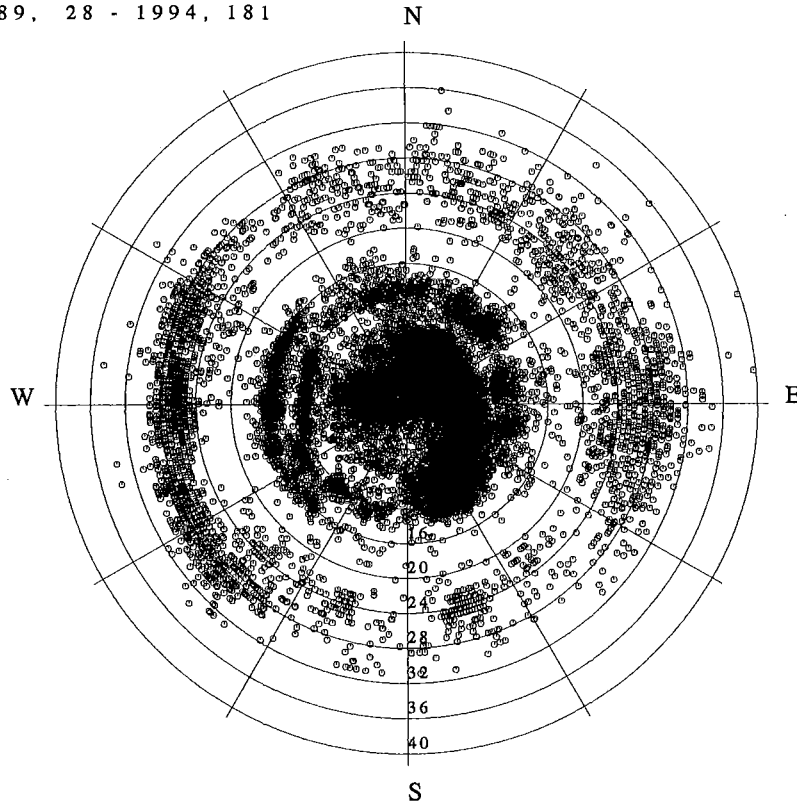
Table 7.5.3: Phases for which ray parameter and azimuth values were used in this study to estimate the mislocation vectors. For core phases all branches were used (i.e., ab, bc, and df). mag = phase was used only if event magnitude was not lower than 4.0; * = phase was used only if another earlier onset from the same event was observed. del = distance.

Array	No. of detections		Mean scatter			Mean scatter after slowness corrections		
	Associated	Used	Slowness	Ray parameters	Azim.	Slowness	Ray parameter	Azim.
			[s/deg]	[s/deg]	[deg]	[s/deg]	[s/deg]	[deg]
Apatity	3 654	1 882	2.77	2.24	19.44	1.66	1.51	14.45
ARCESS	42 521	29 738	1.87	1.65	21.83	1.32	1.11	18.99
FINESS	22 798	15 482	2.20	1.79	23.99	1.59	1.28	21.74
GERESS	23 499	17 852	2.00	1.77	23.97	1.47	1.29	20.64
NORESS	34 987	26 083	2.09	1.85	17.01	1.56	1.36	15.58
Spitsbergen	1 267	253	1.89	1.96	27.46	1.25	0.94	22.73
GERESSr		8 000	1.54	1.28	26.97	1.29	1.08	22.91
GERESSa		10 579	1.66	1.40	30.75	1.42	1.16	26.33

Table 7.5.4: Some numerical results of the mislocation study. GERESSr gives the results for analyst-reviewed P-type onsets (ray parameter ≤ 10 s/deg) and GERESSa is the corresponding subset of the automatically estimated data from GERESS (see text and Fig. 7.5.8).

OBSERVED RAY PARAMETER AND AZIMUTH VALUES

NRA0 1989, 28 - 1994, 181



THEORETICAL RAY PARAMETER AND AZIMUTH VALUES

NRA0 1989, 28 - 1994, 181

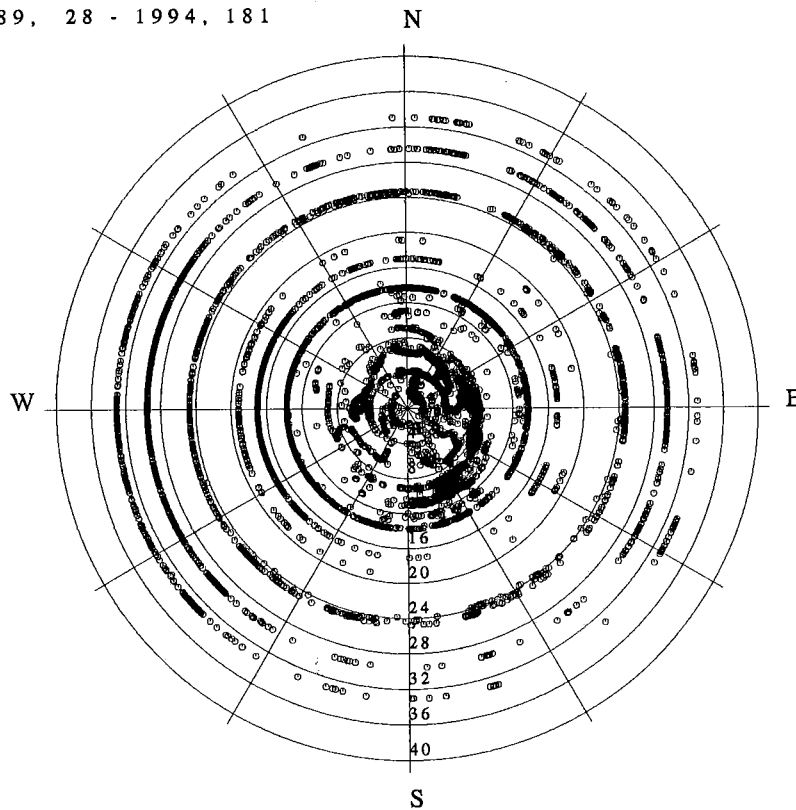
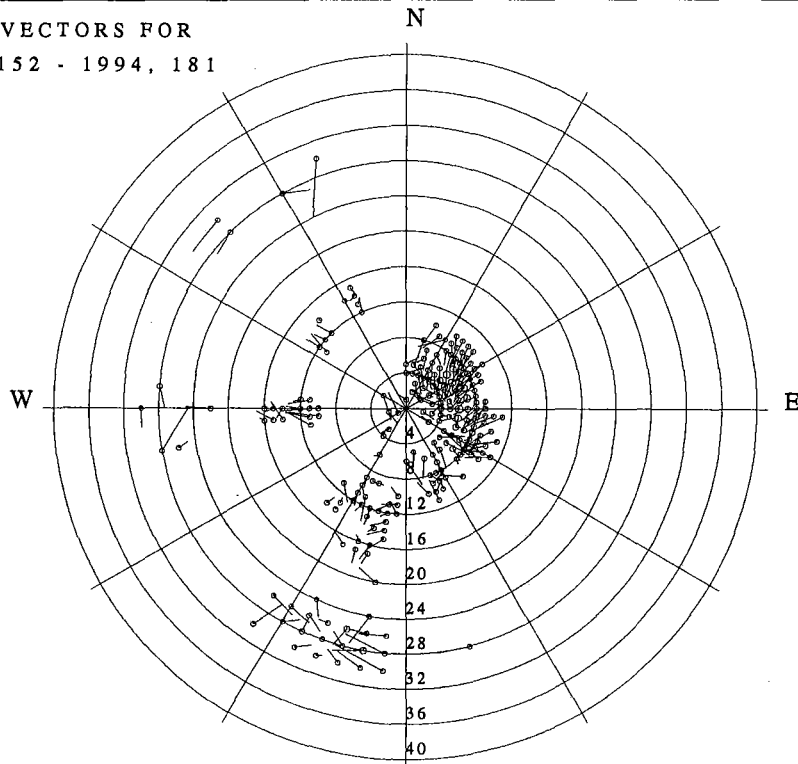


Fig. 7.5.1: The upper plot shows all 26 083 NORESS slowness observations used in this study and at the bottom all corresponding theoretical slowness values are seen.

CORRECTION VECTORS FOR
 APA0 1992, 152 - 1994, 181



CORRECTION VECTORS FOR
 APA0 1992, 152 - 1994, 181

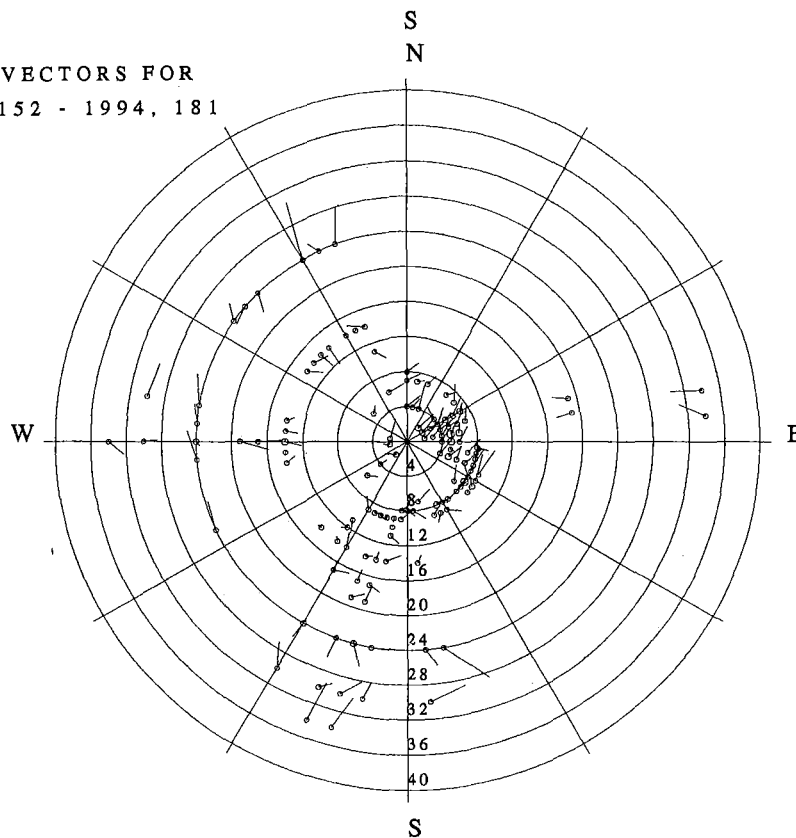
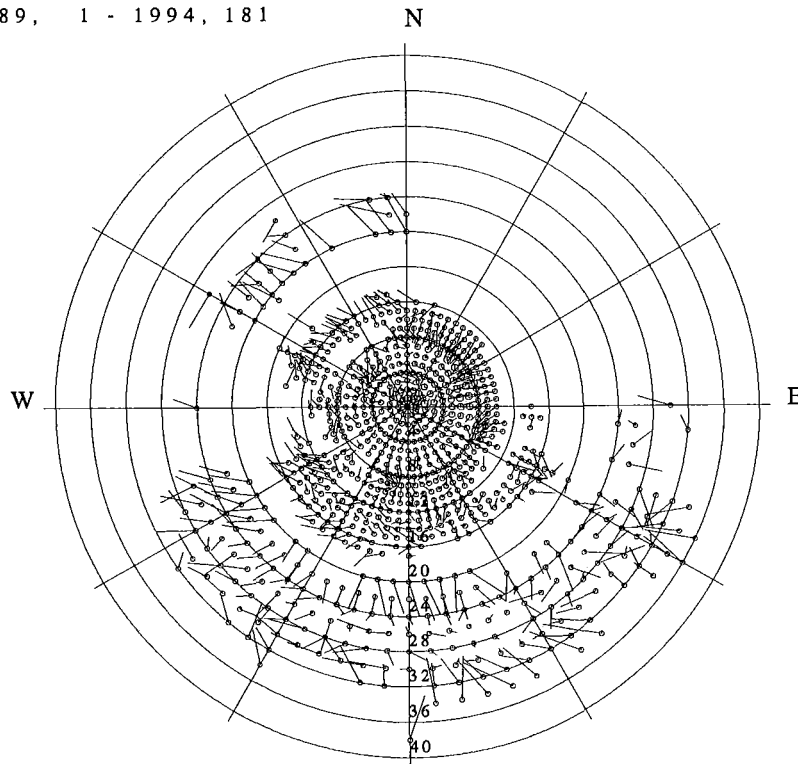


Fig. 7.5.2: The upper plot shows 222 Apatity slowness mislocation vectors relative to the observed values. At the bottom the 134 corresponding mislocation vectors relative to the theoretical values (predicted mislocations) are seen. The symbol size corresponds to the number of single observations per bin. The maximum number of observations per mislocation vector is 25 (top) and 84 (bottom).

CORRECTION VECTORS FOR
 ARA0 1989, 1 - 1994, 181



CORRECTION VECTORS FOR
 ARA0 1989, 1 - 1994, 181

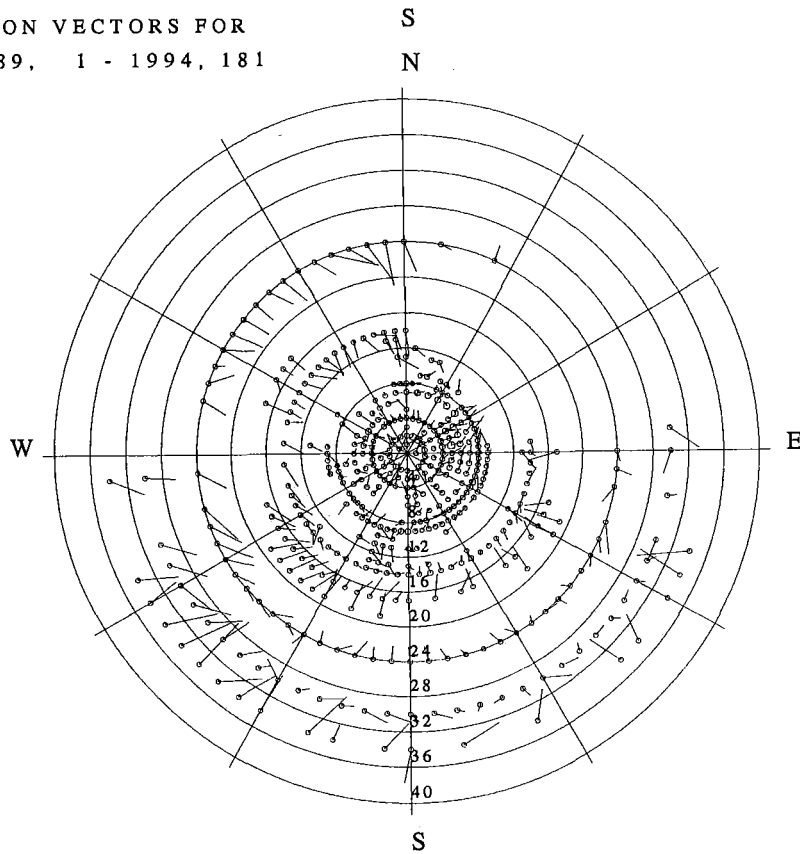
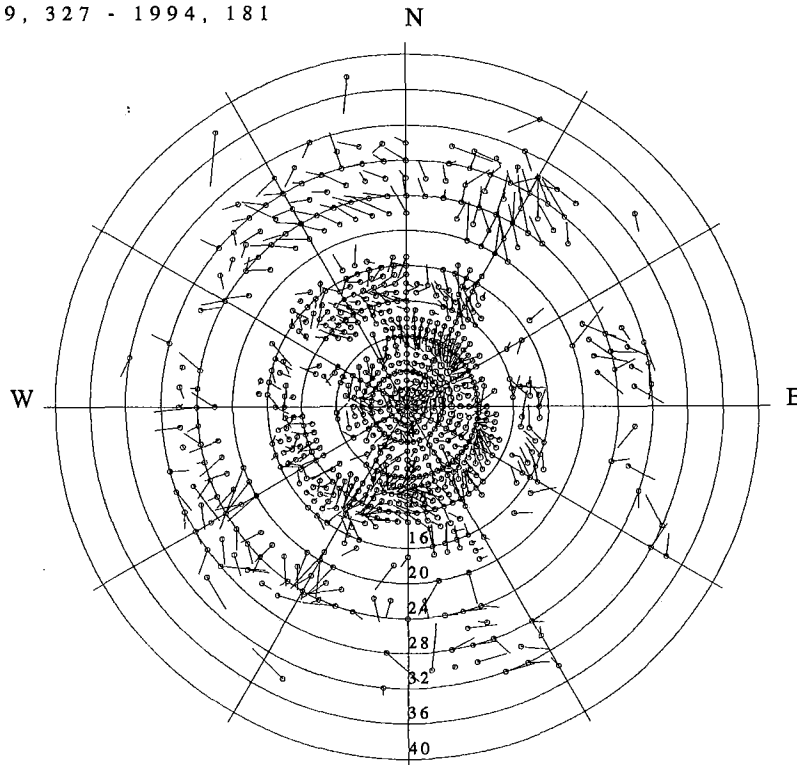


Fig. 7.5.3: As Fig. 7.5.2 but for ARCESS. The number of mislocation vectors is 796 (relative to observation) and 435 (relative to the theory). The maximum number of observations per mislocation vector is 631 (top) and 2419 (bottom).

CORRECTION VECTORS FOR
FIA0 1989, 327 - 1994, 181



CORRECTION VECTORS FOR
FIA0 1989, 327 - 1994, 181

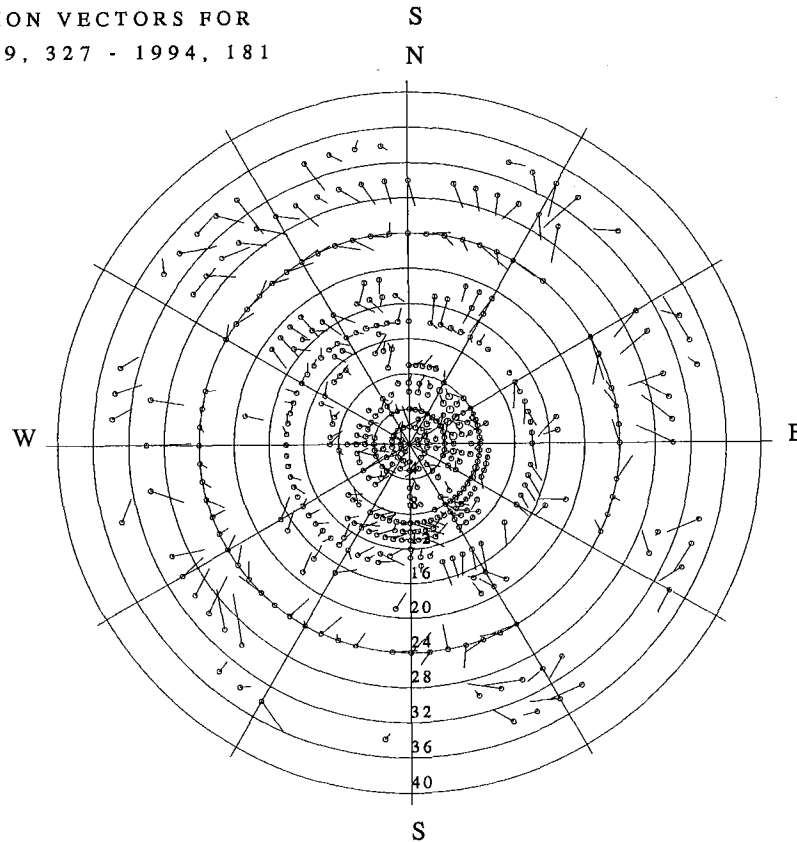
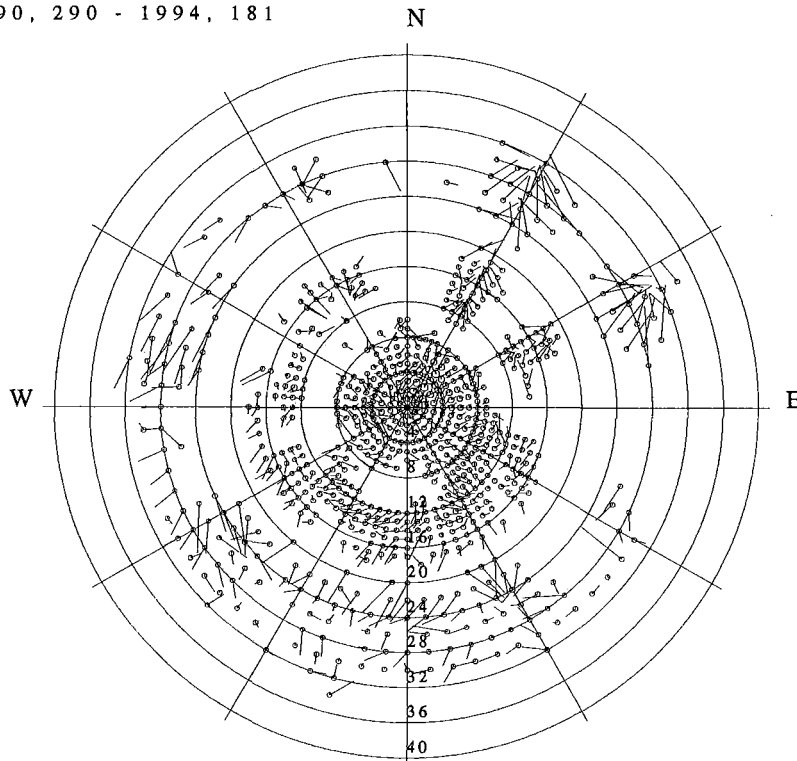


Fig. 7.5.4: As Fig. 7.5.2 but for FINISS. The number of mislocation vectors is 806 (relative to observation) and 446 (relative to the theory). The maximum number of observations per mislocation vector is 298 (top) and 996 (bottom).

CORRECTION VECTORS FOR
GEC2 1990, 290 - 1994, 181



CORRECTION VECTORS FOR
GEC2 1990, 290 - 1994, 181

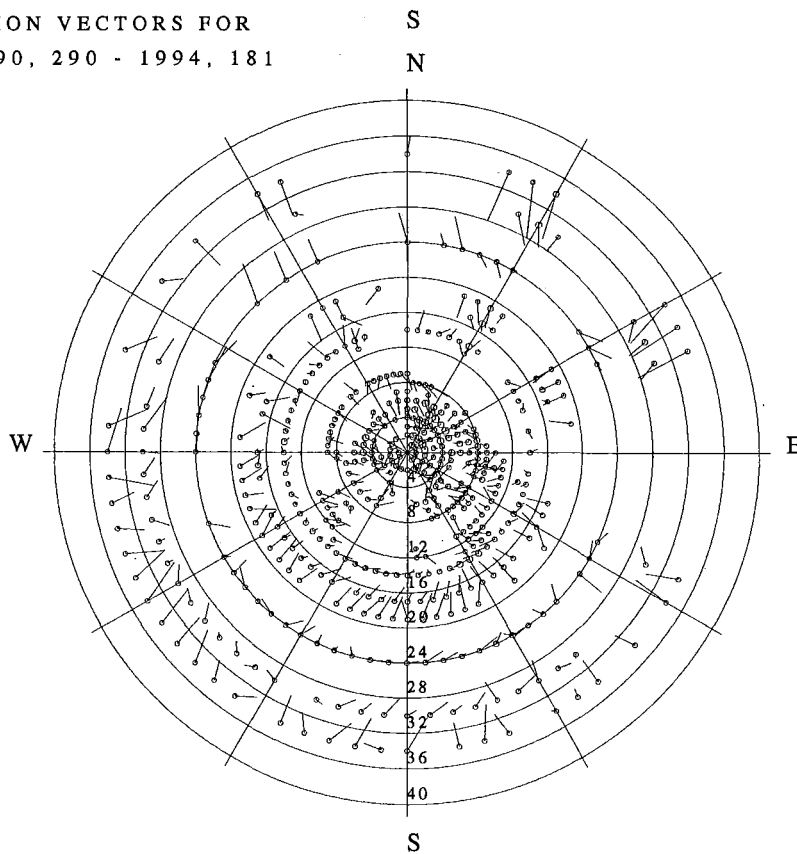
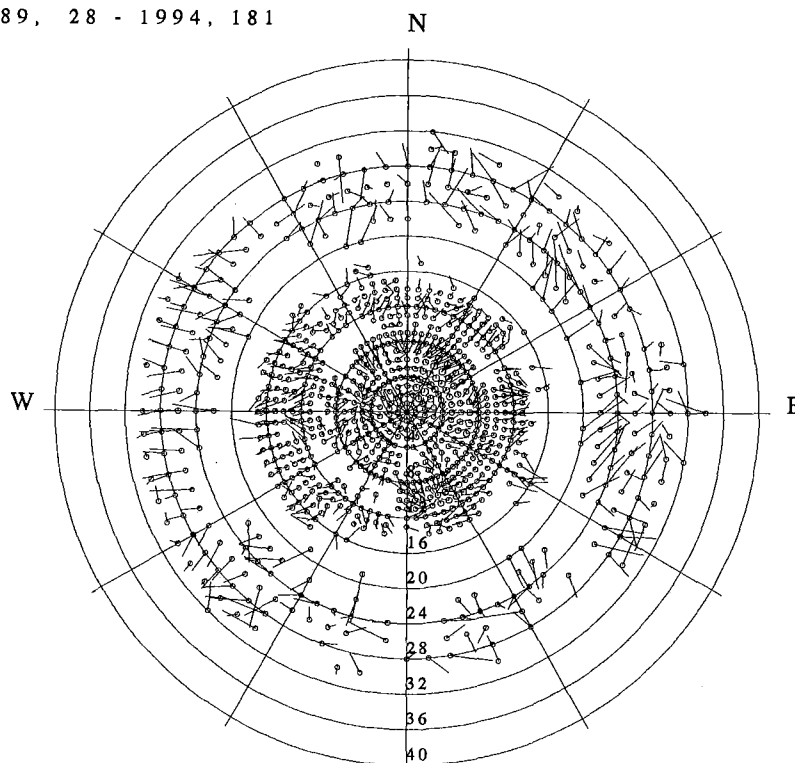


Fig. 7.5.5: As Fig. 7.5.2 but for GERESS. The number of mislocation vectors is 760 (relative to observation) and 469 (relative to the theory). The maximum number of observations per mislocation vector is 325 (top) and 619 (bottom).

CORRECTION VECTORS FOR
NRAO 1989, 28 - 1994, 181



CORRECTION VECTORS FOR
NRAO 1989, 28 - 1994, 181

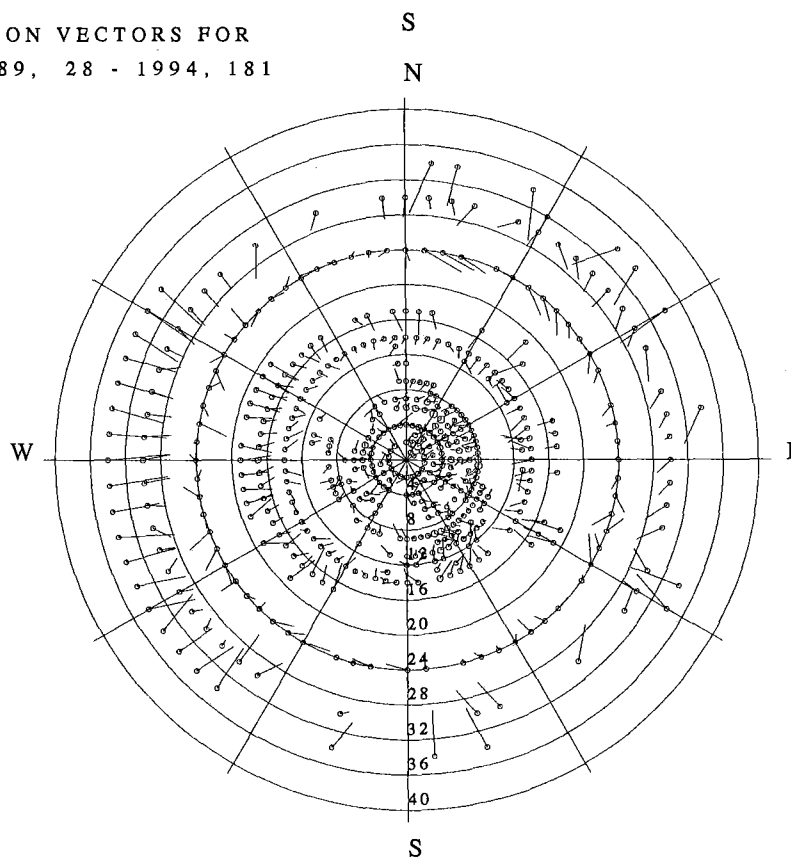
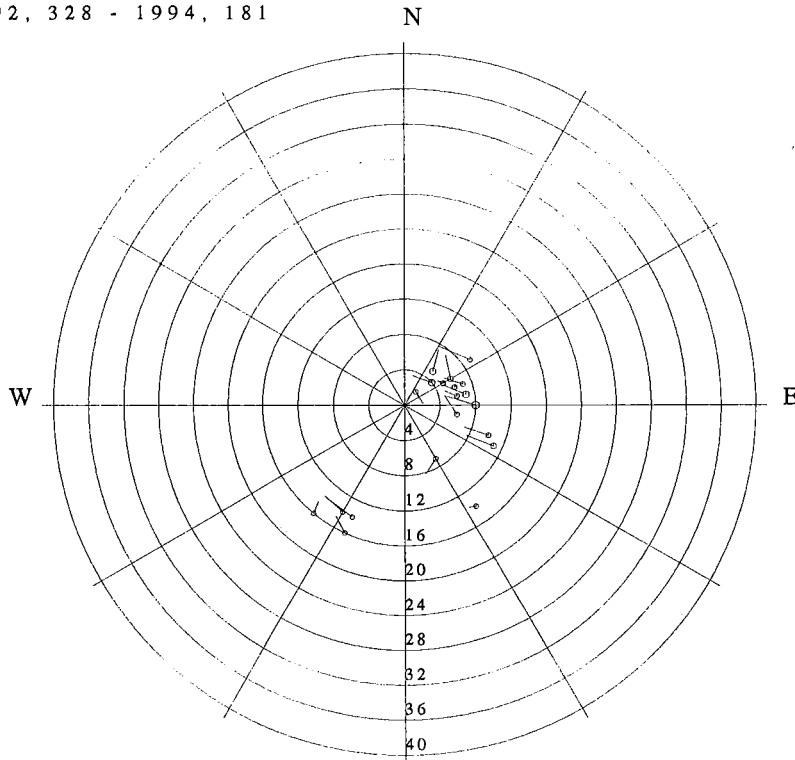


Fig. 7.5.6: As Fig. 7.5.2 but for NORESS. The number of mislocation vectors is 934 (relative to observation) and 497 (relative to the theory). The maximum number of observations per mislocation vector is 614 (top) and 1282 (bottom).

CORRECTION VECTORS FOR
SPA0 1992, 328 - 1994, 181



CORRECTION VECTORS FOR
SPA0 1992, 328 - 1994, 181

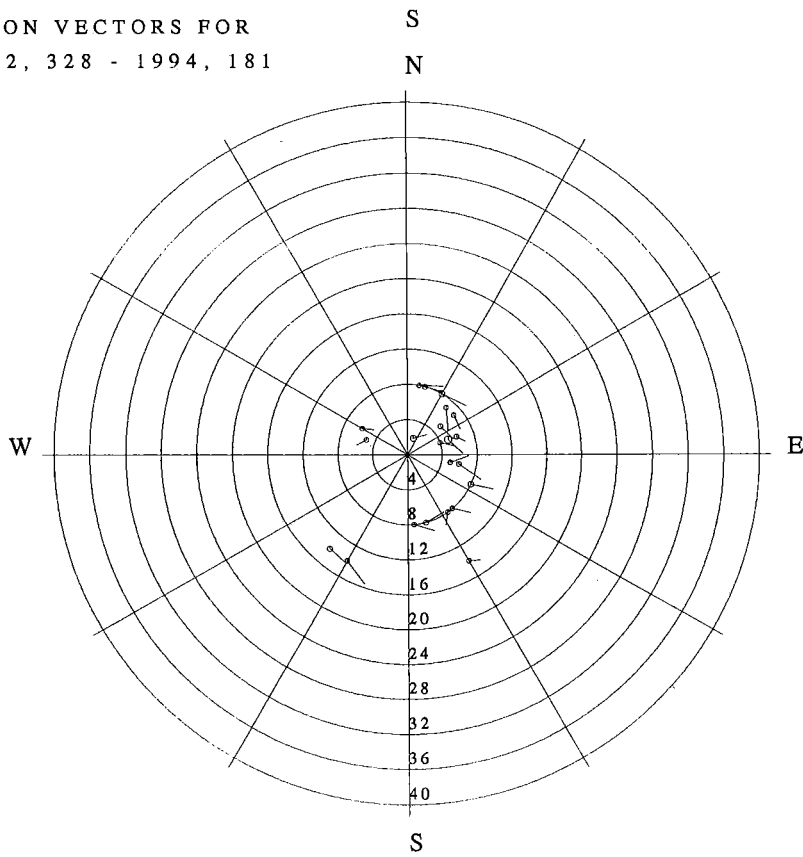
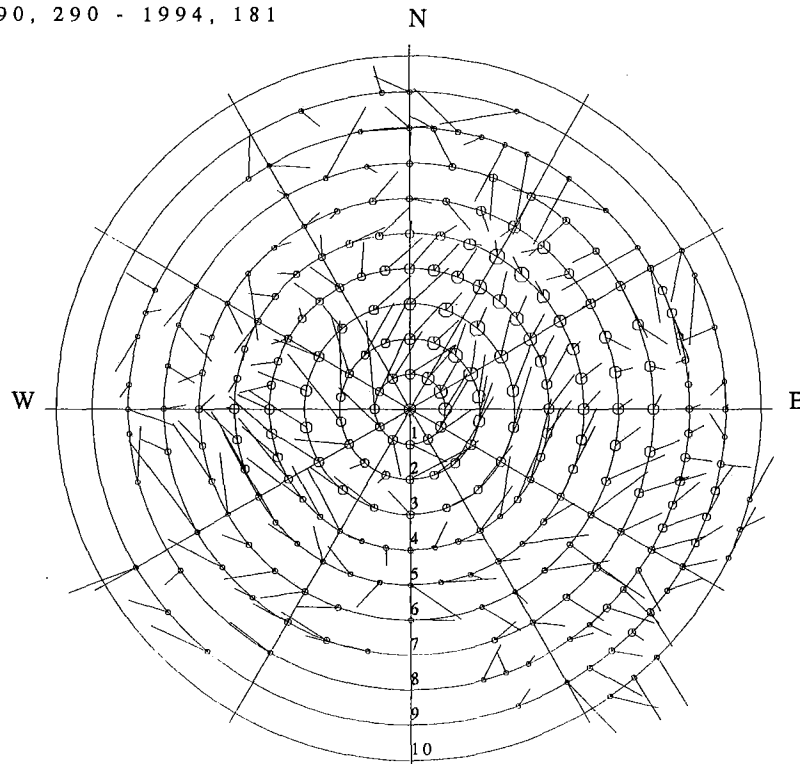


Fig. 7.5.7: As Fig. 7.5.2 but for Spitsbergen. The number of mislocation vectors is 20 (relative to observation) and 22 (relative to the theory). The maximum number of observations per mislocation vector is 6 (top) and 26 (bottom).

CORRECTION VECTORS FOR
GEC2 1990, 290 - 1994, 181



CORRECTION VECTORS FOR
GEC2 1991, 112 - 1994, 181

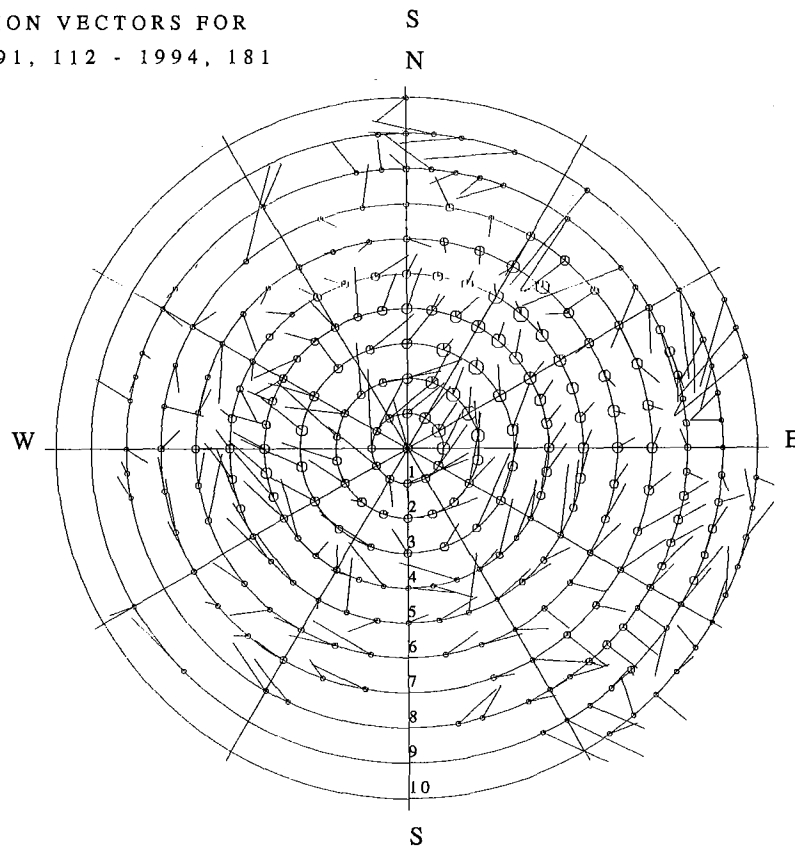


Fig. 7.5.8: Mislocation vectors for GERESS P-type onsets. On the top a subset is shown of the data from Fig. 7.5.5 (top), and at the bottom the mislocation vectors for a collection of GERESS analyst-reviewed slowness values are shown.

7.6 On the reliability of event location estimates from automatic and interactive processing

Introduction

The technique of automatic post-processing of seismic events (Kværna and Ringdal, 1994) has been shown to give a substantial improvement in location accuracy when applied to seismic events in the Khibiny Massif, Kola Peninsula. As shown in that paper (see also Ringdal et al, 1993), the improvement is significant not only relative to automatic processing by the Intelligent Monitoring System (IMS), but also compared to interactive analyst-reviewed solutions.

The improvements are particularly noteworthy since the IMS already shows an excellent location capability in this area (median location error 10.6 km for the automatic solutions and 3.3 km for the analyst-reviewed solutions). By the automatic post-processing method, the median error is reduced to 1.9 km, even when no calibration is carried out. The improvements are even larger when considering the 90% quantile in the location errors; the corresponding numbers being 48.4 km, 9.7 km and 3.6 km for the three cases.

In order to take full advantage of the improved accuracy, it is essential to provide realistic confidence ellipses for the location estimates. In this contribution we discuss the confidence ellipses associated with the various processing methods, and make some observations regarding their reliability as an uncertainty measure. The data base established in the studies described above has been used.

The Khibiny Massif events

Six apatite mines are located within an area of about 10 km² in the Khibiny Massif on the Kola Peninsula of Russia (see Fig. 7.6.1). A detailed description of these mines and the mining activity is found in Mykkeltveit (1992). Although we have no explicit information on the exact sizes of these mines, interpretation of various maps suggests that the typical size is about 1 km². The Kola Regional Seismological Centre has since the beginning of 1991 provided NORSAR with information on mining blasts in the six Khibiny Massif mines. Detailed information on the events used in this study is given in Kværna (1993).

Data analysis

As reported by Kværna (1993), available data for this study have comprised 4 arrays (NORESS, ARCESS, FINESS, Apatity) as well as the 3-comp Apatity station APZ9. We have considered the location results using four different analysis methods:

1. Automatic IMS analysis, based on available array data (4 arrays)
2. Interactive analyst results using the Analyst Review Station (ARS) (4 arrays + APZ9)
3. Automatic post-processing without calibration (2 arrays: ARCESS and Apatity)

4. Automatic post-processing with calibration (2 arrays + APZ9)

For each event in the data base, we computed the associated 90% confidence ellipse for each of the four methods. For methods 1 and 2, we used the error estimates of time and azimuth provided by the IMS processing system for calculating the error ellipses. As explained by Bache et al (1990), these error estimates take into account both a priori model uncertainties and uncertainties resulting from actual signal-to-noise ratios. For methods 3 and 4, we used error estimates of time and azimuth computed by Kværna (1993). These latter estimates were set to the same value regardless of actual signal-to-noise ratio. An example comparing the uncertainties used for each method is shown for one typical event in Table 7.6.1, using phases from the ARCESS and Apatity arrays.

We then plotted the solutions and the confidence ellipses for all events, as shown in Figs. 7.6.2-7.6.4. For clarity, different colors have been used for each of the six mines, and each figure shows the solutions in two different scales.

Our general observations, also discussed in Ringdal et al (1993), are:

- The interactive IMS solutions (Fig. 7.6.3) are significantly more accurate and consistent than the automatic IMS solutions (Fig. 7.6.2).
- The automatic post-processing solutions are still better than the interactive IMS solutions, even without calibration (Fig. 7.6.4). This is in spite of the fact that post-processing makes use of only 2 arrays.
- With calibration, the results are even more accurate. Fig. 7.6.5 shows the "optimum" results achieved by post-processing with calibrated data, where also the Apatity 3-comp station has been used.

Information on the percentage of events for which the 90% confidence ellipse includes the actual location is given in Table 7.6.2. The following observations are made:

IMS automatic processing:

Only 54% of the error ellipses cover the actual epicenter. This means that these ellipses do not represent the accuracy of the solutions properly.

IMS interactive processing:

93.9% of the error ellipses cover the actual epicenter. Thus the error ellipses are quite representative of the actual accuracy in this case.

Automatic post-processing (uncalibrated):

98.0% of the error ellipses cover the actual epicenter. Thus, the error ellipses are probably too conservative in this case.

Automatic post-processing (calibrated):

90.0% of the error ellipses cover the actual epicenter. Thus the error ellipses represent very well the actual uncertainty for this method.

Conclusions

For the automatic IMS, the error ellipses are currently too small. The main reason is probably that they do not take into account effects of occasional erroneous phase identification by the automatic system. It is noted here that the formal calculation of error ellipses assumes that the phases are correctly identified.

For the interactive IMS solution, the error ellipses are quite representative. This indicates that the a priori uncertainties in the phases used by the location program have been well estimated. Consequently, the interactive IMS solutions have an accuracy that is well represented by their error ellipses, at least for the region processed here.

For the post-processing method using uncalibrated data, it seems necessary to reduce the a priori uncertainties, thus producing smaller error ellipses. With calibrated data, the ellipses are representative for this particular data set. However, it is important that other regions be studied as well before making any firm conclusions.

F. Ringdal
T. Kværna

References

- Bache, T.C., S.R. Bratt, J. Wang, R.M. Fung, C. Kobryn and J. Given (1990): The Intelligent Monitoring System, *Bull. Seism. Soc. Am.*, 80 (Special Issue), 1818-1832.
- Kværna, T. (1993): Accurate determination of phase arrival times using autoregressive likelihood estimation, *NORSAR Semiannual Tech. Summ. 1 Oct 1992 - 31 Mar 1993*, Scientific Rep. No. 2-92/93, Kjeller, Norway.
- Kværna, T. and F. Ringdal (1994): Intelligent post-processing of seismic events, *Ann. Geofysica*, Vol XXXVII, No 3, 309-322.
- Mykkeltveit, S. (1992): Mining explosions in the Khibiny Massif (Kola Peninsula of Russia) recorded at the Apatity three-component station. Report PL-TR-92-2253, Phillips Laboratory, Hanscom AFB, MA, USA.
- Ringdal, F., T. Kværna and B.Kr. Hokland (1993): Onset time estimation and location of events in the Khibiny Massif, Kola Peninsula, using the Analyst Review Station, *NORSAR Semiannual Tech. Summary 1 Apr - 30 Sep 93*, Scientific Rep. No. 1-93/94, Kjeller, Norway.

Phase	Method 1 (IMS)		Method 2 (ARS)		Method 3 & 4 (Post-proc.)	
	Time	Az	Time	Az	Time	Az
Apatity Pg	1.0	5.4	1.0	5.4	0.1	-
Apatity Lg	3.0	6.5	3.0	-	0.25	-
Apatity Rg	-	-	3.1	3.2	-	4.0
ARCESS Pn	1.0	6.0	1.0	6.0	0.1	4.0
ARCESS Pg	2.1	5.5	2.1	5.5	-	-
ARCESS Sn	2.1	6.6	2.1	6.6	-	-
ARCESS Lg	3.0	5.5	3.0	5.5	-	-

Table 7.6.1. Example of uncertainties used for calculating error ellipses. Note that the estimates for Methods 1 and 2 are identical, whenever the same phase has been used.

Method	Mine						Total	%
	1	2	3	4	5	6		
IMS automatic	9/11	0/2	7/11	7/12	3/10	1/4	27/50	54.0
IMS interactive	10/11	2/2	10/11	12/12	8/9	4/4	46/49	93.9
Post--processing (uncalibrated)	12/12	2/2	11/11	12/12	9/10	4/4	50/51	98.0
Post-processing (calibrated)	10/11	2/2	11/11	12/12	7/10	3/4	45/50	90.0

Table 7.6.2. Number and percentage of events for which the 90% location confidence ellipse includes the actual epicenter. Numbers are given for each of the 6 mines individually and combined.

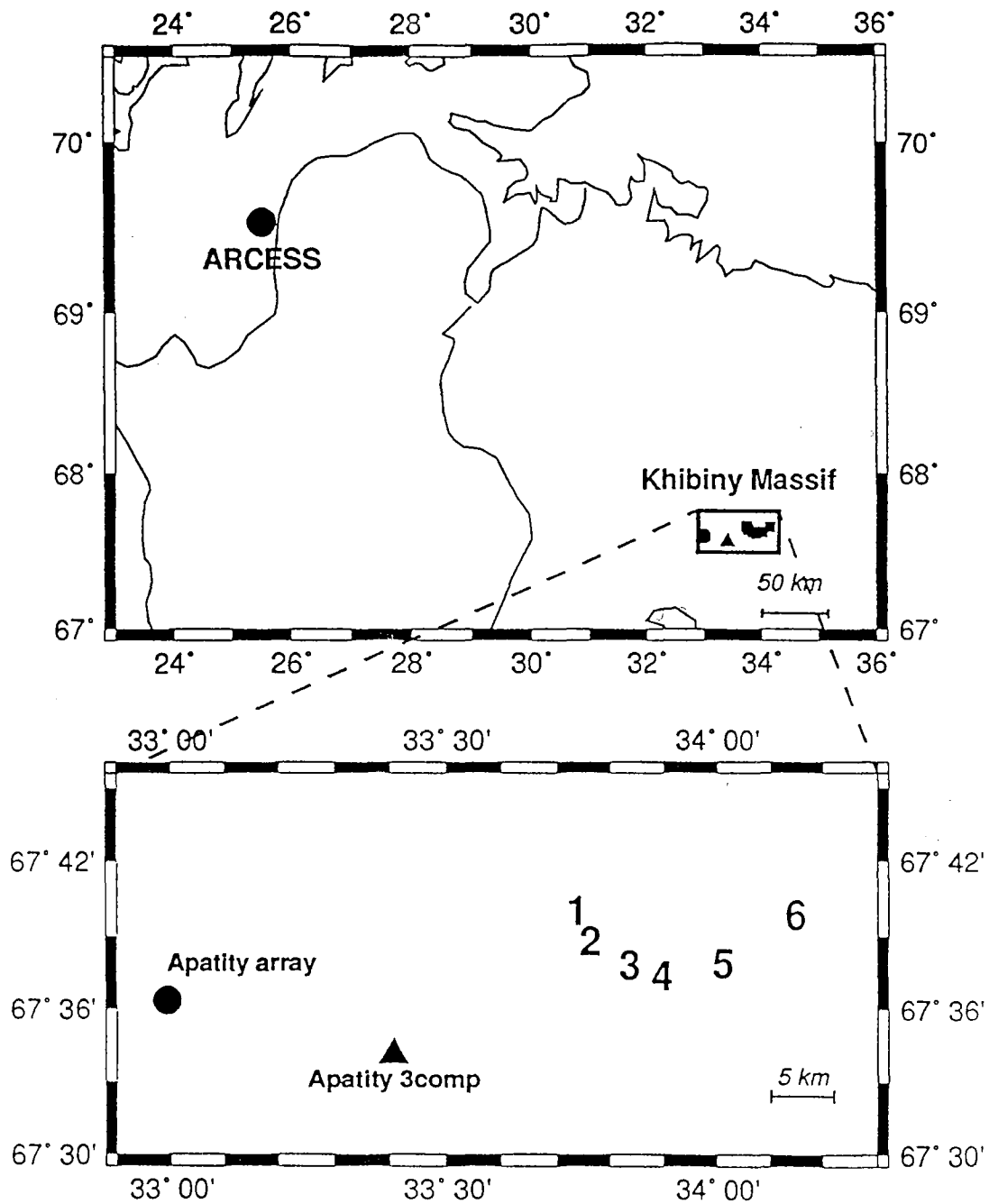


Fig. 7.6.1. In the *upper part*, a large reference area is shown. The location of the ARCESS array is given by a filled circle, and the location of the Khibiny Massif region is shown. The *lower part* shows a detailed picture of the Khibiny Massif region. The locations of the six mining sites are given by large numbers 1-6. The Apatity array (APA0) is shown as a filled circle, and the three-component station (APZ9) in the town of Apatity is shown as a large triangle.

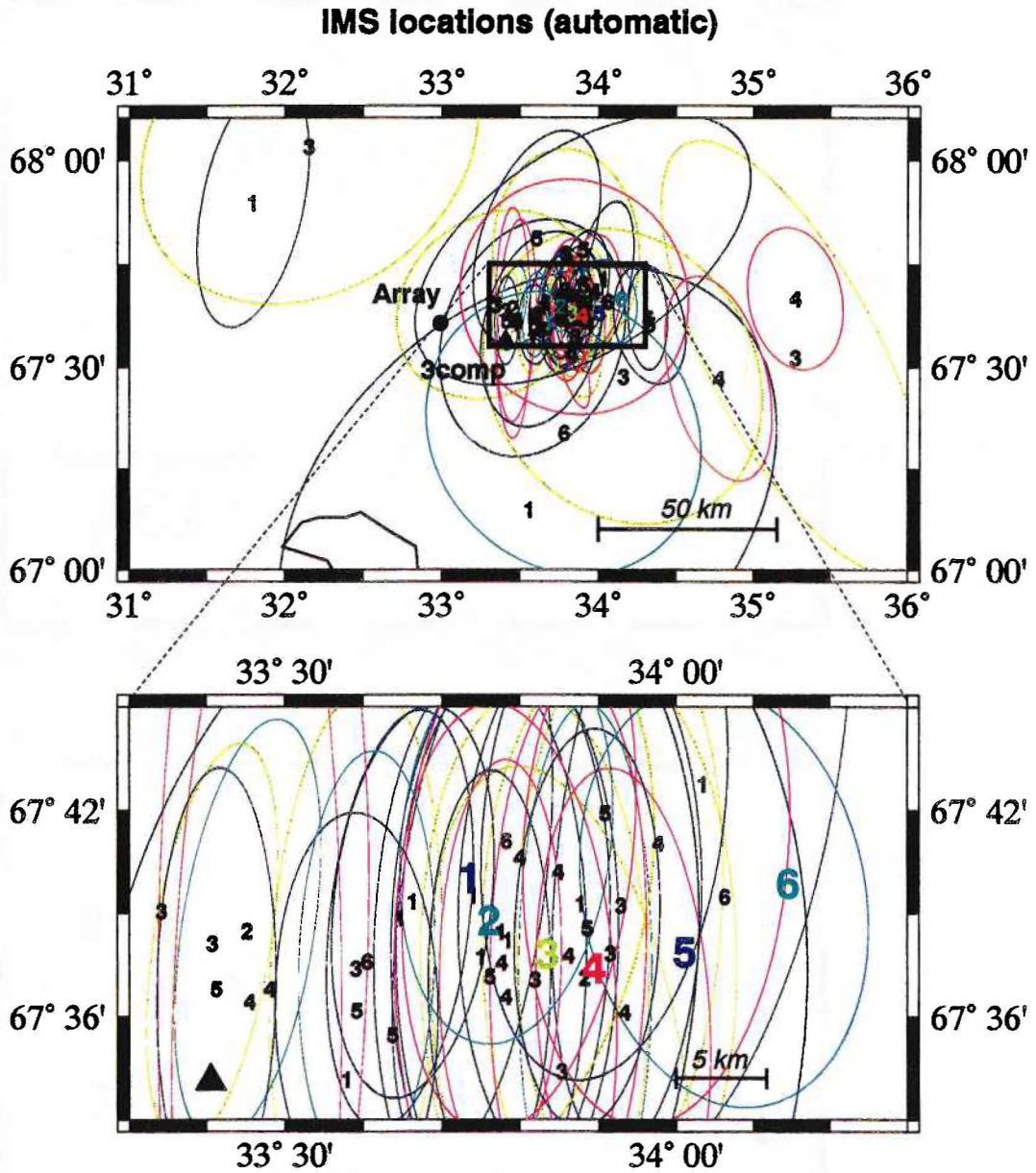


Fig. 7.6.2. Location error ellipses for automatic IMS processed events. The large numbers are actual mining sites, and the small numbers are corresponding location estimates.

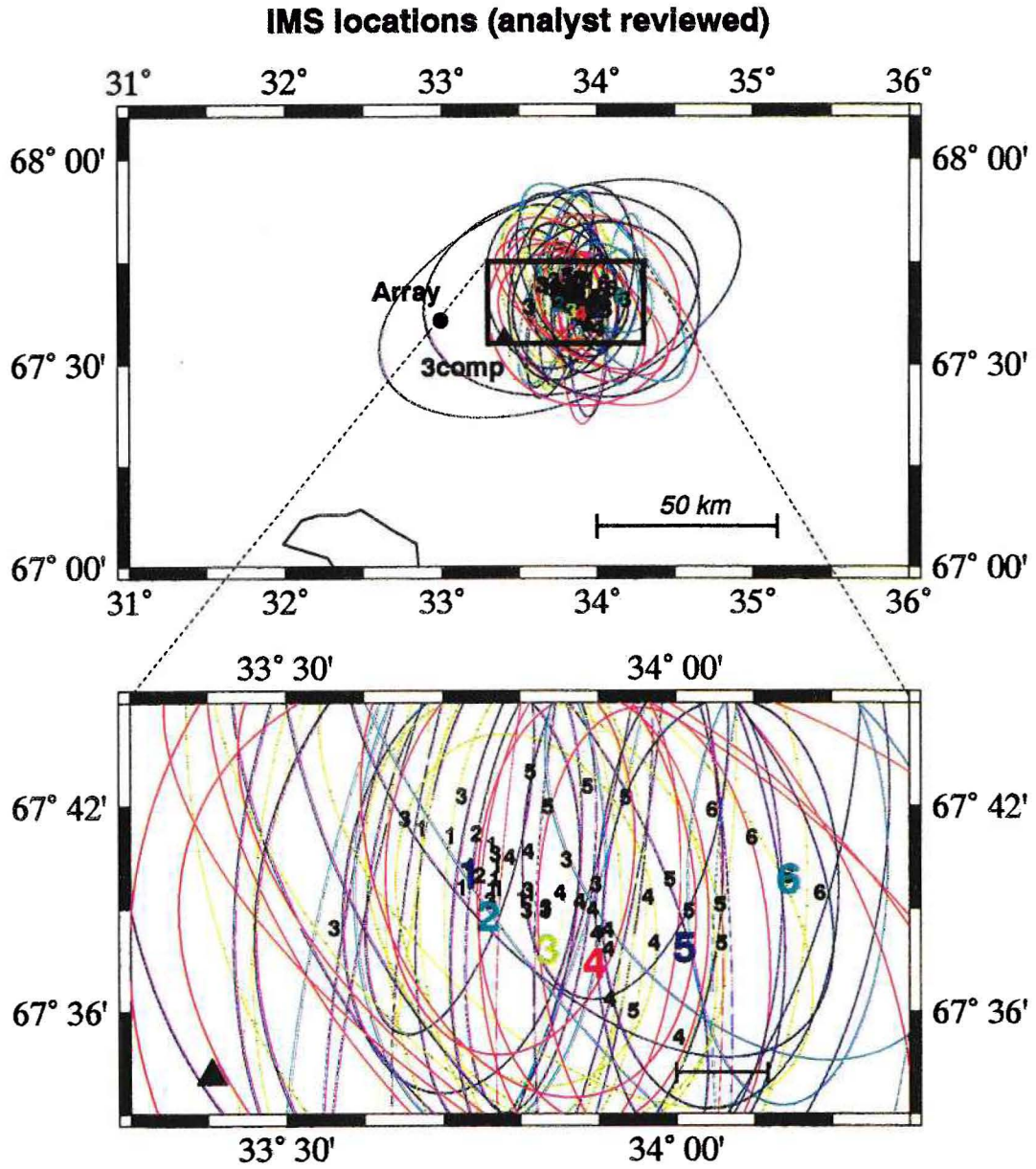


Fig. 7.6.3. Same as Fig. 7.6.2, but corresponding to the IMS analyst-reviewed location estimates.



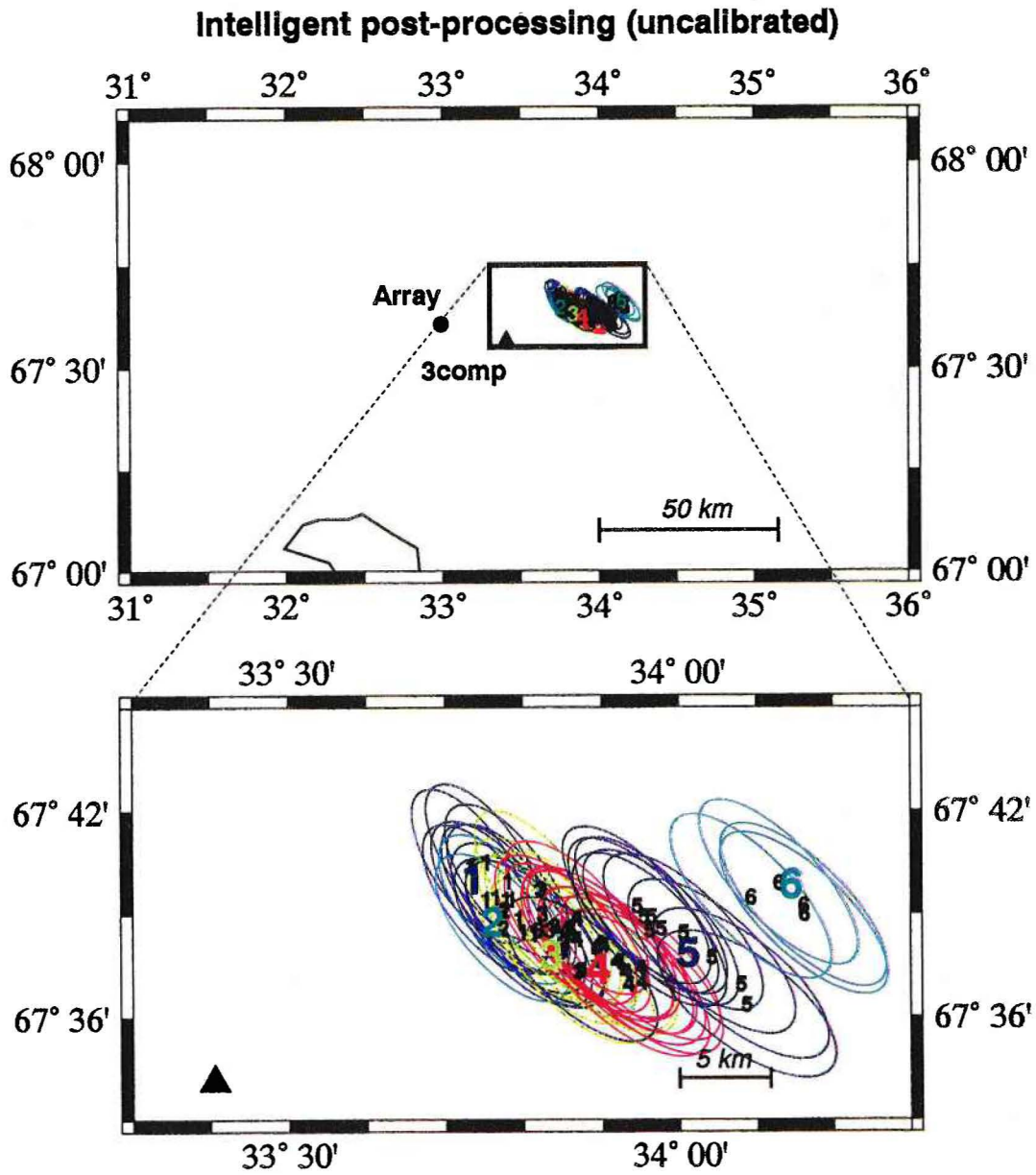


Fig. 7.6.4. Same as Fig. 7.6.2, but corresponding to the automatic post-processing location estimates, using ARCESS and Apatity array data with no calibration.



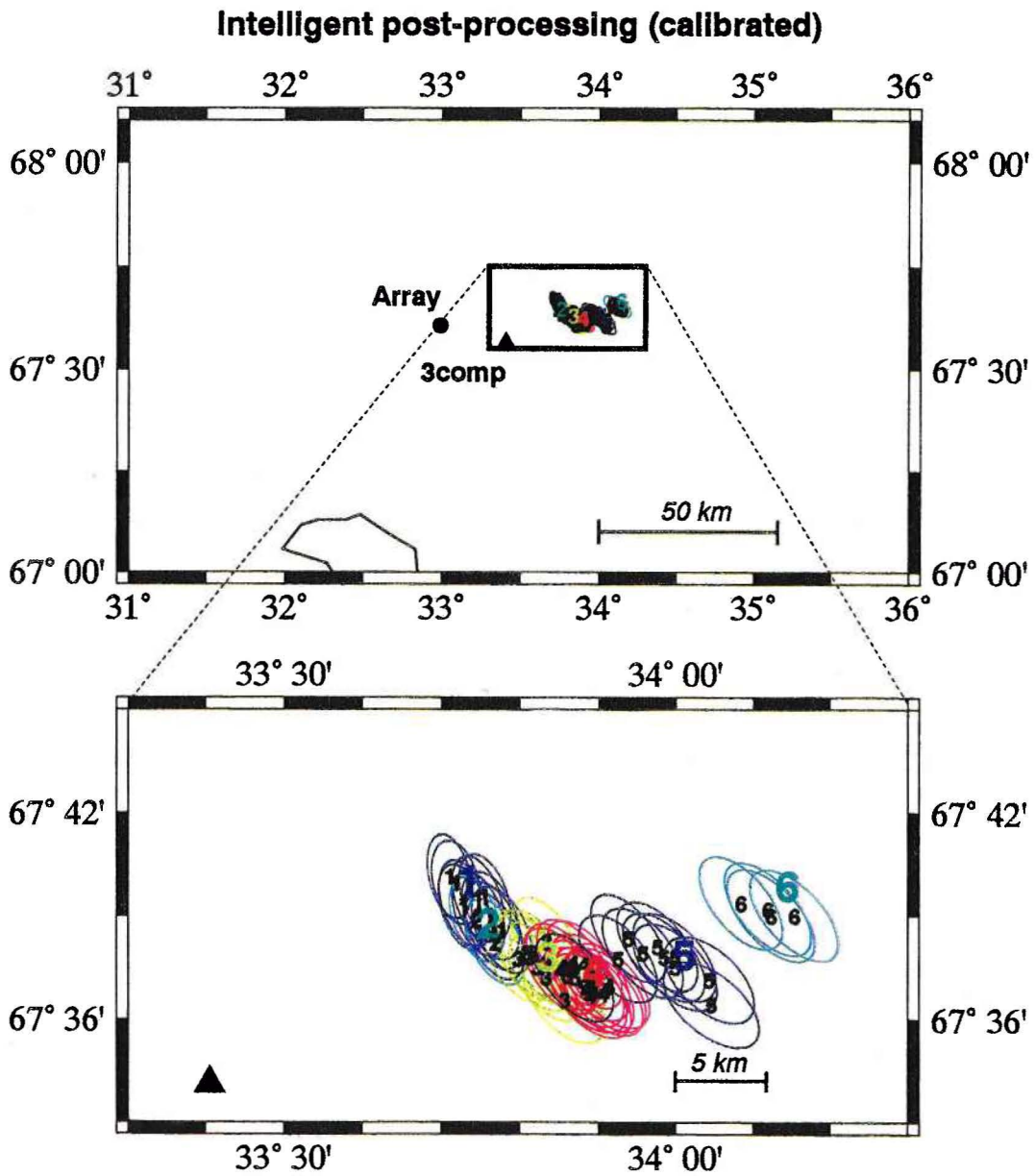


Fig. 7.6.5. Same as Fig. 7.6.2, but corresponding to the automatic post-processing location estimates, using calibrated data from ARCESS, the Apatity array and the Apatity 3-comp station.

Vertical text or markings along the right edge of the page, possibly bleed-through or a margin.